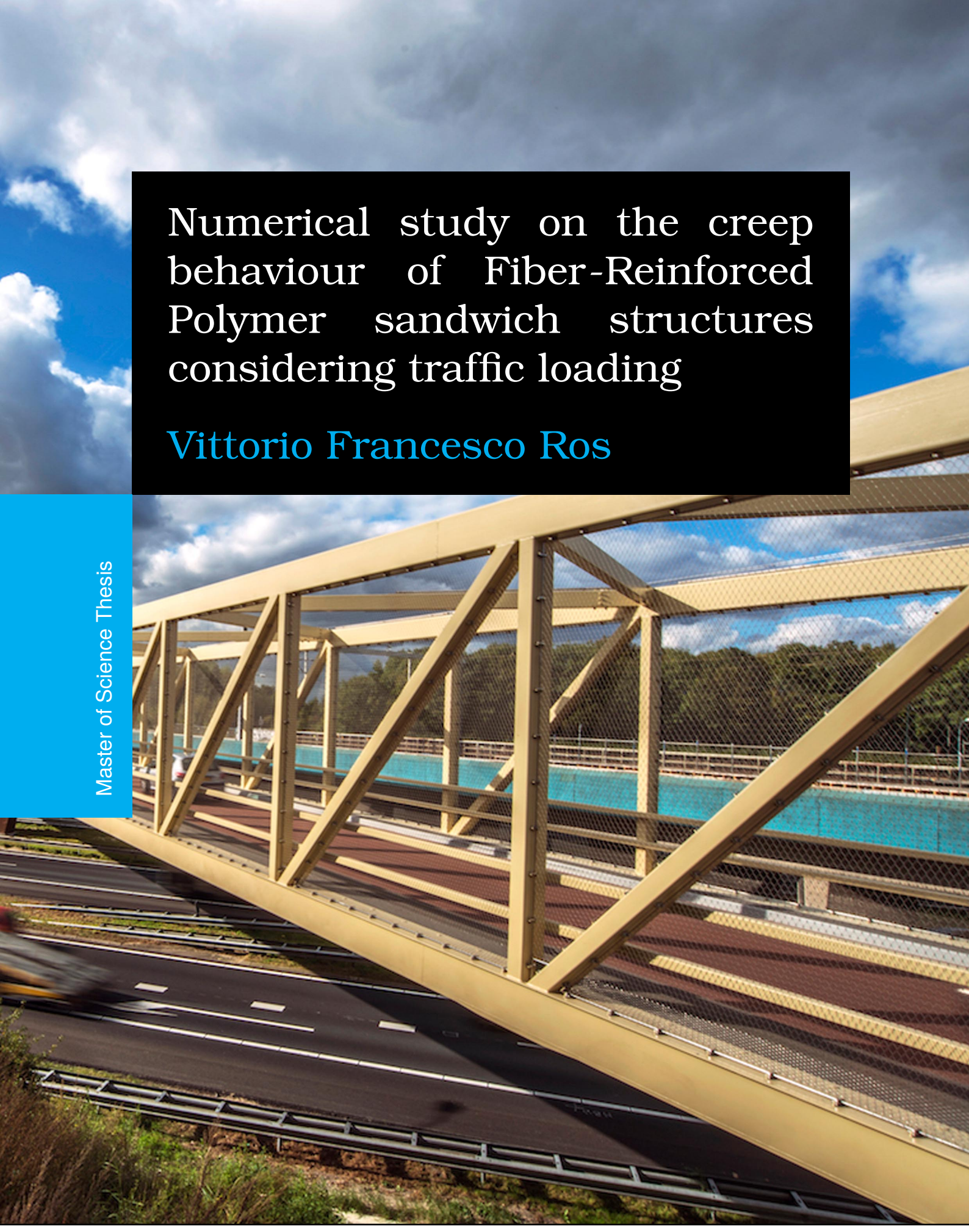

Numerical study on the creep behaviour of Fiber-Reinforced Polymer sandwich structures considering traffic loading

Vittorio Francesco Ros

Master of Science Thesis

TU Delft Delft University of Technology

Faculty of Civil Engineering and Geosciences

Numerical study on the creep behaviour of Fiber-Reinforced Polymer sandwich structures considering traffic loading

MASTER OF SCIENCE THESIS

For the degree of MSc in Structural Engineering: Steel, Timber and Composite structures at Delft University of Technology

Vittorio Francesco Ros

September 25, 2021

Faculty of Civil Engineering and Geosciences · Delft University of Technology

Supervisors and assessment committee:

Dr. Ir. Marko Pavlovic (Chair)
Ir. Angeliki Christoforidou
Dr. Ir. Mladena Lukovic
Ir. Pieter Schoutens
Ir. George Zarifis

The work in this thesis was supported by Engineering Constultancy Witteveen+Bos. Their cooperation is hereby gratefully acknowledged.

Abstract

Ageing of infrastructure leads to an increasing demand for new technologies and design solutions in current bridge engineering. Over the last decades the traffic intensity has grown tremendously, while design codes and regulations have become stricter. Many current steel bridges realised in The Netherlands suffer from fatigue problems. Replacement of the bridges can be expensive, and thus engineers are asked to provide design solutions that can extend the lifetime of these structures. Rehabilitation through the replacement of steel orthotropic decks with Glass Fiber-Reinforced Polymer (GFRP) sandwich deck panels is considered as one of the few possible solution strategies. FRP's are considered a viable option, due to their versatility, high strength-to-weight ratio, fast installation possibilities, low maintenance costs and their resistance against both corrosion and fatigue. The increasing amount of bridges containing FRP structural elements demonstrates the high potential of the material. However, many engineering consultancies address to face difficult challenges when working with FRP. The main concern in the construction and design field is about the long-term performance of the material. Due to the viscoelastic nature of the polymeric matrix, FRP structural elements show complex creep and recovery behaviour under variable traffic loading. Current standards account for this traffic load by conservatively assuming that 40% of this traffic load should be accounted for in creep calculations, which originates from experience with concrete bridges. However, due to the fast recovery behaviour of FRP compared to concrete, this value might be too conservative. Based on current knowledge and experimental results, a numerical model was created that is able to predict the long-term creep deformation including both creep and recovery behaviour. The model uses experimental results based on UD-plies, which enables the model to calculate the long-term deformation of laminates with a wide variety of layups. The Finite Element Analysis (FEA) software package Abaqus has been used to model a FRP sandwich deck panel and calculate the time-dependent response under traffic loading. Finally, a FRP sandwich deck panel has been analysed by both the numerical model and according to the procedure prescribed by current standards. Results have shown that the amount of traffic load that is currently considered as permanent static load for creep calculations could be reduced. However, it is recommended for future research to improve the numerical model by using more accurate creep prediction models supported with profound experimental work. It is expected that this would lead to an even higher reduction of the amount of traffic load that is currently considered in design recommendations.

Keywords: Glass Fiber-Reinforced Polymer; Sandwich deck panel; Viscoelasticity; Creep; Traffic Load

Table of Contents

List of Figures

List of Tables

Preface

This thesis focuses on the long-term creep behaviour of Fiber-Reinforced Polymer composites applied as structural elements in bridges. It is the result of both my literature research on the topic of creep within this material together with the creation of a numerical model that has the findings of this literature research implemented. It is the result of a rough eleven months taking project that functions as the final step in obtaining the Master's degree in Structural Engineering at the Delft University of Technology. The thesis is mainly directed to future researchers and engineers in the field of bridge engineering that want to implement the relative new material FRP. However, the content might be interesting for any engineer or scientist that is interested in FRP.

My interests for bridge design and the challenges that come along by investigating this relatively new material were basis for the subject of this thesis. The research question originated from multiple sessions with my committee members, whom can be considered as true experts in the field of bridge engineering.

Although some times this project seemed a bit rough, I am truly proud of the discipline I had that was needed to gain the knowledge necessary for the accomplishment of such a project. Finally, I would like to point out that I am very grateful to have been given the opportunity to work on such a state-of-the-art project in which I was constantly able to challenge myself.

Acknowledgements

This study has been conducted at the engineering consultancy Witteveen+Bos for the Master's degree in Structural Engineering at the Delft University of Technology. I want to thank Witteveen+Bos for the graduating opportunity, the support and the supervision during the project. In particular, I would like to thank George Zarifis and Pieter Schoutens, who both provided me with their knowledge and insights of the subject.

In addition, I would like to thank the supervisors from the Delft University of Technology. First, I want to thank Marko Pavlovic for his very precious time which he invested in my project and for the clear guidance he provided. I would like to thank Angeliki Christofirodou. She really spent a lot of time helping me with the challenges I had within this project, but also for her mental support during the rough thesis times. Also I would like to thank my friends Mathieu Koetsier and Tim Sluiter, who both have really contributed in my study related successes.

I want to thank all the people that were not directly part of my thesis, but really have encouraged me to finish this project. Especially, I want to thank my girlfriend Daphne Troost, who always supported me during my entire study and was always there for me in tough times. Finally, I would like to thank both of my parents who have always motivated me to achieve my full potential.

Delft, University of Technology
September 25, 2021

Vittorio Francesco Ros

“You never change things by fighting the existing reality. To change something, build a new model that makes the existing model obsolete”

— *Richard Buckminster Fuller*

Glossary

List of Acronyms

ANWB	Algemene Nederladsche Wielrijders-Bond
BSP	Boltzmann Superposition Principle
CLT	Classical Laminate Theory
FE	Finite Element
FEA	Finite Element Analysis
FEM	Finite Element Modelling
FRP	Fiber-Reinforced Polymer
FSDT	First-order Shear Deformation Theory
FTTM	Frequency Time Transformation Method
GFRP	Glass Fiber-Reinforced Polymer
LSS	Laminate Stacking Sequence
SLS	Serviceability Limit State
TTSP	Time Temperature Superposition Principle
TTSSP	Time Temperature Stress Superposition Principle
UD	Unidirectional
UDL	Uniform Distributed Load
ULS	Ultimate Limit State
VARTM	Vacuum Assisted Resin Transfer Moulding

List of Symbols

α_h	TTSSP horizontal shift factor
α_T	TTSP shift factor from WLF equation
α_v	TTSSP vertical shift factor
δ_0	Instantaneous deformation
δ_m	Stress and temperature dependent deformation parameter of Findley
δ_t	Transient part of the creep deformation
$\dot{\varepsilon}(t)$	Creep strain rate
ϵ_0	Initial strain
$\eta(f)$	Loss factor
η_{cf}	Conversion factor for fatigue effects CUR96 and JRC
η_{cm}	Conversion factor for moisture effects CUR96 and JRC
η_{ct}	Conversion factor for temperature effects CUR96 and JRC
η_{cv}	Conversion factor for creep effects CUR96 and JRC
η_c	Conversion factor for reduction material properties CUR96 and JRC
γ_M	Partial factor accounting for unfavourable deviations of the material properties
γ_{Rd}	Partial factor accounting for the uncertainty in the resistance model
λ	Variable for time shift recovery cycle in Schapery integral
μ_m	Fit parameter Bürger model
ν	Poisson's ratio
ν_{12}	Poisson's ratio in 12-direction
ν_{13}	Poisson's ratio in 13-direction
ν_{23}	Poisson's ratio in 23-direction
$\phi(t)$	Creep coefficient from TS19101
$\psi_{0,i}$	Factor that determines the combination value for the variable loading in the characteristic loading combination
$\psi_{1,i}$	Factor that determines the combination value for the variable loading in the frequent loading combination
$\psi_{2,i}$	Factor that determines the combination value for the variable loading in the quasi-permanent loading combination
σ	Applied stress
σ_0	Initial applied stress
τ	Viscosity fit parameter phenomenological mechanical models
ε'_0	Initial elastic strain under reference stress
a_σ	Nonlinear stress dependent shift parameter in Schapery integral
C_1	Experimental constant in WLF equation for the shift factor
C_2	Experimental constant in WLF equation for the shift factor
$D(t)$	Time-dependent creep compliance
D_0	Instantaneous creep compliance

D_m	Transient creep compliance fit parameter of Findley
D_t	Transient creep compliance
E	Elastic modulus
$E''(f)$	Loss modulus
$E'(f)$	Storage modulus
E_0	Initial elastic modulus
E_1	Elastic modulus of UD-ply in longitudinal fiber direction
E_2	Elastic modulus of UD-ply transverse to the fiber direction
E_3	Elastic modulus of UD-ply in out-of-plane direction
E_a	Arrhenius activation energy
E_k	Fit parameter Bürger model
E_t	Stress and temperature dependent modulus fit parameter of Findley
f	Frequency
G	Shear modulus
g_i	Nonlinear stress dependent material parameter in Schapery integral
G_{12}	Shear modulus in 12-direction
G_{13}	Shear modulus in 13-direction
G_{23}	Interlaminar shear modulus in 23-direction
m	Stress and temperature dependent strain fit parameter of Findley
m'	Stress and temperature dependent strain fit parameter of Findley under reference stress
n	Stress independent exponential fit parameter of Findley
Q_{ij}	Stiffness matrix parameters
R	Molar gas constant
R_d	Design value of certain material parameter
t'	Shifted time to reference temperature
T_0	Reference temperature during the creep tests
T_g	Glass transition temperature
T	Temperature
t	Time

Chapter 1

Scope-Objectives

1-1 Introduction

Ageing of infrastructure leads to an increasing demand for new technologies and design solutions in bridge engineering. Design codes and regulations have become stricter in The Netherlands, while traffic intensity has grown a lot over the last decades. This development led to a high number of post-war bridges that are reaching their end-of-life. The ministry of infrastructure, Rijkswaterstaat, has a total of 176 fixed steel bridges and 107 bridges containing a steel deck. Due to the nature of steel and the increasing traffic intensity, these bridges are prone to fatigue failure. In 2008 dangerous fatigue problems such as small fractures in the steel deck were already detected in 25 of these bridges. In recent years it is noticed that these fatigue problems cannot only be found in the steel decks, but can also occur in the entire steel structural frame [25, 26]. Replacement of these bridges can be expensive and authorities have little budget for maintenance [27]. Replacing the steel decks with Fiber-Reinforced Polymer (FRP) sandwich deck panels is considered as a viable solution. FRP is gaining a lot of interest in the last decades due to their versatility, high strength-to-weight ratio, accelerated construction, resistance to fatigue and corrosion and low maintenance costs [28]. A lot of different examples of FRP bridges and buildings have already been realised, which demonstrates the potential of FRP. At this moment in the Netherlands FRP footbridges became a standard product, but also FRP traffic bridges and lock doors are increasingly selected for commercial projects. Where concrete and steel are too heavy, FRP can offer lightweight solutions, reducing structural risks and long-term traffic hindrance during the installation phase. Furthermore, FRP's form freedom enables a wide variety of possible designs of structural elements. The use of light-weight FRP sandwich deck panels as replacement of current steel decks could extend the current life-time of these bridges. However, the lack of design guidance results in additional effort and reduced efficiency in the realisation of FRP structures. Design guidance is called for by engineers: a uniform design standard will contribute to increased transparency, reliability and efficiency of FRP designs. The main challenge in design guidance is the fact that FRP is not just one material, but can be made by many different processes and with many different layups [29]. The guidance for FRP concerning pultruded profiles is most complete, but is still under development for structures containing multi-directional laminates created by the Vacuum Assisted Resin Transfer Moulding (VARTM) production method.

1-2 Problem statement

Although significant advancements have been made from research standpoints, FRP composites have not been accepted worldwide. This could be caused by the fact that the material costs are still relatively high, there is a lack of design guidelines, material specifications and procurement. In addition, compared to other materials FRP has a relatively short application period within civil engineering structures. A survey in which 38 infrastructure agencies participated, showed that the number of construction agencies that participated in FRP projects is quite low. At least 70% of the agencies that participated answered that they attempted difficult challenges working with FRP. These challenges specifically are: insufficient experience (68.0%), lack of design guidelines (60.0%) and lack of design workers (52.0%). Beside these challenges, most of the agencies indicated that they are not certain about the long-term performance and durability of installed FRP composites [30]. Civil engineering structures including bridges are designed to remain in service for more than 50 years, in which such structures are subjected to various combinations of mechanical and environmental loads. Polymeric-based composite materials are viscoelastic, this makes the time-dependent behaviour of such materials one of the most important factors for the analysis and design of FRP structural systems [31]. The viscoelastic nature of the polymer ensures that the material will creep in time under temperature or mechanical loading, which subsequently affects the long-term reliability and durability of FRP structural elements. Creep is described as the time-dependent deformation of materials subjected to an externally applied load over an extended period of time [32]. There is still limited amount of both theoretical and experimental data on this subject, in particular with reference to aramid and glass FRP's. This motivates the interest to study creep phenomena in FRP in more detail [33]. Several studies analysed the creep behaviour of simple coupons or simple pultruded profiles under tensile static stress [8, 34, 9, 14, 35]. However, the extrapolation of such data to structural elements is rarely made. In calculations creep is often accounted for by virtually reducing the stiffness of the material, based on certain reduction factors retrieved from experimental test results. Unfortunately, the amount of test results on ply level in current literature is scarce. Therefore, the creep behaviour of laminates consisting multiple plies placed in different directions misses experimental background. Especially the creep-recovery behaviour caused by variable traffic loading is something that finds almost no scientific background in literature at all. Some of the current structural codes assume that traffic loading will have negligible effects on the creep behaviour. Other codes suggest to take a certain fraction of the traffic load into account for creep deformation. However, how much of the variable traffic load truly should be accounted for in creep calculation seems to be unclear.

1-3 Research question

The problem statement described a global problem about the use of the relative new material FRP. It identifies the problems and insecurities of companies towards such a material. A lot of research on the properties of FRP is done, but there are still a lot to be analysed, especially when the long-term properties are concerned.

1-3-1 Main research question

How much creep deformation is build up in GFRP web core sandwich deck panels applied in road traffic bridges, due to traffic load?

Many steel bridge decks in the Netherlands are struggling with fatigue problems. Rijkswaterstaat is trying different solutions to overcome this problem [36]. Replacing the steel decks by GFRP web core sandwich decks can be seen as one of the most promising solutions [37]. Modern bridge decking systems must meet the criteria of ease to construction, lightweight, economically acceptable and a long service life. GFRP composite deck panels are used in the rehabilitation of existing bridges since the mid-1990s [38]. As stated before, there is limited amount of creep test data available, especially data on how the traffic load influences the accumulation of creep [33]. This study should give more insight on how this traffic load should be accounted for in long-term deformations caused by creep.

1-3-2 Sub-questions

How can the mechanism of creep (in FRP) best be explained and accounted for?

Creep phenomena can influence the structural reliability and durability of structural elements [33]. To make predictions on the long-term creep behaviour of FRP, the mechanism of creep must be fully understood. The virtual reduction of stiffness leads to higher deformations which still need to fulfil the SLS requirements.

How do temperature effects, moisture effects and physical ageing of the composite influence the long-term creep behaviour?

Fiber-Reinforced Polymers are used in various environments, thus external factors that may influence their creep behaviour must be understood. The most important factors include time, temperature, moisture content and physical ageing. Physical ageing relates to the stabilization behaviour of molecular chains over time [39].

Which models describe the creep behaviour of composites and how do these models differ from each other?

A number of empirical and analytical models have been developed to model and predict the creep strain response of polymers and composites under individual and combined influences of stress, moisture and temperature. These constitutive models are typically based on fundamental concepts such as energy methods, damage mechanics and the critical element concepts with residual stresses [40].

How could such analytical models be implemented in a numerical model including Finite Element Analysis (FEA) to determine long-term creep deformation?

FEA offers the opportunity to analyse complex problems. Interactions of parts of the structure in load transfer can effectively be taken into account. Deformations of FRP structures are both affected by shear and axial bending strains. Using FEA the effects of using the orthotropic and layered material together with the additional shear deformations are included directly within the FE simulation. This is very useful as FRP structures, such as sandwich deck panels, can be quite complex on meso-scale [41].

How do current standards treat creep compliance in the long-term deformation verifications (SLS) and how does the TS19101 (Eurocode proposal) deviate from it?

The most common standard used in the Netherlands regarding FRP structures is the CUR96 design recommendation, which takes the creep into account by the use of conversion factors [2]. However, a technical specification (TS19101) is currently developed by the European technical committee CEN-TC250. This committee is responsible for the development of structural codes in Europe. The TS19101 takes creep into account by a formula which reduces the stiffness properties with a time-dependent creep coefficient based on FRP creep tests [42]. The creep coefficient could be seen as the inverse of the conversion factors used in current design recommendations [43]. However, how the background of these factors differs quite from each other.

1-4 Aim and objectives

The overall aim of this thesis is to determine the influence that variable traffic loading has on the creep accumulation in Glass Fiber-Reinforced Polymer web core sandwich deck panels. Based on experimental work and the use of a numerical model, a long-term creep prediction should be made. Given this aim, several objectives and tasks could be defined. These are listed below.

- Literature review about the scientific approaches on predicting long-term creep behaviour
- Literature review on results retrieved from state of the art FRP creep experiments
- Create a state of the art numerical model that has implemented these scientific long-term creep predictors based on experimental work
- Determine how much of the traffic load needs to be accounted for in creep accumulation
- Compare long-term deformation results from the numerical model with results based on long-term deformation calculations prescribed by the TS19101

1-5 Research method

Both analytical formulas and experimental results retrieved from literature are used to formulate curve fits that predict the long-term viscoelastic creep behaviour of FRP. An extensive literature research will contribute to the knowledge that is needed for describing the viscoelastic creep behaviour of FRP in more detail. The literature review will be focused on the current analytical formulas that can predict long-term creep behaviour of FRP. Experimental results from literature will be used to complete the found formulas with the appropriate parameters to describe the behaviour of GFRP laminated sandwich deck panels accurately. No experimental work will be done during this thesis, thus all the parameters used in the numerical model are based on tests found in current literature.

To predict the long-term viscoelastic deformation, a numerical model containing the use of Finite Element Analysis (FEA) will be created. The numerical model should incorporate all the findings from literature and implement the creep predictors with the appropriate fit parameters retrieved from existing experimental results in literature. The numerical model should be based on experimental work done on UD-plies, so that the model can be used for a various range of multi-directional laminates applied in different design scenarios.

Finally a comparison must be made between the long-term deformation, caused by creep retrieved from the numerical model and the results from the long-term creep deformation calculated by using the TS19101 procedure. Based on the differences between these results a recommendation should be given for engineers and future researchers concerning the creep behaviour of FRP under variable traffic loading.

Chapter 2

Literature Study

2-1 Creep behaviour in general

To define how creep works there needs to be an investigation on what creep exactly is and how it behaves in general. Each material will behaves differently under creep, because it is caused by different mechanisms on microscopic scale. This section elaborates on the background of creep in general and the multiple mechanisms there are that can cause a material to creep.

2-1-1 Concept of creep

Creep is the time-dependent deformation of a material subjected to an applied load over an extended period of time [32]. Creep can lead to fracture, partly because the material is weakening mechanically and partly because the true stress over the cross-section of the element increases as the cross-sectional area decreases during the creep process [1]. Figure 2-1 shows the results of a generalized uniaxial creep test in which a specimen is subjected to a constant stress σ_0 over the cross section. From the diagram it can be seen that the specimen momentarily gets an initial strain ϵ_0, which can be build up from both an elastic and plastic strain. Under a constant stress this strain develops in time, which is a phenomenon referred to as **creep**. E. Andrade was the first to identify and study this creep behaviour in metals and called it a viscous flow in metal. Andrade indicated that a material loaded well below its elastic limit becomes proportional to time or becomes viscous in character [44]. He also classified creep into three stages: primary, secondary and tertiary creep stage. These creep stages can easily be recognised in Figure 2-1. The first stage is often characterized as the transient creep stage, which has a accelerating creep rate till some point in time when it starts to decelerate and starts the transition to its second creep stage a. In the second stage, the creep rate becomes more or less steady. This stage is followed by the third and last creep stage in which the creep rate clearly begins to accelerate again and may cause fracture, a phenomenon often referred to as creep rupture [45].

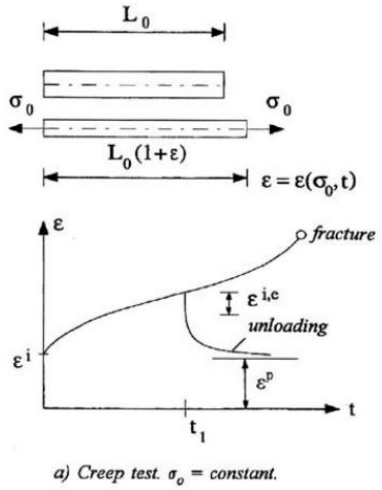

Figure 2-1: Creep development [1]

In most of the given literature, the equations follow Andrade's empirical concept that one may express as the variation of strain over time given by Eq. (2-1). Many of the proposed equations in literature have similar structure containing an initial elastic strain part and a transient creep part. The transient creep part is often calculated by multiplying a material constant by time containing another exponential material parameter.

$$\varepsilon(t) = \varepsilon_0(1 + \beta t^{\frac{1}{3}})e^{\kappa t} \tag{2-1}$$

Creep curves are stress and temperature dependent, and thus the three main parameters that determine the creep rate are: time, temperature and stress. Eq. (2-2) gives the relation between these phenomena with their conventional symbols, where f simply represents a certain yet unknown function of the three input variables taht should give the resulting strain output.

$$\dot{\varepsilon}(t) = f(\sigma, t, T) \tag{2-2}$$

In this equation $\dot{\varepsilon}(t)$ represents the time-dependent strain rate, σ is the applied stress, t is the time and T is the given service temperature. Creep can occur in any material due to different microscopical mechanisms. These mechanisms can roughly be classified into two different creep mechanism groups. These groups are: **diffusion creep** and **dislocation creep**. Both these mechanisms and their sub-mechanisms are explained in Appendix A.

2-1-2 Creep damage and creep fracture

As creep continues to its tertiary stage, damage accumulates. It takes the form of voids or internal cracks that slowly expand and link, eating away the cross-section and causing stress to rise. Voids arise on grain boundaries that lie perpendicular to the tensile stress. These are the boundaries to which atoms diffuse to give diffusional creep, coming from the boundaries that lie more nearly parallel to the stress. If the tensile boundaries have voids on them, they act as sources of atoms too and therefore these voids will grow. These voids cannot support load, which lead to an increase in stress on the remaining intact bits of the boundary, making the voids grow more quickly until the voids snap to link with each other. Reducing the area of the cross section subsequently increases the stress level in the material, which can be identified as the tertiary creep stage Figure 2-1 [3].

2-1-3 Creep mechanics

Creep mechanics is a part of a branch called continuum mechanics, which comprises the modelling of elasticity, plasticity, viscoelasticity and viscoplasticity in materials. Continuum mechanics is concerned with the mechanical behaviour of solids and fluids on macroscopic scale [46]. It is a special branch of physics in which matter regardless of phase or structure, is treated by the same theory until the special macroscopic properties are described through constitutive equations [1]. The physical laws used in the calculation of the stresses and displacements should be independent of the position and orientation of the observer. Therefore, the equations of physical laws are vector functions and tensor functions, since these kind of functions transform from one coordinate system to another in such a way that the vector or tensor equations hold in all different coordinate systems [46]. Creep mechanics involves the study about the constitutive part of continuum mechanics. In pure elastic materials the constitutive variables are constant in time. However, in viscoelastic materials this is not the case. To see how creep evolves in structural elements, use could be made of Finite Element computer Models (FEM). FEM makes use of the fast calculation time that computers offer us to calculate difficult problems within the world of continuum mechanics. By adjusting the constitutive relations, based on experimental creep behaviour, the long-term properties and results can be evaluated [46]. These constitutive relations make up the relation between calculated stresses and strains or forces and deformations. To account for the creep behaviour in these constitutive relations, several viscoelastic models can be used for time-dependent material description. The two models on the right in Figure 2-2 are a representation of linearly viscoelastic materials and are often used to model the material behaviour of polymers. Polymers can be divided into two groups: thermoplastic and thermosetting polymers. Thermoplastics have a fluid-like response similar to the Maxwell fluid from Figure 2-2 and thermoset plastics have a viscoelastic solid similar to the Kelvin bar from Figure 2-2 [1]. The Kelvin solid is mechanically described by a parallel system of a Newtonian damper and a Hookean spring. The Maxwell fluid is mechanically described by a system in series consisting of both a Hookean spring and a Newtonian damper. Solving the equation of motion results in a viscoelastic constitutive relation between stresses and strains.

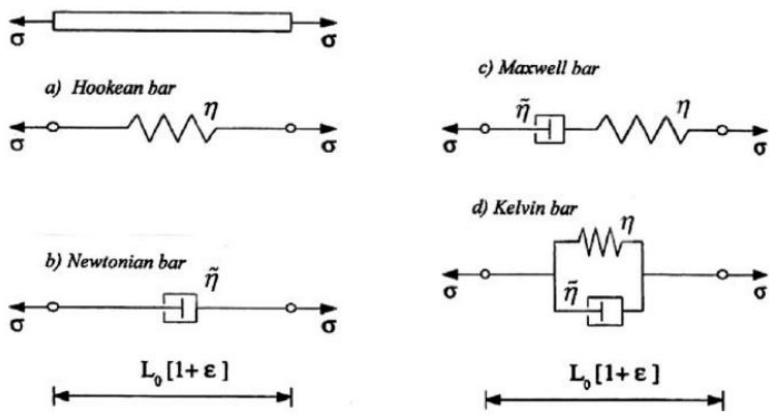

Figure 2-2: Viscoelastic mechanical models [1]

These Maxwell fluid and Kelvin solid mechanical representations are of the most simplest form for the description of viscoelastic behaviour. However, in literature they are often combined to describe the viscoelastic behaviour more accurately. Section 2-3-2 elaborates more on these and other material behaviour descriptions.

2-2 Creep behaviour of FRP

Polymeric-based composite materials are viscoelastic (Section 2-1-1), this makes the time-dependent behaviour of such materials one of the important factors in the analysis and design of FRP structural systems. The big difference in creep behaviour of composites compared to steel, concrete and regular plastics is due to the structure of the composite. The stiffness properties for such classic isotropic materials can be found in the form of an elastic modulus E, the shear modulus G and the Poisson's ratio ν. As explained in Section 2-1-3, the viscoelastic description of the materials is described in the constitutive relationship where the *time-dependent* stiffness properties provide the relationship between stresses and strains. A composite is build up of multiple layers that together create the layup of a so-called laminate. Each layer in this layup is called a ply which can have different properties depending on how the ply is produced. The amount of fibers and the direction of the fibers are mainly responsible for the mechanical properties such as the stiffness and strength of the ply. The general convention of each ply for naming the material properties in composites is represented by Figure 2-3.

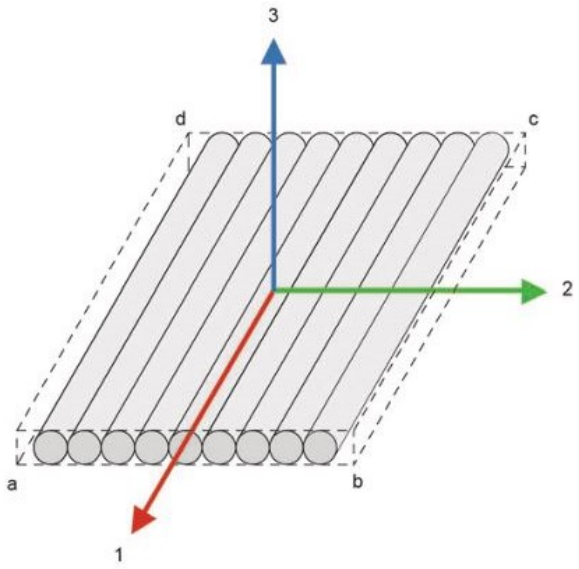

Figure 2-3: Convention for naming the material properties of the ply [2]

The stiffness of composites unidirectional (UD) lamina in 3D can be described by the elastic moduli in three different orthotropic directions (E_1, E_2 and E_3). The same holds up for the shear moduli of the plies, which can be divided into the in-plane shear moduli (G_{12} and G_{13}) and the interlaminar shear modulus (G_{23}). The relation between longitudinal and transverse elongation-contraction is described by three different Poisson's ratio's in each direction (ν_{12}, ν_{13} and ν_{23}). Due to the variety in properties in different directions, it can be an expensive and tedious process to determine all the material properties of a GFRP laminate. The combination of plies with different properties and orientations will result in a certain laminate behaviour as a whole. Classical Laminate Theory (CLT) allows to find the properties of a laminate consisting of multiple different plies or ply-orientations. The general convention for laminates differs slightly from the ply convention, Figure 2-4 shows this convention and how the local coordinate systems of each ply could be implemented.

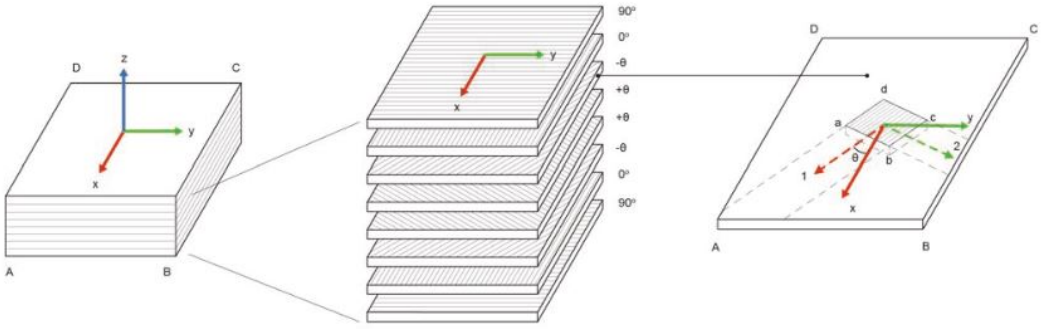

Figure 2-4: Convention for naming the material properties of the laminate [2]

Since a large number of laminates can be made using multiple ply orientations with different material properties, a method is searched for that predicts the long-term viscoelastic behaviour of a variety of laminates with possible different layups. In short, to model the behaviour of the laminate, the multiple stiffness properties of each ply listed below need to be known [14].

- The behaviour along the fiber direction (E_1)
- The behaviour transverse to the fiber direction (E_2, E_3)
- The shear behaviour (G_{12}, G_{G13} and G_{23})

Due to the viscoelasticity of each ply, the laminate can also be characterised as a viscoelastic material. However, plies that are not oriented in the direction in which the biggest stresses occur will be more susceptible to creep. Therefore, the stresses in each layer change over time and the behaviour of the composite depends on the combination of creep and relaxation. This phenomenon is also referred to as delayed elasticity in the plies [14]. In this section the behaviour of both base materials and the combination of them in one composite will be analysed. Also some models for the prediction of the creep behaviour and the time-dependent strain, which are often used for composites and plastics, are presented.

2-2-1 Creep behaviour of base materials

As described in Section 2-2, FRP composites are created by combining fibers with a polymer-based matrix to form a composite material. Each layer of fibers in that laminate is what is called a ply. In composite materials, one may identify the resin and the interface between the fiber and the resin as the elements which mainly influence the time-dependent behaviour. However, when organic fibers are used, the variation of fiber properties with time is also a factor to be considered in the prediction of the long-term behaviour of the composite [40]. These organic fibers are not considered within the scope of this study.

Polymers and their creep behaviour

The characterization of the long-term performance of FRP composites is important, because of the viscoelastic behaviour of the polymer matrix [47]. Creep in crystalline materials, explained in Section 2-1, is closely related to diffusion. This also holds for polymers, but because they are partly

or wholly amorphous, diffusion is controlled by free volume. When a molecule contains enough thermal energy it can jump into that free volume within the material. This diffusion could be driven by thermal energy, but also by a stress gradient. The free volume increases with temperature and it does so rapidly near the glass transition temperature (T_g). This is the temperature at which the weak inter-chain bonds between the long polymer molecule chains start to melt. In contrast to crystalline solids, which have a well defined melting point, polymer bonding is weaker and more diffusive. Figure 2-5 (a) shows the temperature dependence of the Young's modulus of thermoplastics with amorphous and semi-crystalline structures and Figure 2-5 (b) shows the the temperature-dependence of the Young's modulus of both elastomers and thermosets.

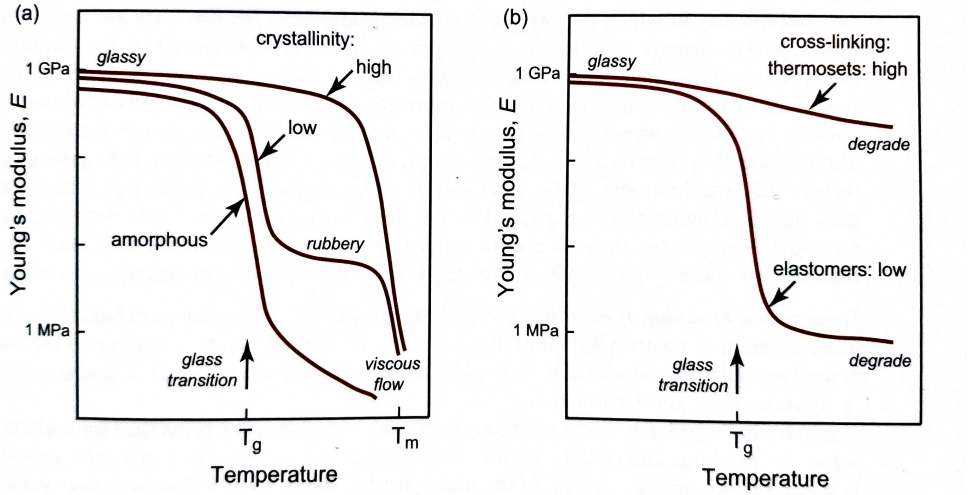

Figure 2-5: Schematic temperature-dependence of Young's modulus [3]

Approaching this T_g creates more open space in the amorphous structure of the polymer, which results in an increasing creep strain rate. Usually the T_g of polymers is relatively low and can be found between 50-150 °C [3]. Although the creep strain rate is closely related to the the glass transition temperature of a material, polymers still show a clear dependence on time and temperature below this T_g [4]. Unlike creep in metals, creep in polymers is recoverable at low strains when the applied load is removed. Eq. (2-3) gives a nonlinear relation between the input stress and the output strain. The **creep compliance** $D(\sigma, t, T)$ from Eq. (2-3) provides the direct relation between the input stress and the time, stress and temperature dependent strain. It could be seen as the inverse of a time-, temperature and stress dependent elastic modulus. The function that describes this creep compliance could be determined by using analytical formulas from literature. Experimental results should provide the correct coefficients or parameters within these formulas.

$$\varepsilon(\sigma, t, T) = \sigma[D(\sigma, t, T)] \tag{2-3}$$

Fibers and their creep behaviour

Due to their low cost, relative high tensile strength, impact and chemical resistance, **glass fibers** are used extensively in commercial civil applications. The three glass fibers commonly used in composites

are E-glass, S-2 glass and quartz. From which E-glass is the most common and least expensive. Some of the mechanical properties are given in Table 2-1.

Properties of different type of glass fibers			
Glass fiber type	Tensile strength (MPa)	Young's modulus (GPa)	Elongation at failure (%)
E-glass	3500	70	4.7
S-2 glass	4500	87	5.6
Quartz	3400	70	5.0

Table 2-1: Overview properties of glass fibers

Like polymers, glass is an amorphous material, which means that the atoms are packed in a non-crystallographic way [3]. It consists of a silica (SiO_2) backbone with various oxide components to give specific compositions and properties. Glass fibers are made from silica, sand, limestone, boric, acid and minor amounts of other ingredients such as clay, coal and fluorspar [48]. These fibers have a relative high glass transition temperature of around 840 °C, which means that they will most likely show no viscoelastic behaviour in practical applications. This is in contrast with the applied polymer matrix, which has a glass transition temperature that is much lower. Due to the relative high strength, stiffness and glass transition temperature it could be assumed that the creep behaviour of the composite is mainly determined by the properties of the polymer. The very low viscoelastic behaviour of the fibers are considered to be negligible.

2-2-2 Creep behaviour of a FRP composite

Based on Section 2-2-1 it could be stated that in practical applications of FRP composites, the creep behaviour is predominantly determined by the properties of the polymeric matrix resin. Therefore, when both materials are combined into one composite, the properties of the composite depending on the polymer matrix are influenced by creep to a greater extend. Stresses perpendicular to the fiber direction and shear stresses will have a greater influence on the creep behaviour than the stresses along the fiber direction will have. The classical laminate theory (CLT) for laminated FRP composites can also be extended to describe this time-dependent behaviour for a multi-directional laminate. The basic orthotropic properties of a ply are based on experimental work and CLT can be used to find the overall behaviour of the laminate. The creep behaviour for the conditions of off-axis loading is then evaluated via the transformation relations similar to the ones used in evaluating the elastic properties. Analysing the creep behaviour of a composite under a constant stress is relatively simple, but if the stress distribution is changing due to stress transfer between the fibers and the matrix, the analysis becomes more complex and continuous re-evaluation of the current stress state is required to ensure strain compatibility [31]. Although numerical simulations based on CLT can possibly predict the time dependent creep behaviour in laminated composites accurately, the predictions for laminates with more than two directions in which fibers are oriented seem to obtain different experimental results [14]. Predictions for laminates with more than two fiber orientations have been accurate at short times, but have fallen well below the longer time experimental results obtained on specimens. The numerical procedure to obtain the time-dependent strains provided CLT, assumes that normals through the laminate remain straight an normal. When the fibers are present in at least three directions, the CLT assumptions imply that the fibers act as pinned trusses which form a vast network of triangular

truss elements. These triangular trusses are rigid and therefore the numerical predictions tend to approach an upper limit. This phenomenon is often referred to as the **fiber-truss effect** with the upper limit called the fiber truss limit. This limit can be obtained by assuming that the matrix properties completely relax and thereby forcing the elastic fibers to carry all the load. This fiber-truss effect ensures an increased stiffness and strength, which can be attributed to the presence of the fiber trusses imposed by three or more fibers and the assumptions of CLT. At the free edges these assumptions are not valid, yet for practical structures the region affected by the free edges is relatively small. It has been demonstrated that specimens with three or more fiber directions experience considerable less creep than laminates consisting of only two fiber orientations [49].

2-3 Creep prediction in FRP

As stated before, it is mainly the polymer resin that influences the time dependent viscoelastic behavior of the composite. It shows a clear dependency on time and temperature even well below its glass transition temperature T_g, which overlaps with the service temperature in which FRP structural elements are applied. Therefore, the mechanical behaviour of FRP composite systems are also dependent on both time and temperature [4]. Examples of these relations are shown by Aboudi et al., Sullivan, Gates and Miyano et al. [50, 51, 52]. A number of analytical models have been developed to model and predict the creep behaviour of polymers and composites under the combined influences of stress, temperature and moisture [32]. To support these analytical and empirical models and provide them with the appropriate material parameters, creep testing is needed. However, determining these long-term properties of FRP is not easy, because it requires a range of multiple tests over a longer period of time at different stress and temperature ranges. Since the molecular structure of the polymers changes over time, the physical ageing of the polymer should be taken into account as well. To predict this time-dependent behaviour, several accelerated testing methods have been developed. These methods are briefly explained in Section 2-3-1. These accelerated test methods support the use of the analytical and empirical models, as they could provide the right model parameters to the analytical description of the creep behaviour. The models that are most often used for predicting the long-term creep response of FRP laminates are: Findley's power law and the Boltzmann superposition principle (BSP), which have both semi-empirical and analytical basis. Other mechanical models, such as the Bürger model, are based on a more physical or phenomenological background. Such mechanical models are often created by combining Hookean springs and Newtonian dashpots, which both obey Hooke's law and Newton's law of viscosity respectively. In Section 2-1-3 these elements are explained in their most elementary combination.

2-3-1 Accelerated test methods

It seems obvious that experiments to determine the long-term properties of a material will take a lot of time. A lot of studies contain experimental work in which the researchers made use of long-term creep test results. However, different experimental models have been proposed to predict the long-term properties of polymers and fiber-reinforced polymers. With these models, the results based on relative short-term tests are extrapolated to predict possible deformations on the long-term. The tests make use of both the differences in behaviour under different temperature and stress inputs and shifting the corresponding output over time, which reduces the testing time significantly. Some methods make use

of dynamical loading and try to describe the time-dependent material behaviour through the complex modulus (damping) and the storage modulus (stiffness).

Time-Temperature Superposition Principle

One of the methods that could be used to obtain the viscoelastic properties of a FRP composite is the so-called time-temperature superposition principle (**TTSP**). This principle was developed around 1950 and is used extensively in research about the time-dependent behaviour of polymers [14]. The method was later adopted by Yeow et al. in the application on fiber-reinforced polymers [53]. The method is based on the assumption that the effects of temperature on the time-dependent behavior of a material is equivalent to a stretching or shrinking of real-time for temperatures above or below the reference temperature [31]. Thus, when plotted on a log-scale based graph, the individual creep curves at different temperatures can be shifted horizontally to obtain a continuous master creep curve. Figure 2-6 shows how this shifting of the curve graphically. However, as shown in this figure, elevated temperatures below T_g cannot be superimposed smoothly by only horizontal shifting. A much more smooth curve could be obtained by shifting the curve both vertically and horizontally as shown in Figure 2-6 (b). This vertical shifting is well known as the thermal correction based on the entropy elasticity at the temperature above T_g [4].

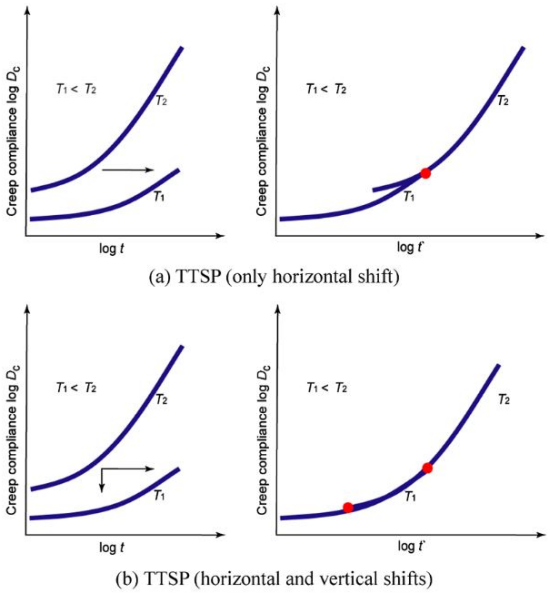

Figure 2-6: Construction of creep master curve according to TTSP [4]

This accelerated test method can predict the long-term behaviour quite accurately and the reason behind this relatively good performance can be found in the field of polymer kinetics. The creep movement of polymer chains increases, due to an increase in volume at higher temperatures [54]. Using the kinetic theory of polymers, which is only valid above T_g, the shift factors can be derived. Willams et al. applied the TTSP to a large number of polymers and empirically found the expression given in Eq. (2-4) and called it the WLF equation for the shift factor α_T.

$$log(a_T) = \frac{-C_1(T - T_0)}{C_2 + (T - T_0)} \tag{2-4}$$

In this equation both C_1 and C_2 are constants that could be determined from experimental tests. The parameter T_0 represents the reference temperature of the test data and the parameter T represents the temperature for which the creep master curve is created. If T_g is used as the reference temperature, the values for both the constants C_1 and C_2 are 17.44 and 51.6 respectively. However, this relation cannot be used for temperatures below T_g. A shift factor related to temperatures below T_g could be found with Eq. (2-5), which makes use of the Arrhenius activation energy (E_a).

$$log(a_T) = \frac{E_a}{2.303R}(\frac{1}{T} - \frac{1}{T_0}) \tag{2-5}$$

In this equation, E_a is the activation energy and R is the molar gas constant. Implementations of TTSP involve the use of a new time scale t', which is called the shifted time to reference temperature. The relation between time and this shifted time is given in Eq. (2-6).

$$t' = \frac{t}{a_T} \tag{2-6}$$

The shifted time can be implemented in analytical approaches such as Boltzmann's superposition principle and Schapery's integral procedure [14].

Time-Temperature-Stress Superposition Principle

The Time-Temperature-Stress Superposition Principle (**TTSSP**) has the same principle as TTSP, but is extended to predict the creep master curve on the applied stress level as well. TTSSP is based on the assumption that the effects of temperature and stress on the time-dependent behaviour of a material are equivalent to stretching or shrinking of the real-time for temperatures and stresses above or below the reference temperature and stress. Yen and Morris used TTSSP in tensile creep tests on glass and polyester composite sheet molding compound. Four stress levels per temperature were analysed. The stress levels were: eleven, twenty, thirty and thirty-six percent of the ultimate strength at given temperature level. All of these tests were done at temperatures of: 23 °, 40 °, 70 °and 100 °C. The results are used in the power law model of Findley (Section 2-3-2) and had an excellent agreement with a 1000 min creep test [55]. Other researches done by Brinson et al., Dillard et al., Gramoll et al. and Yen also came to good agreements between the modified predictive law of Findley and long-term creep results retrieved from testing as well [56, 57, 58, 59]. All these agreements led to the conclusion that using the power law model of Findley together with the modification based on TTSSP, produces reliable results for the prediction of the long-term performance of FRP composites [31]. Using Eq. (2-3), the relation between the time-temperature-stress dependent strain at a given stress state, a horizontal and vertical shift factor could be obtained and implemented in the power law of Findley. The shift factors α_v and α_h could be obtained through both Eq. (2-7) and Eq. (2-8) [55].

$$a_v = \frac{D_0(\sigma, T)}{D_0(\sigma_0, T_0)} \tag{2-7}$$

$$a_h = \frac{D_0(\sigma_0, T_0)D_t(\sigma, T)}{[D_0(\sigma, T)D_t(\sigma_0, T_0)]^{-1/n}} \tag{2-8}$$

In these equations the D_0 is the instantaneous creep compliance, which could be seen as the inverse of the initial elastic modulus of the composite. The D_t parameter is the transient creep compliance, which could be determined from a single creep test at a certain stress level and a certain temperature. These parameters could be used in analytical models, such as the already mentioned power law model of Findley to predict the creep behaviour of FRP composites on the long-term.

Frequency-Time Transformation Method

The accelerated testing techniques for long-term creep results discussed above are based on the use of elevated temperatures. However, Gibson et al. expressed their caution in using such techniques, because of the possible physical ageing of the material due to aggressive environmental conditions [5, 60]. Therefore, alternative techniques for characterizing the long-term properties of FRP composites have been developed. The Frequency Time Transformation Method (FTTM) is one of these techniques. This method, as described by Gibson et al., uses results from the frequency domain hysteresis loop (see Figure 2-7) measurements to develop an expression for the time-domain creep compliance [5].

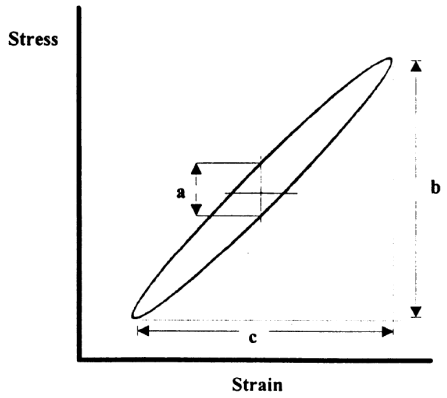

Figure 2-7: Hesteresis loop method for calculating the storage modulus [5]

The experimental data from these hysteresis loop is used to develop an expression for the complex modulus (in terms of a loss factor) and a storage modulus, which are a measure for the damping and stiffness within the material respectively. Eq. (2-9) shows how this compressive complex modulus could be determined.

$$E*(f) = E'(f) + iE''(f) = E'(f)(1 + i\eta(f)) \tag{2-9}$$

In this equation $E'(f)$ is the storage modulus, $E''(f)$ is the loss modulus, $\eta(f)$ is the loss factor and f is the frequency. The loss factor and the storage modulus could be determined from Figure 2-7, by using both Eq. (2-10) and Eq. (2-11).

$$\eta(f) = \frac{a}{b} \tag{2-10}$$

$$E'(f) = \frac{b}{c} \tag{2-11}$$

To transform from the frequency into the time domain, use is made of the complex compliance $D*(f)$ = $(1/E*(f))$. The time-dependent creep compliance could then be calculated using the inverse fast Fourier transform and numerical integration, given in Eq. (2-12).

$$D(t) = \int_0^t (F^{-1}[D*(f)])\, dt + D_0 \tag{2-12}$$

In this equation $D(t)$ is the time-dependent creep compliance, D_0 is the instantaneous creep compliance and F^{-1} is the inverse Fourier transform. Gibson and Kathawate performed tests on unidirectional laminates and chopped glass fiber and polyester sheet molding [5]. Data from these tests as well as the

frequency response function were imported to a computer program which calculated the corresponding loss factor $\eta(f)$ and storage modulus $E'(f)$. These values were used with the Zener model to form the time-dependent expression for the creep compliance, given in Eq. (2-13). The Zener model is a constitutive representation of a viscoelastic material and could be created by combining multiple Hooke springs and Newtonian dashpots together, see Section 2-1-3.

$$D(t) = \frac{1}{E_1}[1 - \frac{E_2}{E_1 + E_2} \exp(-\frac{E_1 E_2}{(E_1 + E_2)\mu} t)] \tag{2-13}$$

In this equation $D(t)$ is the time-dependent creep compliance, E_1 and E_2 are the elastic moduli in the direction of interest and μ is the dashpot viscosity [31, 5].

2-3-2 Analytical models

Next to the discussed accelerated test methods presented in Section 2-3-1, analytical models have been developed to describe the long-term creep behaviour of FRP composites. The models each have different backgrounds and are sometimes used for different purposes. However, each model still tries to provide a certain function for the creep compliance that could be used to find time-dependent strains based on input stresses. Findley's power law model is one of the most popular models used in literature, due to its simplicity. It tries to predict the time-dependent strain based on a constant stress state [61]. Other models, such as the Bürger model and the generalized Maxwell and Kelvin models are based on a varying combinations of Hooke's springs and Newtonian dashpots and therefore find more basis in physical laws than Findley's power law does [6]. Both the Boltzmann superposition principle and Schapery's integral procedure determine the final strain at time t based on a varying stress history input.

Findley's power law

The power law developed by Findley has become one of the most widely used analytical models to describe the viscoelastic behaviour of FRP composites under a constant stress. The general forms for both axial and shear strain are given in Eq. (2-14) and Eq. (2-15). The power law of Findley has a direct relation with Eq. (2-1), which gives the final strain in metals and was formulated by Andrade [44, 45].

$$\varepsilon(t) = \varepsilon_0 + mt^n \tag{2-14}$$

$$\gamma(t) = \gamma_0 + mt^n \tag{2-15}$$

In this equation the $\varepsilon(t)$ is the total time-dependent creep strain, ε_0 is the stress- and temperature-dependent initial elastic strain, m is a stress- and temperature dependent strain fit parameter, n is the stress independent material parameter and t is the time at which the strain is evaluated. Findley's power law can also be used in terms of creep compliance, which is an inverse of the elastic modulus at a given time. To obtain this time-dependent creep compliance, a similar relation could be used. This relation is given in Eq. (2-16).

$$D(t) = \frac{\varepsilon(t)}{\sigma} = D_0 + D_m t^n \tag{2-16}$$

In this relation the D_0 is the instantaneous creep compliance, or the inverse of the static elastic modulus at starting time. The parameter D_m is the fit parameter of the transient creep compliance, which can

be determined from creep tests and n is the same parameter as described before. The power law of Findley is used to develop an expression for the time-dependent modulus of a FRP composite system, given in Eq. (2-17) and Eq. (2-18) [31]. According to literature, the non-linear power law of Findley seems to predict the creep and recovery behaviour quite accurately [6].

$$E(t) = \frac{E_0 E_t}{E_t + E_0 t^n} \tag{2-17}$$

$$G(t) = \frac{G_0 G_t}{G_t + G_0 t^n} \tag{2-18}$$

In this equation E is the viscoelastic modulus in the direction of interest, E_0 is the initial elastic modulus independent of time and E_t is the modulus which characterizes only the time-dependent behaviour.

Bürger model for viscoelastic behaviour

In contrast to the given power law of Findley, the Bürger model has more physical basis and can be seen as a semi-empirical model instead of an empirical model. Weissman-Berman modelled creep deformation behaviour through a simple linear viscoelastic model which was used to develop the creep compliance function for an average sandwich beam material response [62]. The model that was used to predict this time-dependent response of the material was the Bürger model, given in Figure 2-8. The Bürger model is one of the possible combinations that could be made from Hookean springs and the Newtonian dashpots. It gives a more accurate representation of the viscoelastic behaviour of a fiber-reinforced polymer laminate than the basic mechanical models, presented in Figure 2-2. It is a result of combining the Kelvin solid and Maxwell fluid into one viscoelastic model, which displays all aspects of viscoelasticity such as instantaneous elastic strain, steady state creep, decelerating creep, recovery and stress relaxation [6].

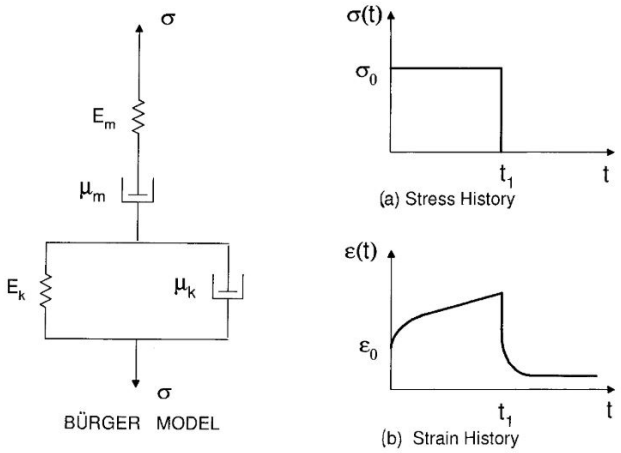

Figure 2-8: Schematic representation of the Bürger model [6]

The relation between the load (stress) and the displacement (strain) is achieved through the creep compliance function $D(t)$, given in Eq. (2-19).

$$D(t) = \frac{1}{E_0} + \frac{t}{\mu_m} + \frac{1}{E_k}(1 - e^{-t/\tau}) \tag{2-19}$$

The four constants E_0, E_k, μ_m and τ can be gained from creep experiments. E_0 is a constant that governs the magnitude of static deflection, E_k is a measure of the elastic modulus in the primary creep range, μ_m governs the rate of steady state creep and τ is a retardation constant which determines the rate of transition from primary creep into steady state creep. The creep displacements vary over time and are derived from the elastic problem by replacing the elastic modulus with the inverse of the creep compliance. This means that the final axial strain in the face sheets could be determined by Eq. (2-20) and the final shear strain can be determined by Eq. (2-21).

$$\varepsilon(t) = \sigma D(t) \tag{2-20}$$

$$\gamma(t) = \tau D(t) \tag{2-21}$$

Using Bürger's model the application of Boltzmann's superposition principle is also valid. For a step-input stress function it means that when the load gets removed, an initial decrease of the instantaneous elastic strain will occur followed by a slow decrease recovery strain. The stress input can be modelled by using the Heaviside step function under the assumption that the superposition principle is valid. The removal of the stress can be treated as a negative stress with the same magnitude of the applied stress that is removed. This is illustrated in Figure 2-11.

Generalized viscoelastic models

As indicated in Section 2-1-3, a single Maxwell or Kelvin model could describe the behaviour of a polymer. However, these elements are limited in representing the actual stress-strain response of polymers. A more realistic model can be developed by considering a series of such elements. If the Maxwell model is considered, the simple combination of the spring and the dashpot could be repeated N times to form a so-called **Generalized Maxwell model**. One extra spring element is added to describe the elastic behaviour of the material. Adding the extra spring results in a model known as the Wiechert model, Figure 2-9(a). The solution for the relaxation modulus could be obtained by solving the corresponding N^{th} order differential equation or by solving the system of N first order differential equations. This solution for the relaxation modulus is given by Eq. (2-22).

$$E(t) = \sum_{i=1}^{N} E_i e^{-t/\tau_i} + E_\infty \tag{2-22}$$

This type of representation is often referred to as a **Prony series** and such an exponential expansion is often used to describe the relaxation modulus of a viscoelastic material even without reference to the corresponding mechanical model [7].

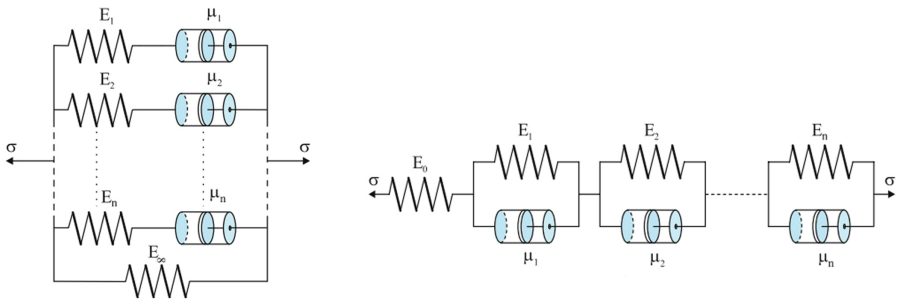

(a) Wiechert model **(b)** Generalized Voigt-Kelvin model

Figure 2-9: Schematic representation of the generalized models [7]

The **Generalized Kelvin model** is composed of N Kelvin elements in series. The model has no instantaneous elasticity and therefore an extra spring is added to the series resulting in the so-called Generalized Voigt-Kelvin model, shown in Figure 2-9(b). The procedure for finding the creep compliance belonging to this model is the same as with the Generalized Maxwell model. The creep compliance that could be found in relation to the given Generalized Voigt-Kelvin model is given in Eq. (2-23).

$$D(t) = \frac{1}{E_0} + \sum_{i=1}^{N} \frac{1}{E_i}(1e^{-t/\tau_i}) \tag{2-23}$$

Due to the the forms of the differential equations and ease of the solution, Maxwell elements in parallel are typically used for the relaxation behaviour and Kelvin elements in series are used for describing the creep behaviour of polymers [7].

Boltzmann Superposition Principle

The Boltzmann Superposition Principle (BSP) gives a relation between the creep strain and the stress for a certain time and can be considered to be a fundamental theorem in the field of viscoelasticity [63]. It states that the sum of time-dependent strain outputs resulting from each component of stress input is the same as the strain output resulting from the combined stress inputs. This statement is mathematically described by Eq. (2-24), where D_0 is the instantaneous creep compliance and D_t is the transient creep compliance. The creep compliance function used in BSP can be described by one of the analytical models discussed in the previously described paragraphs of this section.

$$\varepsilon(t) = D_0\sigma + \int_0^t D_t(t-\tau)\frac{d\sigma(\tau)}{d\tau}\,d\tau \tag{2-24}$$

The creep compliance is independent of the stress if it is assumed that the material is linear viscoelastic. BSP is not applicable for nonlinear viscoelastic material behaviour. Leaderman, Findley and Lai eventually developed a modified version of the Boltzmann principle to account for such nonlinearities [31, 64]. However, Schapery developed a much easier procedure than the modified version proposed by these scientists. In addition, the procedure prescribed by Schapery also found much better agreement with experimental data. In the case of a step-wise constant stress input on a certain specimen, that is placed on the specimen at $t = 0$ and removed on $t = t_1$, the subsequent strain can be considered to arise from the superimposed effect of $+\sigma$ applied at $t = 0$ and a superimposed stress of $-\sigma$ applied at time $t = t_1$. At time t_1 the rate of change deformation changes sign and the body slowly returns to its original state [63]. The remaining deformation or strain after unloading at time t can be calculated with Eq. (2-24).

$$\varepsilon(t) = \sigma[D(t) - D(t-t_1)] \tag{2-25}$$

Such a given state of constant stress for a certain amount of time could be modelled with a so-called Heaviside function. The Heaviside function of a constant stress is given in Figure 2-10 (a). The related strain output corresponding to the step-wise stress input is given in Figure 2-10 (b).

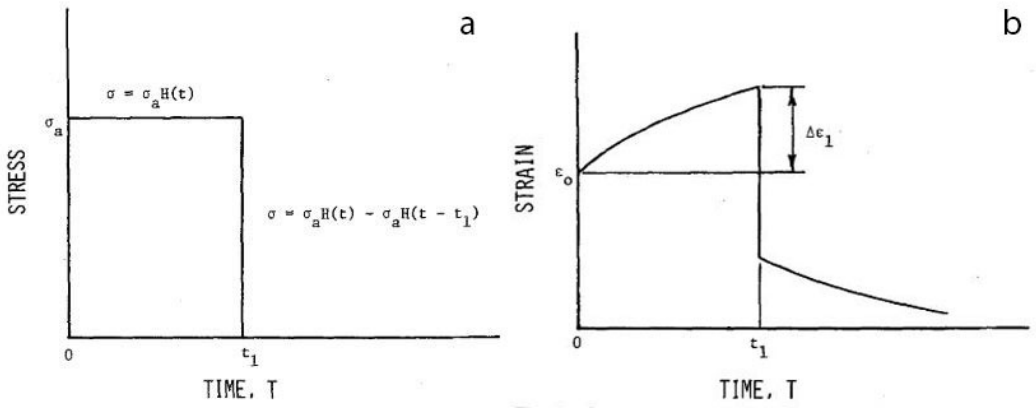

Figure 2-10: Creep-recovery stress history corresponding strain Boltzmann [8]

Modelling a Heaviside function could be difficult when using the numerical approaches such as FEA. Modelling how the recovery will look like cannot be based on unloading, because calculation will simply give the trivial zero state equilibrium of a structure. Therefore, the creep-recovery stress input can be represented by the superposition of two Heavisidal step inputs [7]. The stress inputs of such a single superposition is given in Figure 2-11.

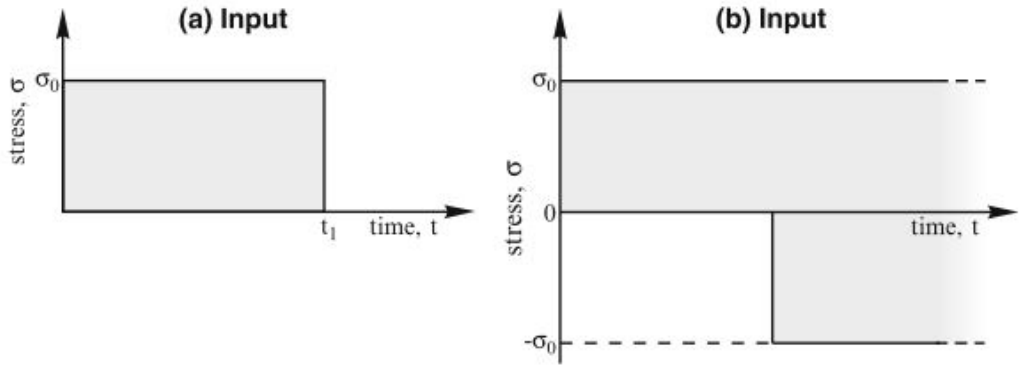

Figure 2-11: Creep-recovery stress input (a), which can be represented by the superposition of two step inputs (b) [7]

Following Boltzmann's superposition principle, the strain output could be modelled according to multiple load and recovery cycles [65]. Implementing the power law of Findley as the creep compliance part within BSP results in the constitutive relation between the time-dependent train and the input stress that is given in Eq. (2-26).

$$\varepsilon(t) = \sigma \cdot \sum_{i=0}^{N} (-1)^i \cdot [D_0 + D_m(\sigma) \cdot (t - t_i)^n] \tag{2-26}$$

Multiplying the creep compliances with the stress will lead to the summation of the time-dependent strains, as BSP states that this is possible. This will result in the relation between all the smaller

additive strains with the final overall strain and can mathematically described by Eq. (2-27).

$$\varepsilon(t) = \sum_{i=0}^{N} (-1)^i [\varepsilon_0 + m \cdot (t - t_i)^n] \tag{2-27}$$

These strains can be extrapolated to deformation by simply using Euler beam theory, Timoshenko beam theory or Finite Element Analysis. The resulting time-dependent relation that could then be found for the final deformation based on certain input loading scenarios could then mathematically described by Eq. (2-28), which can be used to find the final deformation as consequence of multiple creep and recovery cycles.

$$\sum_{i=0}^{N} (-1)^i [\delta_0 + \delta_m \cdot (t - t_i)^n] \tag{2-28}$$

In this equation the variable δ_0 is the instantaneous deformation and δ_m could be determined from tests, but can also be calculated if the correct parameters are used in Eq. (2-26) for stiffness reduction. Then Eq. (2-29) could be used to find the final deformation and the parameter δ_t corresponds to the viscoelastic creep increment due to the decrease in stiffness according to Findley.

$$\sum_{i=0}^{N} (-1)^i [\delta_0 + \delta_t] \tag{2-29}$$

Schapery single integral procedure

The Schapery integral is a nonlinear viscoealstic equation that can be used for the study of time-dependent behaviour of FRP composites. In the case of uniaxial loading, the constitutive equation for the multi-stress state is given by Eq. (2-30). In this equation D_0 is the instantaneous creep compliance and D_t is the time-dependent transient creep compliance. All the g_i parameters are nonlinear material parameters, ψ is a time parameter given by Eq. (2-31) and Eq. (2-32) in which the a_σ is the shift factor for the reducing time parameter. This reducing time parameter is governed by the physical ageing of the material. Schapery's integral could be seen as an extension of Boltzmann's superposition principle, but Schapery simply added nonlinear terms to the equation provided by BSP and given in Eq. (2-24). When the applied stress is small the material behaves more or less linearly, which means the parameters g_i and a_σ are equal to one [31, 66]. In such a case, the Schapery's integral transforms into the Boltzmann integral for linear superposition.

$$\varepsilon(t) = g_0 D_0 \sigma + g_1 \int_0^t D_t(\psi - \psi') \frac{d}{d\tau} [g_2 \sigma(\tau)] \, d\tau \tag{2-30}$$

$$\psi = \int_0^t \frac{dt'}{a_\sigma} \tag{2-31}$$

$$\psi = \int_0^\tau \frac{d\tau'}{a_\sigma} \tag{2-32}$$

The nonlinear stress-dependent material properties g_i and a_σ can be determined from creep and recovery data retrieved at different stress levels, temperatures and humid boundary conditions. The transient creep compliance could be modelled with the help of Findley's power law or other mechanical models. If a constant state of stress is applied to the viscoelastic material again, the integral gets

removed from the equation by the Heaviside function. The same principle holds up as with the Boltzmann integral, only with the Schapery integral the nonlinear parameters will be left. The result for the time-, stress- and temperature dependent strain in this case can be described by Eq. (2-33).

$$\varepsilon(t) = \sigma[g_0 D_0 + \frac{g_1 g_2}{a_\sigma^n} m t^n] \tag{2-33}$$

The step-wise constant stress state can modelled with a Heaviside function, given in Figure 2-10 (a) and the strain that results from such a stress input is given in Figure 2-10 (b). However, the strain outputs could be shifted in this diagram due to nonlinear behaviour. As with the superposition principle of Boltzmann, Schapery's procedure allows for modelling of the recovery strain as well. How this recovery strain could be calculated according to Schapery is given in Eq. (2-34).

$$\varepsilon_{rec} = \frac{\Delta\varepsilon_1}{g_1}[(1 + a_\sigma \lambda)^n - (a_\sigma \lambda)^n] \tag{2-34}$$

In Eq. (2-34) the $\Delta\varepsilon_1$ represents the creep strain of the load cycle. The new introduced variable λ shifts the time of the recovery cycle to the time at which the load is removed, in this case represented by t_1. Both the parameters $\Delta\varepsilon_1$ and λ could be calculated according to Eq. (2-35) and Eq. (2-36) respectively.

$$\Delta\varepsilon_1 = [C\frac{g_1 g_2}{a_\sigma} t^n] \tag{2-35}$$

$$\lambda = \frac{t - t_1}{t_1} \tag{2-36}$$

2-4 Internal and external influences

From both the empirical and analytical models together with the reviewed experimental test results, it becomes clear that creep is highly influenced by several internal and external factors. The most important environmental and material related parameters that could influence the creep behaviour of a material are explained in the following subsections. The description and implementation of these factors within the selected analytical model(s) will be evaluated as well.

2-4-1 Stress level

In a research done by Najafabadi et al. it was observed that by increasing the stress ratios, the creep strain rates increased as well [67]. Moreover, the creep ratios decreased by increasing the stresses from 20% to 30% of the ultimate strength and remain constant for higher stress levels. A study done by Ascione et al. showed that by increasing the stress from 25% of the ultimate strength (f_u) to 75% of f_u results in a negligible strain ratio ($\frac{\Delta\varepsilon}{\varepsilon_0}$) increase of 0.58%. The reason for the slight difference observed in creep ratios at different stress levels between FRP laminates may be due to the different mechanical characteristics, cross section geometries and manufacturing processes. However in general, it could be stated that the creep ratios do not change significantly by changing the value of applied stress higher than $0.2 f_u$. Najafabadi observed from tests that in GFRP bars the amount of creep strain increases by raising the stress ratio, while the creep ratio converges to an almost constant value reaching stress ratios more than $0.3 f_u$ and less than $0.6 f_u$ [67]. However, the power law of Findley [Eq. (2-14)] is

non-linear with respect to stress level [16]. The stress-dependent terms ε_0 and m can be expressed in hyperbolic form. These relations are given in Eq. (2-37) and Eq. (2-38) [31].

$$\varepsilon_0(\sigma, T) = \varepsilon_0' \, sinh(\frac{\sigma}{\sigma_0}) = \sum_{i=1}^{n} \varepsilon_0'(\frac{\sigma}{\sigma_0})^i \tag{2-37}$$

$$m(\sigma, T) = m' \, sinh(\frac{\sigma}{\sigma_t}) = \sum_{i=1}^{n} m_i'(\frac{\sigma}{\sigma_0})^i \tag{2-38}$$

In these equations the ε_0' represents the initial strain during the experimental test and m' represents the transient strain retrieved by fitting the power law on experimental results at a given reference stress σ_0. The parameter σ represents the applied stress level for which the creep strain is calculated. Implementing these findings in the power law of Findley, shown in Eq. (2-14), results in the relation for the final creep strain described by Eq. (2-39) [16].

$$\varepsilon(\sigma, t) = \varepsilon_0' \, sinh(\frac{\sigma}{\sigma_0}) + m' \, sinh(\frac{\sigma}{\sigma_0}) t^n \tag{2-39}$$

Using a Taylor series expansion for both parameters given in Eq. (2-37) and Eq. (2-38) and considering only the first order approximation will result in a simplified relation without the hyperbolic sine function. This relation is given in Eq. (2-40).

$$\varepsilon(\sigma, t) = \varepsilon_0' \frac{\sigma}{\sigma_0} + m' \frac{\sigma}{\sigma_0} t^n \tag{2-40}$$

This approximation of the time- and stress dependent strain is confirmed to be a good predictor without a lack of accuracy by many researches done by Sá et al., Bottoni et al., Nabafajadi et al., Scott D. and Zureick A. and other researchers [13, 16, 67, 68].

M. Sá proposed another modification to the power law of Findley, which originates from shifting the creep curve based on TTSP (Section 2-3-1) test methods [13]. TTSP can be used to extrapolate short-term test data to longer-term data, considering the range of load levels performed. Such a methodology allows to conclude that the viscoelastic response of the laminated material to high load levels is comparable to the response to lower stress levels, but with a higher duration. In this way Findley's power law (Eq. (2-14)) can be modified by introducing its transient creep component into a superposition principle, which is expressed in the stress-dependent form given in Eq. (2-41).

$$\varepsilon(\sigma, t) = a_V \cdot [\varepsilon_0(\sigma_0) + \varepsilon_t(\sigma_0) \cdot (\frac{t}{a_H})^n] \tag{2-41}$$

The parameters a_v and a_h have the meaning of shifting factors and can both be defined for a reference stress σ_0. Both these shifting factors are given by Eq. (2-42) and Eq. (2-43) [13]. These shift factors are comparable to some of the nonlinear parameters used in the Schapery integral method, which can also be found by experimental work based on TTSP or TTSSP.

$$a_V = \frac{\varepsilon_0(\sigma)}{\varepsilon_0(\sigma_0)} \tag{2-42}$$

$$a_H = [\frac{\varepsilon_0(\sigma_0) \cdot \varepsilon_t(\sigma)}{\varepsilon_0(\sigma) \cdot \varepsilon_t(\sigma_0)}]^{-1/n} \tag{2-43}$$

2-4-2 Temperature

A wide range of properties depends on the temperature, most of the times properties like the density or the elastic modulus are linearly related to the increase of temperature. However, the creep rate is quite unique, because the creep rate increases exponentially with temperature [3]. Especially, when it comes to the properties of the matrix resin, because of their low glass transition temperature T_g (Section 2-2-1). Short-term high temperatures can cure the resin and even increase its T_g, which increases other mechanical properties of the resin. However, long-term exposure to elevated temperatures will soften the matrix resin which leads to a fast degradation in material properties. Typical damages from exposure to these elevated temperatures can be gloss or color defects and the presence of blistering or air bubbles within the matrix. Relatively low differences in temperatures can cause residual stresses in the material microstructure, caused by the big difference in the thermal expansion coefficient between the matrix and the fibers. However, unless in severe cold, these microcracks will not occur as a result of low service temperature. Mainly microcracking is caused by multiple cycles of temperature differences. Microcracks in the structure of the matrix have a great contribution in the reduction of stiffness of the material. Increased temperatures affect the initial stiffness of the matrix of the laminate, but it will also affect the long-term creep rate. As explained before, these properties are used in the time-temperature superposition principle (TTSP) to predict the long-term behaviour at a certain reference temperature. At high temperatures close to or above the T_g the viscoelastic behaviour becomes non-linear, because the material softens. TTSP gets more scatter in the results when it comes to these temperatures, but is still used up to T_g + 100 °C. Analytical methods, like a modified version of the power law or the Schapery integral procedure, account for these temperature differences in several ways. In Schapery's integral procedure the differences in temperature are accounted for by the use of the shift factor a_σ, which can be determined from tests based on TTSP [14]. Using Findley's power law (Eq. (2-14)), both parameters of Findley are assumed to be affected by the differences in temperature. Temperature affects both the elastic and viscoelastic behaviour of FRPs for wide ranges of temperatures. For temperature well below T_g of the material, the elastic properties are not expected to be significantly influenced by the temperature. However, the parameters m and n are expected to be dependent on temperature changes within the range below T_g. Their variations reflect temperature activated physical processes affecting the polymer chain mobility. Such temperature dependent processes are frequently well described by the Arrhenius equation given in Eq. (2-44).

$$m(T) = A_m \exp(-\frac{E_m}{RT}) \tag{2-44}$$

In this equation the parameter T is the service temperature with its units in Kelvin, E_m is the activation energy, R is the universal gas constant ($8.314\frac{J}{molK}$) and E_m is a pre-exponential factor. Eq. (2-44) could also be used to determine the reference parameter m', which is needed to calculate the time-dependent strain at different stress levels (Section 2-4-1). In a study done by Garrido et al. the Findley parameters for calculating the time-dependent strain at different temperatures are based on certain constant stress levels [69]. The parameter n was assumed to be temperature independent, due to the small variations in test results. However, it was found that m' was the one temperature dependent factor among the two fit parameters of Findley. For a reference elastic stress of σ_e = 467.5 MPa and a reference creep stress level of σ_m = 80.4 MPa, the relation given in Eq. (2-45) was found.

$$m'(T) = 6.16E^{16} \exp(\frac{84498}{8.314T}) \tag{2-45}$$

The n parameter was averaged over the tests based on multiple different input stresses and compared with the other n values. Results presented a slight reduction in trend with the increase in temperature.

Such a result was unexpected as typically higher temperatures lead to higher creep rates, which translates to higher creep amplitudes and time exponents. It was unclear whether it resulted from the variability of material properties of the GFRP laminates or because of a real temperature dependency [69].

2-4-3 Moisture

The long-term behaviour of composite materials may be effected by the physical ageing (next subsection) and the chemical ageing of the material. Chemical ageing is a collective term describing the changes in the oxidation, change in density and molecular weight. Swelling, plasticization, slow hydrolysis of the resin and the slow attack of a liquid to the fiber/resin interface affects the material properties that will influence the creep and fatigue behaviour of the composite [40]. Moisture affects the chemical ageing of the material and should be considered when the time-dependent behaviour of FRP composites is investigated. Clearly service environments of most structures subjected to long-term loading cannot be completely climate controlled over the entire life-time [31]. Glass fibers are known to degrade in the presence of water, acidic and alkaline solutions [14, 70, 71]. As discussed in Section 2-2-1, the glass-transition temperature T_g of the polymer matrix is an important material property that determines what the strength and stiffness will be at a certain service temperature. An increase in moisture concentration within the composite subsequently will lead to a decrease of the T_g of the polymer matrix. This is due to plasticization of the matrix which is a result of the interruption of Van Der Waals bonds between the polymer chains. This will eventually lead to a decrease in the matrix mechanical properties of the composite. Therefore, it is necessary to determine the maximum moisture content of a composite. By testing at the highers moisture concentration, the corresponding lowest mechanical properties could be retrieved [70]. Tests done by Mohan and Adams involved specimens subjected to moisture [8]. Results from these experiments involving glass fiber epoxy specimens subjected to relative humidities of 57%, 75% and 100% showed that moisture greatly affects some of the nonlinearizing parameters in Schapery's integral and thus have an effect on the nonlinear viscoelastic behavior of the system [8]. Panasyuk et al. performed creep tests on unidirectional glass fiber epoxy laminates under elevated temperatures and in liquid media [72]. Results showed that the initial and steady-state creep were encountered at considerably low stresses for the liquid media creep test specimens compared to identical specimens tested in air. Also, the creep rate increased under the effect of the liquid media. It was concluded that their investigation showed that to some extent the nature of creep of FRP composites is connected with the regrouping of the macro-molecules of the polymer matrix. This was the result of the swelling of the polymer matrix in the liquid medium under the effect of temperature [31].

2-4-4 Physical ageing

Physical ageing the manifestation of a polymer slowly getting to its thermodynamic equilibrium. It is manifested by time-dependent changes in the state variables such as the mechanical properties of the polymer, the volume, enthalpy and entropy [73]. The properties of a polymer can vary over time due to a change in molecular structure, which can happen without any applied stress. The changes that occur in the molecular packing of the polymer is a phenomenon referred to as physical ageing. As a result of physical ageing the molecular packing will be increased, which means that the free volume in the polymer will decrease over time. At temperatures well below T_g, there is a continuation of glass formation until an equilibrium state is reached for the free volume [14]. This is a very slow

process which never equilibrates in a practical time frame for temperatures below $T_g - 15$ °C [73]. At temperatures near or above T_g a thermodynamic equilibrium is reached almost instantly, which can be used to rejuvenate the material. Physical ageing ensures that the material becomes stiffer, but more embrittled over time. This means that the damping of the material decreases and viscoelastic properties are affected [14]. Short-term creep is the viscoelastic response of a FRP composite to an applied load at a certain temperature with a constant age. However, long-term creep is not a fundamental material response, because a significant ageing occurs during the period in which the system is loaded. Long-term theoretical predictions can be made by using the effective-time theory. This effective time is often referred to with the symbol λ as replacement for the real time t. The effective time λ appears in the hereditary integral equation of Boltzmann, given in Section 2-3-2, where λ is a function of the ageing history. From this theory, the long-term creep compliance $\bar{D}$ is related to the corresponding momentary creep compliance D. This relation is symbolically described in Eq. (2-46).

$$\bar{D}(t, T, t_{age}) = D(\lambda, T, t_{age}) \tag{2-46}$$

In this relation the parameter t represents the real time and t_{age} represents the reference ageing parameter. The shifted time parameter λ could be calculated according to Eq. (2-47) for $\mu = 1$ and can be calculated according to Eq. (2-48) when $\mu < 1$.

$$\lambda = t_{age} \ln(1 + \frac{t}{t_{age}}) \tag{2-47}$$

$$\lambda = t_{age} \frac{(1 + t/t_{age})^{\alpha} - 1}{\alpha} \tag{2-48}$$

These equations are based on μ being constant, while the sample is ageing and $0 < \alpha = 1 - \mu < 1$. Results from tests done by Sullivan et al. show that the value for μ ranges between 0.6 and 0.9 and appear to be independent of the fiber content. The presented time-ageing superposition corresponds quite well for amorphous polymer systems [73].

2-5 Creep in verifications

From multiple structural codes or design recommendations, it becomes clear that the concept of creep is tackled quite differently. Both the Dutch recommendation CUR96 and the JRC policy report make use of conversion factors, which reduce both the stiffness and strength in different ways [2, 20]. The technical specification TS19101, which can be seen as the pre-draft of the new Eurocode concerning FRP structures, makes use of certain creep coefficients or ϕ-factors which reduce only the stiffness of the composite [42]. According to the TS19101, strength properties are not affected by creep behaviour. This approach on creep involvement is comparable with the methods proposed in the current Eurocodes for concrete structures. The following subsections elaborate on the different creep methods used in the different design recommendations mentioned above.

2-5-1 Creep in CUR96

The design recommendation CUR96 makes use of conversion factors that reduce certain material properties applied in the structural analysis of FRP elements. This conversion factor depends on multiple internal and external influences that could lead to a lower reliability of structural integrity.

The total conversion factor can be determined according to Eq. (2-49), which is created by multiplying multiple different phenomena specific conversion factors. Each of these conversion factors is dependent on different input parameters such as moisture, temperature and fatigue performance.

$$\eta_c = \eta_{ct} \cdot \eta_{cm} \cdot \eta_{cv} \cdot \eta_{cf} \tag{2-49}$$

In this equation the η_c is the total conversion factor used for reducing the material property of interest, such as the stiffness or the strength. The η_{ct} accounts for the influence of temperature differences, η_{cm} takes moisture effects into account, η_{cf} is a reduction for fatigue effects and η_{cv} reduces the properties caused by creep effects. Some of the conversion factors can be excluded for certain verifications in the CUR96. In Figure C-1 (Appendix C), Table 2-6 from the CUR96 is given, which shows for what kind of verifications certain conversion factors need to be applied. Creep is accounted for through the creep conversion factor within the verifications concerning maximum deformations, stresses and stability issues. Figure C-1 in Appendix C shows exactly for which verifications this creep conversion factor needs to be accounted for. How the creep conversion factor of a FRP laminate could be calculated is given in Eq. (2-50).

$$\eta_{cv} = \frac{1}{r_v \cdot t^n} \tag{2-50}$$

The parameter r_v is a factor that accounts for the theoretical strain increase in the ply of interest. When axial loading is considered, this factor can be determined from Eq. (2-51).

$$r_v = \frac{E_i \cdot t}{\sum(E_{v,i} \cdot t_{v,i})} \tag{2-51}$$

In this equation the E_i parameter represents the stiffness of the entire laminate in the direction of interest and t is the total thickness of the laminate. The sum $\sum(E_{v,i} \cdot t_{v,i})$ is the axial stiffness of the laminate in the direction of interest with the stiffness of each ply that has a different fiber direction equal to 0.0 GPa. The t^n factor in Eq. (2-50) represents the duration in hours in which the exponent n depends on the type of fiber reinforcement. If the fibers are positioned in the direction of the axial loading the exponent is: $n = 0.01$ for an UD-ply, $n = 0.04$ for a bi-directional ply and $n = 0.10$ for mat plies [2].

2-5-2 Creep in JRC

The design recommendation JRC also makes use of conversion factors to reduce certain material properties as a result of internal and external influences. It uses the same conversion factors to account for temperature, moisture, fatigue and creep effects, see Eq. (2-49). However. these conversion factors are not applied in each same verifications as it is done within the CUR96. Figure C-2 represents Table 2.4 from the JRC design recommendation and it can be seen that the conversion factor is applied in the same verifications as in the CUR96 Figure C-1. However, the method to determine the creep conversion factor differs from the CUR96. The Tables 10.1 (Figure C-3) and 10.2 (Figure C-4) from the JRC could be used to determine creep conversion factors for both strength and stiffness reduction in a time span of 20 years. If the creep conversion factor for 20 years ($\eta_{cv,20}$) is found using these tables, the creep conversion factor for the time span of interest (η_{cv}) could be calculated by using both Eq. (2-52) and Eq. (2-53) [20].

$$\eta_{cv}(t_v) = (\eta_{cv,20})^T \tag{2-52}$$

$$T = 0.253 + log(t_v) \tag{2-53}$$

2-5-3 Creep in TS19101

As stated in Section 2-5-1, the CUR96 transforms the influence of creep into a specific conversion factor. The influence of creep in the technical specification is tackled in a different way. The technical specification does not reduce any strength properties used in the ultimate limit state. Instead, it reduces the initial mean values of the relevant elastic moduli of the material through the creep coefficient. The formula that takes this creep reduction into account is given in Eq. (2-54).

$$X_m(t) = \frac{X_m(0)}{1 + \phi(t)} \tag{2-54}$$

In this formula the $\phi(t)$ is the creep coefficient, $X_m(t)$ is the time dependent mean elastic modulus and $X_m(0)$ is the instantaneous mean elastic modulus. Annex A of the TS19101 provides different values for the creep coefficients of unidirectional (UD), woven [0°/ 90°] and chopped strand mat (CSM) plies or laminates [74]. In contrast to the CUR96, the TS19101 has no further elaboration on how the creep coefficient is influenced by combining UD plies into multi-directional ply based laminates. This $\phi(t)$ factor originates from the way that creep is accounted for within other materials in structural design. In essence, it is the ratio between the final strain after creep and the instantaneous strain. These relations or ratios are given in Eq. (2-55). The possibility to easily define simple functions for the creep parameter $\phi(t)$ is useful for practical structural design [43].

$$\phi_E(t) = \frac{\Delta\varepsilon(t)}{\varepsilon(0)},\ \phi_G(t) = \frac{\Delta\gamma(t)}{\gamma(0)} \tag{2-55}$$

2-6 Summarizing and concluding remarks

Creep could be explained as the time-dependent deformation of a material subjected to an applied load over an extended period of time [32]. It could be categorized into three different phases: primary, secondary and tertiary creep. The primary creep stage is characterized by a fast increase of creep strain and is also called transient creep stage followed by a decelerating transition period towards the second creep stage. In the second creep stage, the creep rate starts to become more or less steady. Under normal loading conditions, this stage accounts for the longest period during the entire creep lifetime. The tertiary and final creep stage is characterized by an accelerating creep rate until creep rupture occurs.

Fiber-Reinforced Polymers are considered as viscoelastic materials, which means that their material behaviour could be characterized as both elastic and viscous. This time-dependent viscoelastic behaviour is mainly caused by the polymer matrix, as the creep behaviour of the fibers is negligible. There are multiple ways to predict how creep deformation accumulates over time. This could be done by: creating a deformation master curve based on accelerated test methods or by using analytical formulas with fit parameters found in creep tests. These analytical formulas could be used to describe time-dependent material behaviour, which serves as the constitutive relation between stresses and strains. The factor that eventually depends on time and relating both of these quantities together is often expressed as the creep compliance $D(t)$, which could be seen as the inverse of the time-dependent elastic modulus $E(t)$. Multiple models have been presented to describe this creep compliance function. However, using this function directly as the constitutive relation between stresses and strains only enables to predict long-term behaviour under constant loading conditions. To account for a variable stress input, other models have been proposed such as the superposition principle of Boltzmann (BSP)

or the Schapery integral procedure. These methods make it possible to calculate the strain at a certain moment in time given a certain stress function. Using the Heaviside step function for the stress input enables the modelling of creep and recovery response.

Creep behaviour can be influenced by multiple external factors. Creep in polymers is closely related to diffusion (Appendix A) controlled by the free volume in its amorphous structure. This diffusion of molecules ensures restructuring of the molecules in the material and is induced by changes in temperature or applied stress gradients. Therefore, these two aspects are the most important factors in creep. Due to the low glass transition temperature (T_g) of polymers, FRP materials can experience relatively high creep deformations in practical applications under common service temperatures. Chemical and physical ageing of the polymer can have a negative influence on this T_g, which causes the FRP to creep more easily in time. These external factors could be accounted for in the description of the creep compliance. The unknown parameters in these creep compliance function could be found by fitting the proposed equations to experimental work. These parameters could each be dependent on one or multiple of these internal and external influence factors.

Current standards such as the Dutch CUR96 and the JRC take creep into account by providing engineers from certain creep conversion factors (η_{cv}), which must be used to reduce stiffness properties. The reduction is based on the time at which stiffness is evaluated and on parameters that are based on experimental work. The TS19101 makes use of creep coefficients ($\phi(t)$), which can be seen as the inverse of the creep conversion factor presented in current recommendations. Creep coefficient values for varying stiffness properties and varying reinforcement types are tabulated in Table A.2 of the TS19101.

Chapter 3

Viscoelastic creep model

3-1 Viscoelastic analytical model

Several creep models, retrieved from literature, are analysed and explained in Chapter 2. Together with the amount of experimental data from literature and their relevance, some of the models are taken and used for the prediction of creep in FRP web core sandwich deck panels. The following sections explain which models are used, how they are modified and finally how they are implemented into a numerical model.

3-1-1 Selection creep model

From literature it becomes clear that the procedure prescribed by Schapery is most complete. It takes into account the influences of nonlinear stress ranges, changes in temperature, physical ageing and the moisture content. However, current knowledge lacks experimental data on what these Schapery parameters g_i and a_σ exactly are. In addition, it is unknown how all these phenomena will occur in the wide variety of structural design applications. Therefore, in creep calculations of FRP elements it is often assumed that the stress will be sufficiently low, so the nonlinear effects are negligible. In case of FRP structures, such an assumption could be made based on the fact that FRP elements have a relative high strength-to-weight ratio. This means that the stability issues (ULS) and maximum deformations (SLS) will most likely be governing. Thus, the strength capacity verification will be very conservative which means that the highest stresses in the structural application will be far below the ultimate strength of the FRP. Therefore, Findley's power law can be a suitable creep model to use for the prediction creep deformations. The model is also used most often in literature compared to the other possible models and is supported by more experimental data. An overview of the experimental literature on Findley's power law and its parameters is given in Appendix B. The model is also recommended by the American Society of Civil Engineers (ASCE), the Dutch advisory regulations (CUR96) and the TS19101, which functions as a pre-draft for the new Eurocode (TS19101) [10, 2, 74]. However, Findley's law estimates only the creep accumulation or the virtual stiffness reduction in time and does not account for unloading and recovery behaviour. For this, Boltzmann's superposition can be

used. As stated before, this superposition principle makes it possible to account for different stress levels in time. This means that it can account for unloading or recovery as well. Summarizing, both **Findley's power law** and **Boltzmann superposition principle** will be used in the analysis of the creep development within FRP web core sandwich deck panels applied in road traffic bridges. According to literature both the Findley's power law model and the superposition principle of Boltzmann can predict the material behaviour quite accurately [61, 6].

3-1-2 Creep models validation Maple

To validate the proposed models, one of the creep tests done on a FRP pultruded I-section by M. Sá et al. is remodelled [9, 13]. The background of the creep research done by M. Sá et al. is given in Appendix B, but the bullet points below summarize the most important characteristics of the creep test.

- Four-point flexural bending test done on FRP pultruded I-section
- Two concentrated loads of 11.4 kN each on $\frac{1}{3}L$ and $\frac{2}{3}L$
- At midpoint, both the axial strain in the top flange and the deflection are measured
- Duration of creep test was 1680 h and duration of the recovery test was 148 h
- Dimensions: l_{beam} = 1800 mm, $t_f = t_w$ = 8 mm, b_f = 75 mm and b_w = 150 mm

The experimental setup of the I-profile flexural test included the following elements: a closed steel loading frame, a metallic distribution H-profile, an Enerpac hydraulic jack, TML displacement transducers with a stroke of 50 mm and precision of 0.01 mm, strain gauges placed in the web (and flanges) at different cross-sections and a beam support system materialised by steel rollers placed in-between steel plates [9]. The setup is given in Figure 3-1.

Figure 3-1: Four point bending creep test setup [9]

Fitting Findley's power law onto the results for the displacement or the axial strain at the middle cross section of the beam gives two of the corresponding Findley parameters for the deformation of the entire beam. The parameters are found by fitting the power law through the experimental results. The found parameters are listed below [9].

- $\varepsilon_0 = 2.305$ ‰ $\rightarrow$ $E_0 = 28.4$ GPa
- $\varepsilon_t = 0.036$ ‰ $\rightarrow$ $E_t = 1809.2$ GPa
- $n = 0.31$

To check if the found parameters could indeed be used for modelling the creep behaviour of the beam, a simple Euler-Bernoulli beam has been modelled with the calculation software Maple. This calculation can be found in Appendix D, where the time-dependent elastic modulus is based on the power law of Findley and the corresponding found Findley fit parameters. The test results of the deformation at the middle cross section during the creep tests are shown in Figure 3-2(a) and are expressed as the percentage of the initial elastic deformation. Figure 3-2(b) shows a plot of the modelled beam based on Euler beam theory with a decreasing stiffness based on Findley's power law and the found parameters. In this plot the results are also expressed as the percentage of the calculated initial elastic deformation.

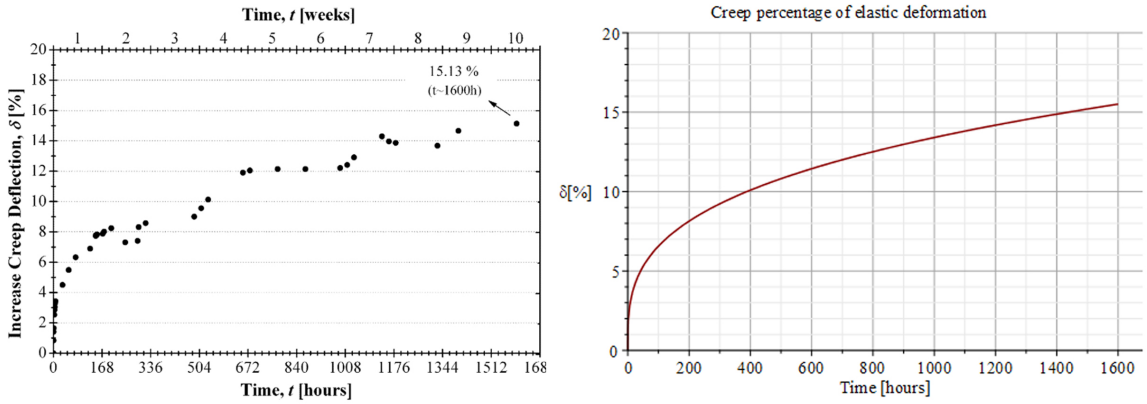

Figure 3-2: Deformation creep test results (a) and plot based on Euler beam theory and Findley (b)

The total deformation recorded after 1600 hours of testing was 15.13% of the initial elastic deformation and the calculated deformation after 1600 hours resulted in 15.23% of the initial elastic deformation. Based on both those values and a visual comparison, it could be stated that the power law predicts the creep behaviour quite accurately. The axial strain at the top flange of the middle cross-section was monitored as well. The results of the creep cycle were processed until unloading of the beam at 1600 hours. However, the measurements of the strain gauge continued to record the recovery strain for 148 hours after unloading. Based on BSP, the superpositioning of both the creep strain in this time interval with the recovery strain should result in a residual deformation curve. However, superimposing a recovery strain based on the same Findley parameters used for the creep calculation did not result in a residual strain that corresponded well with the experimental results. Thus, for the recovery deformation, new Findley parameters needed to be found. This is done by fitting a power law through the results of the recovery strain, see Figure 3-6. The corresponding parameters are used in the modelled Euler beam and are, in accordance with the superposition principle, subtracted from

the creep cycle results at the recovery time interval. This resulted in a prediction of deformation with a good accuracy. The axial creep strain experimental results are given in Figure 3-3(a) and the plot based on Euler beam theory, Findley's power law with the correct parameters and the superposition principle of Boltzmann is given in Figure 3-3(b).

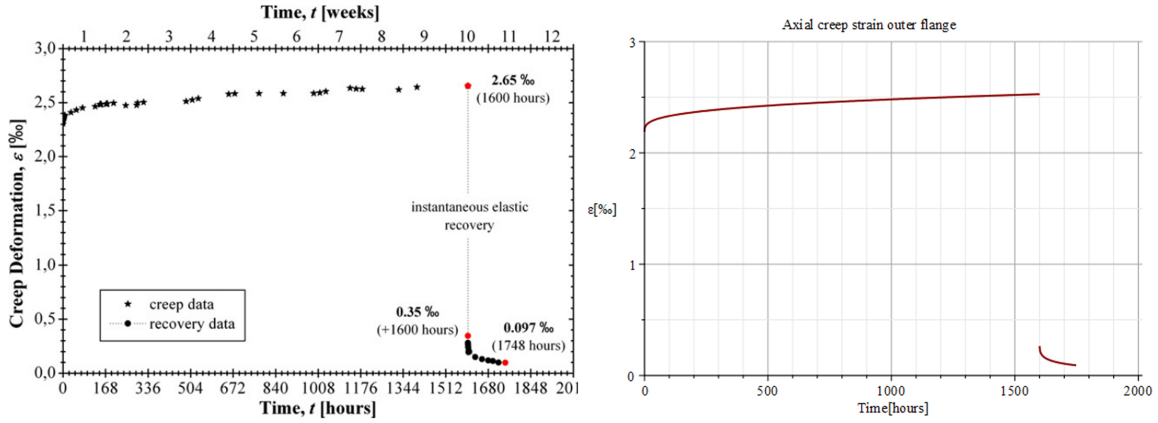

Figure 3-3: Axial strain creep test results (a) and plot based on Euler beam theory and Findley (b)

As stated before, the combination of the power law and the superposition principle with the appropriate fit parameters seem to predict the creep and recovery behaviour quite well. At the time of unloading the recorded axial strain in the top flange of the beam was 2.65‰and the calculated axial strain is 2.53‰. The residual deformation that resulted from the experiment was 0.097‰and the calculated residual axial strain was 0.092‰.

3-1-3 Modification of the creep model

As stated in Chapter 2, the power law of Findley can be modified for multiple different influences. One of the most important influences of the creep behaviour of FRP composites is the stress level that is applied. When a sandwich deck panel is applied in a road traffic bridge, each part of the panel experiences different stress levels and therefore influences the global creep behaviour differently. Therefore, the Findley parameters found in experiments, which are based on a constant stress level, cannot directly be used. However, by using the relationship given in Eq. (2-37) and Eq. (2-38) the parameters from experiments can be used. The difference in strain output based on different stress inputs could be accounted for by taking the hyperbolic sine function of the ratio stress over reference stress. The hyperbolic sine function can also be approached with a first order Taylor series, presented in Eq. (2-40), with a quite good accuracy. The theory behind this modification can be found in Section 2-4-1. The influence of temperature has also an important role in the creep behaviour of the material. However, there is lack of experimental data on how this temperature could influence the power law of Findley and how the temperature development within the FRP composite element actually looks like over the entire lifetime. Therefore, it is assumed that the service temperature of the sandwich deck panel corresponds to the temperature used in experimental tests and is within the limiting values presented by the TS19101. The influence of moisture in combination with changes in temperature, which can lead to multiple degradation forms such as hydrolysis and plasticization of the resin, are

assumed to be of no influence on the parameters of Findley. In the technical specification (TS19101) boundary values for these three phenomena are given, so that the linear Boltzmann superposition principle holds. The limiting values for the creep coefficient at 50 years are given below.

- Minimum fiber volume fraction of 35%
- Service temperatures up to 25 °C
- Relative humidity up to 65%

To obtain the correct stiffness parameter at time t, the creep compliance form of Findley's power law is going to be used (Eq. (2-16)). The instantaneous creep compliance D_0 is a constant that could be taken as the inverse of the modulus of interest. The transient creep compliance fit parameter of Findley D_m could be determined from creep tests. The equation used for the creep compliance is given in Eq. (3-1). The corresponding time- and stress dependent moduli of interest can simply be calculated by taking the inverse of the entire creep compliance, see Eq. (3-2). This equation can be used for the calculation of the moduli in both the longitudinal and transverse direction (E_i, $i = 1, 2$). The same equation could be used for the shear moduli, where the parameter E_i is simply replaced by the notation G_{ij}.

$$D_i(t, \sigma) = D_0 + D_m(\sigma) \cdot t^n \tag{3-1}$$

$$E_i(t, \sigma) = \frac{1}{D(t, \sigma)} \tag{3-2}$$

As stated before, the transient creep compliance parameter has a strong dependence on the stress input and thus will be dependent on the stress in the model. From literature it is retrieved that when the stress level is lower than 30% of the ultimate strength, a stress based linear relationship between the transient creep compliance could be found [14, 31]. The determination of the transient creep compliance is given in Eq. (3-3), where $D_{m,0}$ and C_σ are determined from test results retrieved from literature.

$$D_m(\sigma) = \cdot D_{m,0} + C_\sigma \cdot \sigma \tag{3-3}$$

The final time- and stress dependent modulus of interest based on Findley can be used to predict each creep and recovery cycle. The results for each cycle can then be used in the superposition principle of Boltzmann Eq. (2-24). How this two models can be merged together and used to determine the deflection or strain at time t, as a result of a variable loading history, is explained in Section 3-2-2.

3-1-4 Findley's parameters

Now that the formula for the elasticity during one creep or recovery cycle based on Findley is clear, the appropriate Findley parameters need to be implemented. Multiple studies have tried to find these parameters for specific design and loading scenarios considering FRP pultruded sections [9, 15, 16, 75, 17, 18, 10, 19]. However, data on UD-plies is scarce and literature review resulted in just one study about the creep behaviour of UD-plies done by J. Siccama at TU Delft [14]. The following sections describe the parameters used in given the formula based on Findley for both the creep- and recovery cycles. Further information on the experimental research done on these parameters is given in Appendix B.

Creep cycles

To simplify the creep analysis for the traffic loading, a conservative loading scenario is chosen. Each traffic jam will be modelled as a constant Heavisidal input loading condition. Both the longitudinal and transverse moduli are based on the tests done by J. Siccama [14]. In these tests the fiber volume fraction was 55%, which corresponds to the fiber volume fraction of the face sheets of the sandwich deck panel analysed in the case study presented in Chapter 5. The parameters for the shear behaviour are retrieved from a research done by M.Bottoni et al. on pultruded wide flange sections [16]. The needed parameters for each creep cycle per ply in the model are listed below. Unfortunately, based on the limited data from literature, only a stress based relation could be found for the stiffness in the longitudinal direction of the plies. Further experimental research on the stress-dependency of the transverse stiffness and the shear stiffness should give a more precise Findley power law parameter.

- Longitudinal (+): $n_1 = 0.10$ and $E_{t,1} = 943.0 + 7.5 \times \sigma$ [GPa]
- Longitudinal (-): $n_1 = 0.10$ and $E_{t,1} = 416.5 + 14.7 \times \sigma$ [GPa]
- Transverse: $n_2 = 0.22$ and $E_{t,2} = 23.0$ [GPa]
- Shear: $n_{12} = 0.25$ and $G_{t,12} = 22.8$ [GPa]

The linear relationship between a variable stress input and the Findley fit parameter E_t is based on Eq. (2-40) and on findings from literature [9, 16, 67, 31, 14]. A linear fit is found for the longitudinal tensile E_t parameter, based on the experimental results from tests that described the creep behaviour of UD-plies done by J.Siccama [14]. Also a linear fit is found for the longitudinal compression parameter E_t, but these experimental results were from tests done on a pultruded I-section by M. Bottoni [16]. Both the fits and the experimental results are given in Figure 3-4.

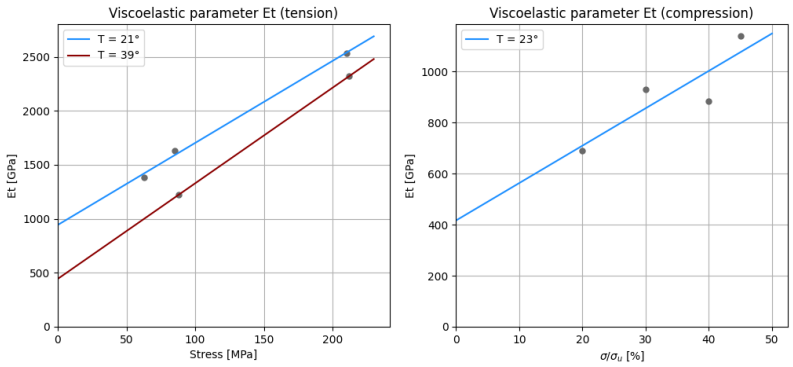

Figure 3-4: Linear fits on the found E_t parameters based on different stress levels and temperatures

It must be noted that the tests for the transverse elastic properties of the UD-plies had a big variety in results. Fitting a power law to these results seemed to be more difficult than the power law fits done on the longitudinal tests. More research should be done on the Findley fit parameters for the transverse elastic behaviour of UD-plies. The same holds up for the parameters used to describe the elastic shear behaviour of the UD-plies. By performing multiple creep tests at different temperatures and stress levels on UD-plies, these parameters can and should be improved by further research.

Recovery cycles

Experimental results on the recovery behaviour are also very scarce. No experimental results concerning UD-plies could be found during a thorough literature review. Therefore, some of the few researches from literature on pultruded sections are taken to describe and model the recovery behaviour of FRP UD-plies. Recovery parameters are found for three different recovery experiments retrieved from literature and TU Delft creep data. The creep and recovery results of tests done by P. He, M. Sá et al. and G. McClure et al. are used to find the magnitude of both the exponential and linear fit parameter used in the power law of Findley [9, 10]. The experimental results together with a nonlinear power law fit are plotted and are given in Figure 3-5, Figure 3-6 and Figure 3-7, in which the blue curve is the nonlinear fit. The Findley parameters found are shown at the right bottom of each plot.

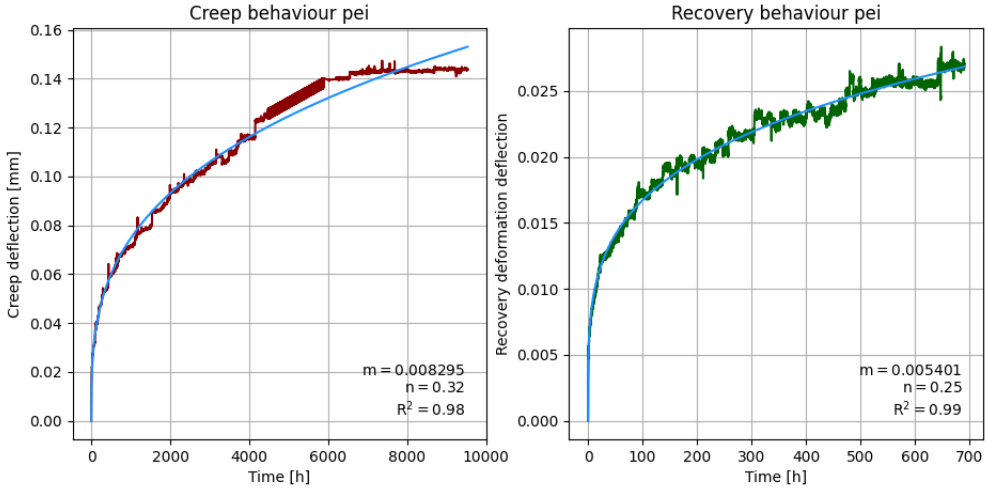

Figure 3-5: Creep/recovery test results performed on wrapped joints by P. He on TU Delft

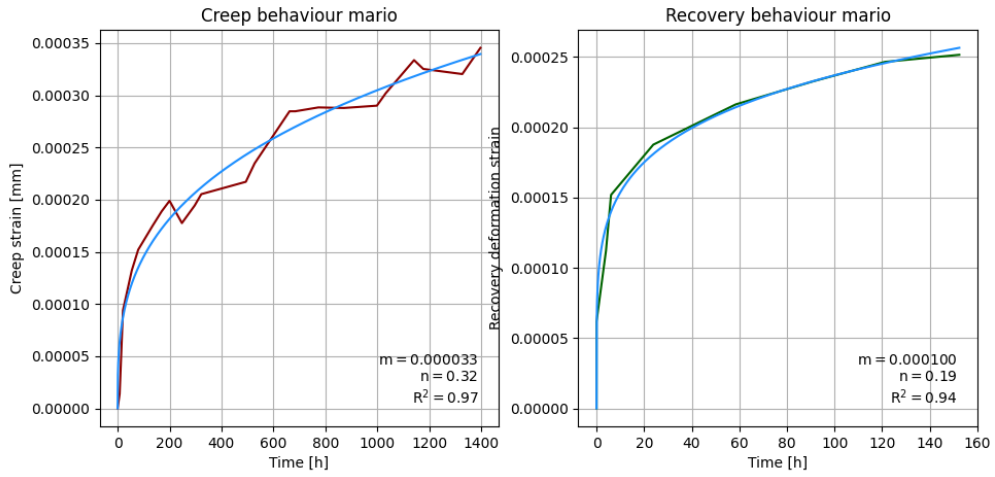

Figure 3-6: Creep/recovery test results performed on pultruded I-sections by M.Sá [9]

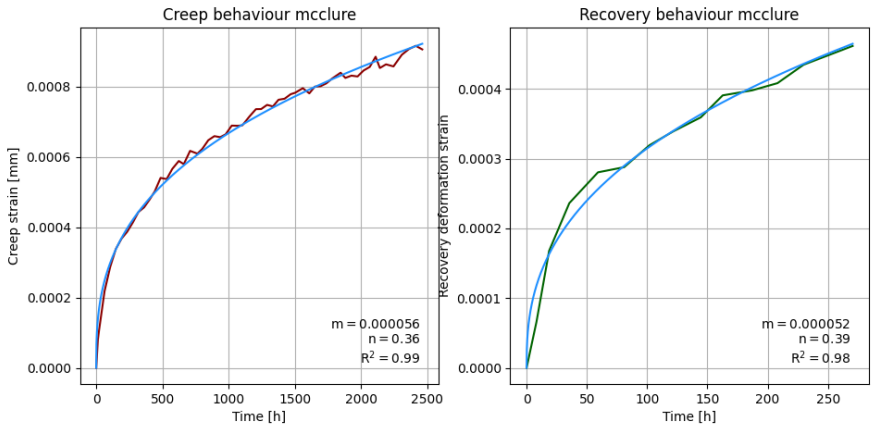

Figure 3-7: Creep/recovery test results performed on pultruded angle stubs by G. McClure [10]

Figure 3-3 in Section 3-1-2 shows that for a certain loading and recovery duration, the use of Findley´s power law and the superposition principle of Boltzmann has great correspondence with experimental results. This correspondence is achieved by using different parameters of Findley for both the creep and recovery prediction of the beam. However, using these different parameters for shorter loading and longer recovery times resulted in weird outcomes for the residual deformation. Figure 3-8 (a) shows that using the parameters for the creep and recovery, found by fitting the power law of Findley, results in negative residual deformations on the same timescale as the test. This clearly does not correspond with what will happen in reality. Figure 3-8 (b) also shows that on a larger timescale the superposition of one creep and one recovery cycle will eventually be dominated by one of the two superimposed exponential functions.

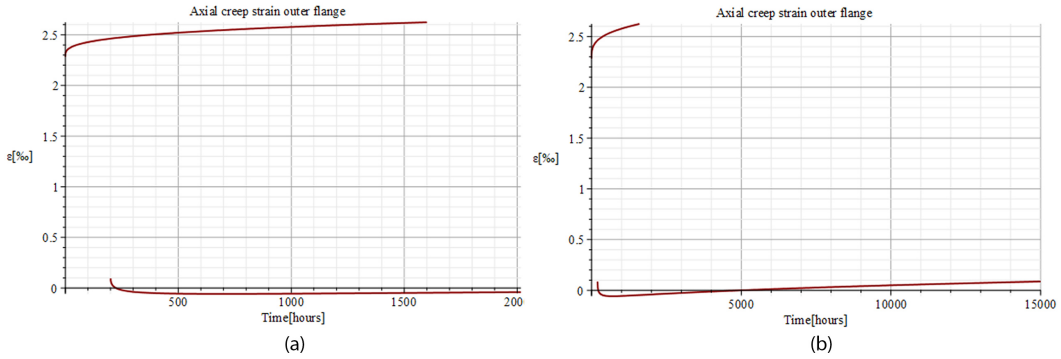

Figure 3-8: Creep and recovery behaviour prediction I-beam experiment with different cycle durations

Based on these findings, it could be concluded that for long-term prediction of creep caused by variable loading, the power law of Findley containing different parameters for creep and recovery is not quite compatible with the superposition principle of Boltzmann. However, using the same parameters for both creep and recovery cycles result in more realistic values for the residual deformation on the long-term. Therefore, for the analysis of the sandwich deck panel it is chosen to use the same parameters for creep and recovery. Using the same parameters with a relative short loading duration and long recovery duration will lead to a residual deformation, which eventually goes asymptotically back to 0.

Figure 3-9 shows how the graph for the residual strain in the I-beam experiment done by M.Sá will look like.

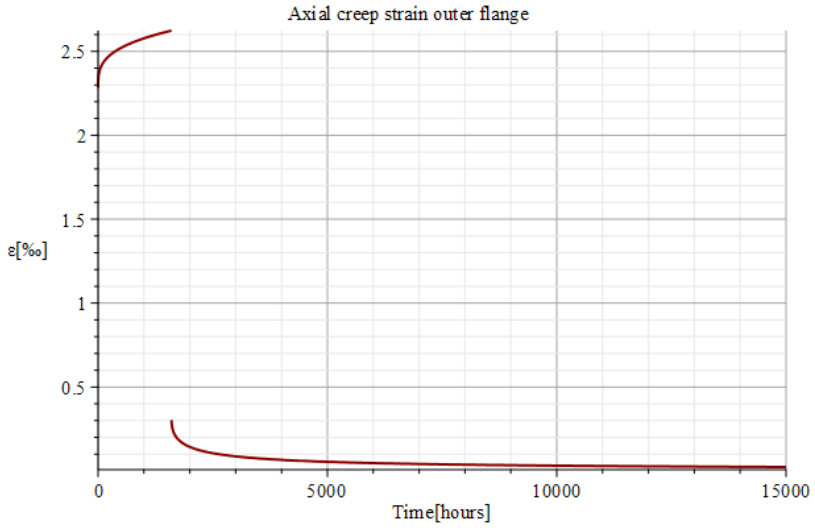

Figure 3-9: Residual deformation I-beam experiment using the same parameter for creep and recovery

The use of the same parameters in the validation of the I-beam experiment lead to a prediction which did not perfectly coincide with the experimental results. However, the speed of recovery that is predicted is much slower. It could therefore be stated that the use of the same parameters is a conservative approach. After 148 hours of recovery during the creep experiment the final residual axial strain resulted in 0.097‰. Using the same parameters for creep and recovery behaviour leads to a residual axial strain of 0.187‰, considering the 148 hours of recovery. To achieve the same strain level, a lot of extra recovery hours are needed. It takes 952 extra recovery hours using the combination of Findley with the BSP approach using the same parameters for creep and recovery to result in the same residual axial strain that were found during the experiments done by M.Sá. This is more or less equal to a recovery time-span of 40 days or 5.5 weeks! Although, the results are not exactly in line with the experimental results, the approach is considered as a very conservative approach. Other descriptions of the creep compliance function than the description of Findley have much better compatibility with the superposition principle of Boltzmann. Unfortunately, experimental results including the viscoelastic behaviour described by a Prony series or by the Bürger model are too scarce. Therefore, the numerical analysis in this research is done with the creep compliance described by the power law of Findley using the same parameters for both creep and recovery cycles.

Parameter overview

Based on existing literature, it can be concluded that the the amount of experimental data on ply-level is scarce. Most of the data is based on experimental work done on pultruded sections with in most cases limited or no results on the recovery behaviour of the material. Finding the most appropriate parameters for unidirectional plies is done through literature research. The background together with an elaborate overview of the found parameters is given in Appendix B. However, Table 3-1 gives a short overview of the parameters to be used in the analysis of a multi-directional laminated sandwich deck panel analysed in Chapter 5.

Overview of Findley's parameters		
Parameter	Creep and recovery parameters	Author
E_{1t} (+)	943.0 + 7.5 x σ [GPa]	J. Siccama [14]
E_{1t} (-)	416.5 + 14.7 x σ [GPa]	Y. Choi [19]
E_{2t}	23.0 [GPa]	J. Siccama [14]
G_{12t}	22.8 [GPa]	M. Bottoni [16]
n_1	0.10	J. Siccama [14]
n_2	0.22	J. Siccama [14]
n_{12}	0.25	M. Bottoni [16]

Table 3-1: Findley parameters to be used for multi-directional laminates

3-2 Creep computer model

For the viscoelastic (creep) analysis of the FRP web core sandwich deck panel, use is going to be made of both Finite Element Analysis (FEA) software and Python. The creep data output from FEA will be taken within a Python script to be post-processed. In the following sub-sections the choice of the right FEM software package and the method of implementing the creep model will be explained.

3-2-1 Finite Element Analysis software

In principle all the Finite Element Analysis (FEA) software packages could be classified into two different groups: structural analysis oriented software and research/ mechanical engineering oriented software. Figure 3-10 shows the most popular FEA software packages on the market, with the structural analysis and research oriented classification for each [41].

Figure 3-10: Different FEA packages on the market: structural analysis and research oriented

Most commercial FEA software packages, such as Sofistik, RFEM, SCIA and other packages have implemented viscoelasticity for isotropic materials. This is a severe limitation for users that want to compute an analysis consisting the viscoelastic behaviour of polymer matrix composites. However,

with some software available on the market it is possible to take advantage of the user programmable features in order to implement the formulations presented in Section 3-1-3 [11]. These programmable features can be implemented by the use of either the FEM software package Ansys or Abaqus and by using one or multiple of their so-called **User Subroutine** modules.

Using FEA software to model composite deck systems, it is important to know what kind of elements the software needs to use for calculation. Most composite structures are built as assemblies of plates and shells. This is more efficient in calculation, because the structure only carries the membrane loads. Besides, thick laminates are also more difficult to produce. Plates are simply one specific case of shells, namely flat shells having no initial curvature. Therefore, from now also these will be referred to as shells. Modelling laminated composite structures differs from modelling conventional materials in three different ways. First, the lamina are orthotropic. Second, the constitutive equations of the element depend on the kinematic assumptions of the shell theory that is used and their implementation into the element. Third, material symmetry is as important as geometric and load symmetry when trying to use symmetry conditions in the models. Shell elements are based on different shell theories, which in their turn are based on kinematic assumptions. The most popular composite shell theory is the **first-order shear deformation theory** (FSDT). It is based on the two assumptions listed below.

- A straight line drawn through the thickness of the shell in the undeformed configuration may rotate but it will remain straight when the shell deforms
- The change of the shell thickness is negligible as the shell deforms

These observations are verified by experiments if the following two statements are true. The aspect ratio $r = \frac{a}{t}$ defined as the ration of the shortest side of the surface a to the thickness t is larger than 10. The stiffness of the laminates in the global shell coordinates does not differ by more than two orders of magnitude. This effectively rules out **sandwich shells** containing foam core material, where the core is much softer than the faces. Deformation and stress analysis of composites can be done at different levels: (a) micro-mechanical level, (b) lamina level and (c) laminate level, see Figure 3-11.

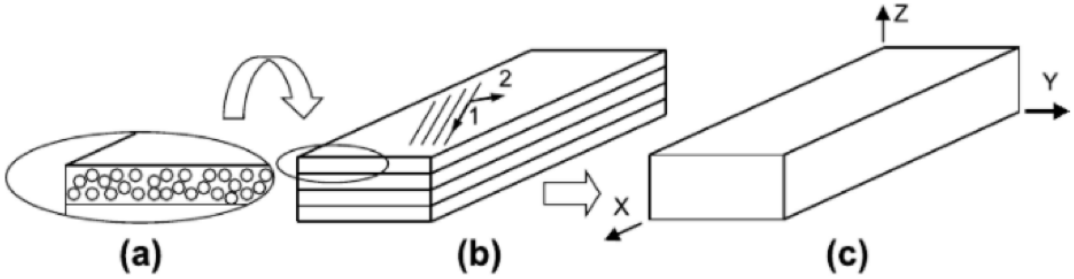

Figure 3-11: Different approaches to model a laminate: micro, meso or macro [11]

When a great level of detail is necessary, the stresses and strains are computed at constituent level. Also when the laminate is very thick or when studying local effects like free edge effects, the composite should be modelled as a 3D solid. A composite laminate can be considered as a homogeneous material when the global displacements, buckling loads and modes of vibration frequencies are analysed. However, the stress distribution within the laminate could not be modelled. To find the internal stresses per ply in the entire laminate, the program needs to know the **laminate stacking sequence**

(LSS). This analysis is often referred to as the **meso-scale level approach**. The different elements that could be chosen within Abaqus are listed below.

- **Conventional shell elements** require the geometry to represent a 2D surface in 3D as opposed to continuum shell elements. Conventional elements include thin shell elements and thick shell elements.
- **Continuum shell elements** require the geometry to model explicitly the thickness of the shell as it would be done with 3D elements, but in contrast to the latter, continuum shell elements enforce the FSDT constraints.
- **Thin shell elements** enforce the Kirchoff plate theory constraints. This means the transverse shear deformations are assumed to be zero or negligible. They are not accurate for composites if the laminate is thick or the transverse shear moduli G_{23} of one of the lamina are small, in which case the shear deformation may be underestimated.
- **Thick shell elements** enforce the FSDT constraints. Therefore, the transverse shear deformations are not assumed to be zero. Thick shell elements can be either conventional or continuum.
- **3D solid elements** discretize the modelled body without using any assumptions done in the different shell theories. Since the assumptions that are done in shell theory are not valid for 3D solid elements, the computation can be expensive.

Composites should be modelled as thick shell elements even if they are geometrically thin, because they have relatively low shear moduli, thus necessitating their shear deformation in the same way as thick shells do. Compared to conventional shell elements, continuum elements have more nodes to depict the thickness in the model. They can be internally laminated to represent a laminate or a sub-laminate with just one element. For sandwich shells the core is much softer than the faces. Transverse shear deformations are significant and thus you need to make use of continuum shell elements [11]. However, when FRP web core sandwich deck panels are considered the mechanical behaviour of the core could be neglected for simplicity reasons. The shear stiffness of the structure is mainly determined by the FRP webs. Therefore to predict the global creep behaviour, using conventional elements without any core material in between the webs is justified.

3-2-2 Creep model implementation

As stated in Section 2-3-2, the Boltzmann superposition principle can be used for different stress levels in time, see Eq. (2-24). The Heaviside function can be used as an interesting way of finding the creep strain during loading and the recovery or residual strain when the element is unloaded. For a simple 1D beam element made from an isotropic material this can easily be done with calculators like Mathcad or Maple. However for a 3D web-core sandwich deck panel containing two different multi-directional layups for both the flanges and the webs, this calculation cannot be simplified in such way. The use of Finite Element Modelling (FEM) software can provide a way to compute the (creep) strains on such structures during a creep or recovery cycle. Use can be made of the Finite Element (FE) software Abaqus, which calculates the stresses and deformations for a given design and loading configuration at every location in the structure. With Abaqus it is possible to assign a certain layup to the possible different elements comprising the sandwich deck panel and calculate the stress in both longitudinal and transverse direction of each ply in its own local coordinate system.

In the Abaqus graphical interface it is possible for the user to provide the viscoelastic relationship of the material through a Prony series. Such a series gives includes a specific function for the description of the time-dependent elastic and shear moduli. It provides the time-dependent creep compliance and finds its origin in mechanical generalized Maxwell and the mechanical generalized Kelvin model, see Section 2-3-2. The Prony parameters needed for this relationship need to be determined from tests. Next to this method of describing the viscoelasticity of a material, Abaqus provides the user with more freedom in prescribing the material behaviour. The user is enabled to write a Fortran code in the form of a so-called User Subroutine. The User Subroutine allows the user to implement time-dependent variables such as a varying load, temperature or material properties. Section 4-1-2 elaborates on one of the User Subroutines called UMAT, which can be used to model the time and stress dependent viscoelastic material behaviour. The constitutive relation between stresses and strains can be represented by a matrix equation, which includes shear deformation and deformations in multiple directions. In the case of 3D solid elements, a 6x6 stiffness matrix must be provided as the constitutive relation between the strains and stresses. However, in the case of using two dimensional shell elements for each ply, a 3x3 stiffness matrix suffices. Therefore, the constitutive relation between the stresses and strains for each ply can be represented by the matrix equation given in Eq. (3-4).

$$\begin{bmatrix}\sigma_1\\ \sigma_2\\ \tau_{12}\end{bmatrix} = \begin{bmatrix}Q_{11}(t,\sigma) & Q_{12}(t,\sigma) & 0\\ Q_{12}(t,\sigma) & Q_{22}(t,\sigma) & 0\\ 0 & 0 & Q_{66}(t,\tau)\end{bmatrix}\begin{bmatrix}\varepsilon_1\\ \varepsilon_2\\ \gamma_{12}\end{bmatrix} \tag{3-4}$$

The stiffness parameters Q_{ij} are based on the elastic moduli of the lamina, which can be determined from testing. How these stiffness parameters can be calculated is taken from both the Dutch design recommendation for FRP composite structures the CUR96 and the TS19101 [2, 74]. For the implementation of the elastic moduli parameters, the viscoelastic theory of Findley from Section 3-1 is used. Therefore, all the stiffness parameters in presented in the stiffness matrix each depend on the input stress and time. Eq. (3-5) gives the composition of each of these time and stress dependent stiffness parameters which can be used in the matrix equation given in Eq. (3-4).

$$\begin{aligned} Q_{11}(t,\sigma) &= \frac{E_1(t,\sigma)}{1-\nu_{12}\nu_{21}}\\ Q_{22}(t,\sigma) &= \frac{E_2(t,\sigma)}{1-\nu_{12}\nu_{21}}\\ Q_{12}(t,\sigma) &= \frac{\nu_{12}E_2(t,\sigma)}{1-\nu_{12}\nu_{21}}\\ Q_{66}(t,\tau) &= G_{12}(t,\tau) \end{aligned} \tag{3-5}$$

3-3 Summarizing and concluding remarks

Based on the amount of current knowledge and experimental work on creep tests at this moment, two analytical models from literature are chosen to implement in a numerical analysis of a FRP web core sandwich deck panel. These models are the power law of Findley and the superposition principle of Boltzmann. The power law of Findley can be used to describe the creep compliance (inverse of the time-dependent elastic modulus). BSP will be used to quantify the response for both creep and recovery cycles in time.

To validate the implementation of both these models in numerical analysis, a creep test done on a FRP pultruded I-section has been remodelled. A simple Euler-Bernoulli beam has been programmed with

a time-dependent elastic modulus based on the power law of Findley and the parameters found in the experiment. By using different parameters for the power law of Findley for the creep and recovery cycles together with BSP, an accurate prediction of the residual deformation and strain was found. However, using these parameters for shorter loading and longer recovery durations has resulted in strange deformation outcomes. These weird results find origin in the fact that the power law creates an ever increasing curve and thus superimposing two of such curves with different parameters will always lead to unstable results for the residual deformation when extrapolated to moments far away in time. Therefore, using the power law of Findley to describe the creep compliance in combination with BSP should be done with the same parameters for each creep and recovery cycle. Although, the prediction of the recovery deformation of the experiment was not entirely accurate, using the same parameters resulted in a conservative prediction of recovery behaviour.

The Findley fit parameters found in experiments done on UD-plies can differ at varying stress levels. Based on the linear relations proposed in Section 2-4-1, it could be assumed that there is a linear relation between the applied stress and the Findley parameter E_t. Figure 3-4 shows the results for the fit parameter E_t retrieved from creep tests done on UD-plies at different stress levels. For both the tensile and compression axial elastic moduli a linear relation between stress and the fit parameter have been found. According to literature, no relation was found between the exponential parameter in the power law and the stress level. Unfortunately, not enough data could be gathered to find a linear relationship for the Findley fit parameters that could be used to describe viscoelastic transverse or shear behaviour.

The analytical models and the experimental data on UD-plies can be implemented in a numerical model to predict long-term viscoelastic behaviour of a sandwich deck panel consisting of multi-directional laminates. Not all FEA software offer the availability to prescribe viscoelastic material properties for anisotropic or orthotropic materials. FEA software package Abaqus offers a feature called the User Subroutine, which allows the user to program a Fortran code that is implemented and used during the FEA. One of the subroutines that can be used to define complex material behaviour is called the UMAT subroutine and it can be used to define the viscoelastic properties in different directions for an orthotropic plate. Eq. (3-4) describes the time-dependent constitutive relation between the stresses and the strains. This equation has been implemented in the UMAT User Subroutine as part of the numerical model. Chapter 4 elaborates more on how this UMAT is programmed and how the relations found in this chapter are implemented.

Chapter 4

Creep analysis Abaqus

4-1 Model overview

As stated in Chapter 3, the analytical equations for predicting creep together with the parameters found are used in a numerical model. This numerical model calculates the creep and recovery deformation based on certain load inputs for certain duration periods in time. Having both the deformation curves for creep and recovery, use can be made of the superposition principle of Boltzmann [31]. The numerical model makes use of the Python programming language as input for the Finite Element Analysis software Abaqus. The User Subroutine module from Abaqus allows the user to program specific user defined material properties, such as viscoelastic properties for orthotropic materials. This User Subroutine module can be programmed with the programming language Fortran. The results that Abaqus gives for each creep and recovery cycle are then analysed (post-processed) with Python.

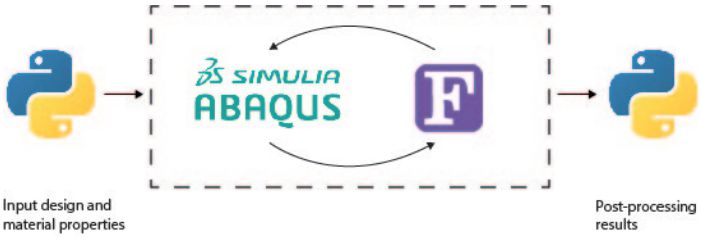

Figure 4-1: Use of programming and FEA within the entire numerical model

The numerical model can be represented in more detail with a flowchart in which all of the processes are given by multiple building block types. Figure 4-2 gives the flowchart corresponding to the numerical model that calculates the creep accumulation due to variable loading. Within this research the same Findley parameters are used for creep and recovery behaviour, which means that the Abaqus calculation only has to be done once [1]. However, when using alternative more precise models, a distinction must be made between the creep and recovery outcomes. The following subsections will each elaborate on the background of certain building blocks within this flowchart.

[1] Using Findley with different parameters for creep and recovery is not compatible with BSP, see Section 3-1-4.

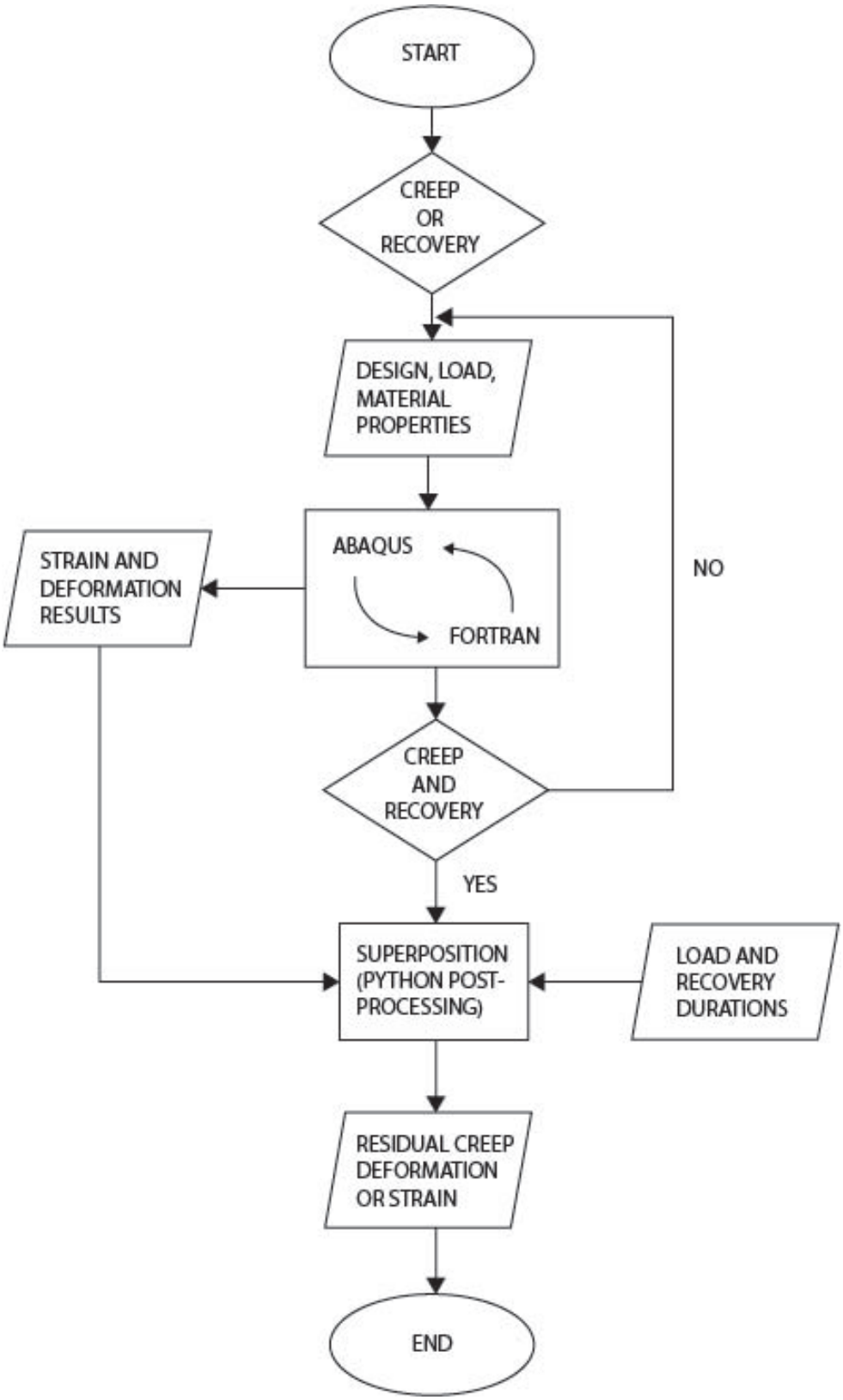

Figure 4-2: Flowchart of numerical model calculating creep under variable loading

4-1-1 Python and Abaqus

The reasoning behind the use of Abaqus is already explained in Chapter 3. It essentially comes down to the fact that it is possible to prescribe viscoelastic material properties in anisotropic and orthotropic materials. Besides, Abaqus enables the user to change the material properties in time and it can evaluate the outcome at multiple time steps during an user defined time interval. Modelling a structure in Abaqus does not differ much from modelling a structure in other FEA software. However, in contrast to other FEA software packages Abaqus enables to script a model by using Python. Python scripting with Abaqus is a very effective tool for pre-processing. It is mostly used for doing a parametric study, create repetitive geometry and to manage multiple job submissions. Post-processing is always done through Abaqus .odb files, which is a database file that contains all the selected results such as stresses, strains, deformations and many other types of output. Abaqus also allows to post-process the .odb output files with Python and enables to automate processes such as the visualisation of results within the model and extracting detailed information of selected nodes or elements.

4-1-2 User Subroutine

The User Subroutine module from Abaqus is quite an unique feature compared to other FEA software on the market. Only the alternative software package Ansys is known to have a comparable kind of feature, which enables the user to code specific material properties, loading configurations, temperature changes and many other varying variables in time. How such a User Subroutine works can be explained by Figure 4-3. for a certain input, Abaqus calculates certain mechanical variables such as stress or strain for each element (1). This data is passed through the User Subroutine to the Fortran compiler (2). The Fortran compiler can be programmed by the user to let some of the discussed properties change for each increment and sends the adjusted data back the element of interest (4). The results at the end of that increment are used as new input for the next increment.

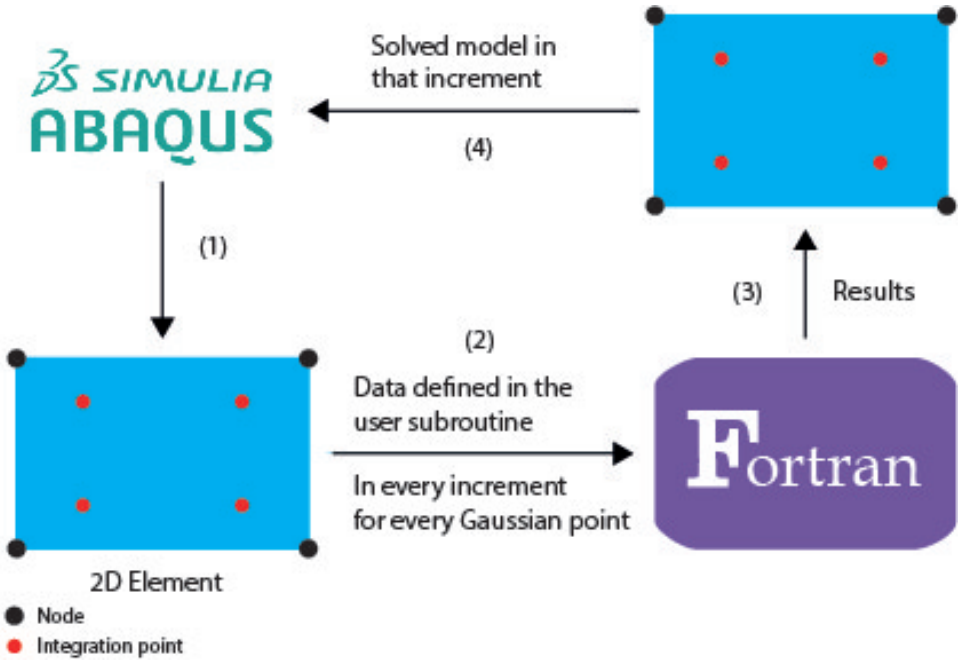

Figure 4-3: Representation user subroutine of one increment step for one element

To perform a viscoelastic analysis on a FRP composite, use could be made of the User Subroutine called UMAT. The User Subroutine UMAT, which stands for user material, allows the user to define the mechanical constitutive behaviour of a material. The definition of the material behaviour or the constitutive relationship between the stresses and the strains in the model can be described by Eq. (3-4) and Eq. (3-5) from Section 3-2-2. The implementation of the User Subroutine within the Fortran compiler, represented in Figure 4-3 (2), is by starting the program with the lines presented in Figure 4-4. These lines can be obtained from the Abaqus Documentation module, provided by Abaqus.

```
      SUBROUTINE UMAT(STRESS,STATEV,DDSDDE,SSE,SPD,SCD,
     & RPL,DDSDDT,DRPLDE,DRPLDT,STRAN,DSTRAN,
     & TIME,DTIME,TEMP,DTEMP,PREDEF,DPRED,MATERL,NDI,NSHR,NTENS,
     & NSTATV,PROPS,NPROPS,COORDS,DROT,PNEWDT,CELENT,
     & DFGRD0,DFGRD1,NOEL,NPT,KSLAY,KSPT,KSTEP,KINC)

      INCLUDE 'ABA_PARAM.INC'
      PARAMETER (EPS=2.22D-16)

      REAL E1o, E2o, PR12o, PR13o, G12o
      REAL E1t, E2t, G12t, G23t, n1, n2, n12
      REAL E1, E2, G12, G23, PR12

      CHARACTER*80 MATERL
      DIMENSION STRESS(NTENS),STATEV(NSTATV),
     & DDSDDE(NTENS,NTENS),DDSDDT(NTENS),DRPLDE(NTENS),
     & STRAN(NTENS),DSTRAN(NTENS),TIME(2),PREDEF(1),DPRED(1),
     & PROPS(NPROPS),COORDS(3),DROT(3,3),
     & DFGRD0(3,3),DFGRD1(3,3)
```

Figure 4-4: User subroutine provided by Abaqus Documentation

In this part of the Fortran code all the variables that are passed by Abaqus are initialized. For the viscoelastic analysis based on time and stress input, a couple of these parameters are of importance and their meanings are listed below.

- NTENS: size of the stress or strain component array
- PROPS(i): user defined material property
- TIME(1): value of time at the beginning of the increment
- DTIME: time difference of start current increment to the next
- STRESS(NTENS): stress tensor at the beginning of the increment (must be updated)
- STRAN: array containing the total strains at thte beginning of the increment
- DTRAN: array containing the strain increment at each increment step
- DDSDDE: Jacobian matrix of the constitutive model

This data can then be accessed by the Fortran compiler for user defined computations. These computations are, in the case of a viscoelastic analysis, based on the theory from Chapter 3. The initial elastic and viscoelastic material properties are passed by Abaqus and then converted to the creep compliance notation. As stated before, this is simply the inverse of the time-dependent elastic modulus. How these variables are defined and converted is presented in Figure 4-5.

```
!   INITIAL PARAMETERS OF THE UD-PLIES
      D1o      = 1/PROPS(1)
      D2o      = 1/PROPS(2)
      D12o     = 1/PROPS(3)
      PR12o    = PROPS(4)

!   STRESS DEPENDENT FINDLEY PARAMETERS BASED ON TESTS
     IF(STRESS(1).EQ.0.0) THEN
          D1t = 0.0
     ELSE IF(STRESS(1).GT.0.0) THEN
          D1t = 1/(PROPS(5)+7.6*STRESS(1))
     ELSE
          D1t = 1/(PROPS(6)+7.1*STRESS(1))
     ENDIF
     D2t   = (1/PROPS(7))
    D12t   = (1/PROPS(8))

!   STRESS INDEPENDENT FINDLEY PARAMETERS BASED ON TESTS (VISCOSITY PARAMETER)
     IF(STRESS(1).EQ.0.0) THEN
          n1 = 0.0
     ELSE IF(STRESS(1).GT.0.0) THEN
          n1 = PROPS(9)
     ELSE
          n1 = PROPS(10)
     ENDIF
     n2    = PROPS(11)
     n12   = PROPS(12)

!    FINDLEY'S POWER LAW FOR ELASTIC REDUCTION (COMPLIANCE NOTATION)
     E1    = 1/(D1o+D1t*(Time(2)+DTime)**n1)
     E2    = 1/(D2o+D2t*(Time(2)+DTime)**n2)
     G12   = 1/(D12o+D12t*(Time(2)+DTime)**n12)
     PR12  = PR12o
```

Figure 4-5: Creating variables from the material properties Abaqus passes through

The final stress and time-dependent moduli at the end of the increment can then be calculated according to the theory of Findley is given in Section 3-1. How this is coded in the Fortran code is given in Figure 4-6.

```
!    FINDLEY'S POWER LAW FOR ELASTIC REDUCTION (COMPLIANCE NOTATION)
     E1    = 1/(D1o+D1t*(Time(2)+DTime)**n1)
     E2    = 1/(D2o+D2t*(Time(2)+DTime)**n2)
     G12   = 1/(D12o+D12t*(Time(2)+DTime)**n12)
     PR12  = PR12o
```

Figure 4-6: Theory of Findley for reduction of the elastic moduli caused by creep phenomenon

These results for the time increment of interest must be rewritten in the form of a 3x3 stiffness matrix to describe the constitutive relation between the strains and stresses. This stiffness matrix can be described by Eq. (3-4) with the stiffness parameters according to Eq. (3-5) from Section 3-2-2. How this is done within the Fortran code is shown in Figure 4-7, where first an empty 3x3 matrix is initialized based on the number of stress or strain components passed by Abaqus. Then, the calculated time and stress dependent elastic moduli are used for the definition of the stiffness parameters in the stiffness matrix.

```
!     SETUP EMPTY STIFFNESS MATRIX
      DO K1=1,NTENS
        DO K2=1,NTENS
          DDSDDE(K1,K2)=0.0D0
        ENDDO
      ENDDO

!     PUT TIME-DEPENDENT ELASTIC PARAMETERS IN EMPTY STIFFNESS MATRIX
       !  PR21   = PR12*E2/E1
       DDSDDE(1,1)  = -1/(-E1+PR12**2.*E2)*E1**2.
       DDSDDE(1,2)  = -PR12*E1/(-E1+PR12**2.*E2)*E2
       DDSDDE(2,1)  = DDSDDE(1,2)
       DDSDDE(2,2)  = -E1/(-E1+PR12**2.*E2)*E2
       DDSDDE(3,3)  = G12
```

Figure 4-7: Stiffness matrix, describing the constitutive time and stress dependent material behaviour

Finally the stress at the end of the increment, corresponding to the new elastic moduli and strain, must be calculated within the Fortran compiler and returned to Abaqus. How this is programmed within the Fortran compiler is given in Figure 4-8. In Figure 4-3 this is illustrated by step (3) and (4). Other results such as deformation of the nodes and strains are automatically calculated and returned to Abaqus.

```
!     CALCULATE STRESS AT THE END OF THE STEP, BASED ON NEW STIFFNESS PARAMETERS
      DO K1=1,NTENS
        STRESS(K1)=0.0D0
        DO K2=1,NTENS
          STRESS(K1)=STRESS(K1)+DDSDDE(K2,K1)*(STRAN(K2)+DSTRAN(K2))
        ENDDO
      ENDDO

      RETURN
      END
```

Figure 4-8: Calculation of stress and returning it to Abaqus

4-1-3 Python post-processing

From Figure 4-2 it can be seen that before the post-processing in Python can be done, Abaqus already calculated the deformation curve for both a creep cycle and a recovery cycle for the entire lifetime. These time-dependent deformation and strain results are caused by decreasing elastic moduli, which find basis in the power law of Findley. This means that the results for deformation and strain will follow some power law like outcome. To find the correct fit parameters, a curve is fitted to the results from Abaqus. A final power law for the creep deformation and recovery deformation is found and both of these can now be superimposed according to the principle of Boltzmann from Section 2-3-2. Figure 4-9 shows how these superposition for one creep and one recovery cycle should look like.

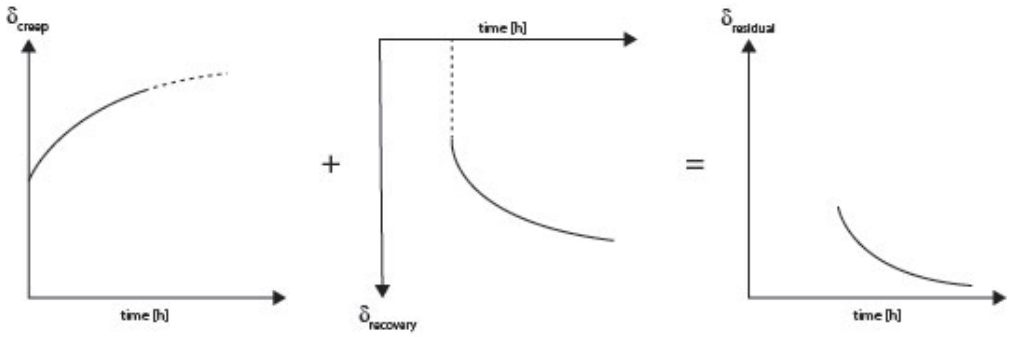

Figure 4-9: Representation of the superpositioning of one creep and one recovery cycle

To calculate the residual deformation at a specific time, each historic creep and recovery cycle should be included in the calculation for that given time. This means that the creep and recovery cycle from day one after installation together with the recovery cycle result in a ever decreasing residual deformation. When the final deformation at the end of the lifetime is analysed the residual deformation resulted from that first creep-recovery cycle at that far away point in time should be considered and not before that point in time. Considering a lifetime of 100 years this means that the contribution of the first creep-recovery cycle is the residual deformation that can be calculated at 100 years. For the second creep-recovery cycle this means the residual deformation at 100 years minus the starting time of the corresponding load cycle should be evaluated. Looping over all these creep-recovery durations should result in many residual deformation results at the time of verification (end of lifetime). The sum of these residual deformations can be seen as the creep deformation formed by a certain amount of creep-recovery cycles, which represents the loading and unloading of both daily morning and evening traffic jams.

4-2 Abaqus model validation

To validate the numerical model, including the User Subroutine Fortran code and the Python post-processing code, the creep-recovery experiment from Section 3-1-2 is remodelled in Abaqus. During this experiment the viscoelastic parameters used in the power law of Findley are determined from the entire flexural beam test. Therefore, during the analysis of the simply supported pultruded I-section beam, these parameters are used and no stress dependency is taken into account. The creep experiment was a four point bending test that took 1600 hours with a recovery time of 148 hours afterwards. The loading configuration that was modelled in Abaqus is given by Figure 4-10.

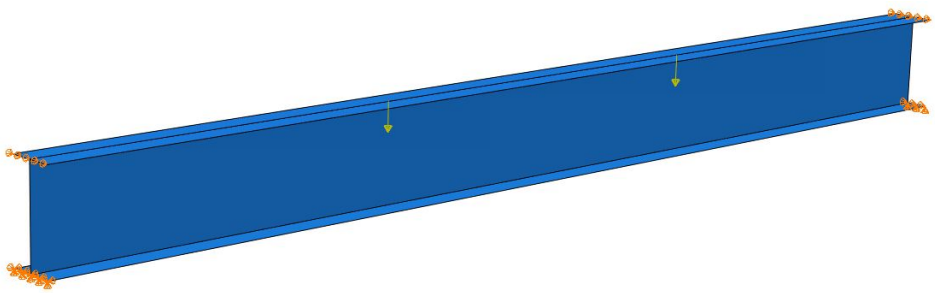

Figure 4-10: Load configuration in Abaqus of experiment M.Sá [9]

All the parameters concerning the design and dimensions of the cross-section, the loading configuration, exact loading duration and the material properties can be retrieved from Section 3-1-2. To see if the model gives results that correspond to the outcome of the experimental tests done by M.Sá, the longitudinal strain (ε_{11}) of the middle element is monitored during the analysis. This data from Abaqus is then compared with the data from the strain gauge placed on top of the flange in the middle of the beam during the experiment.

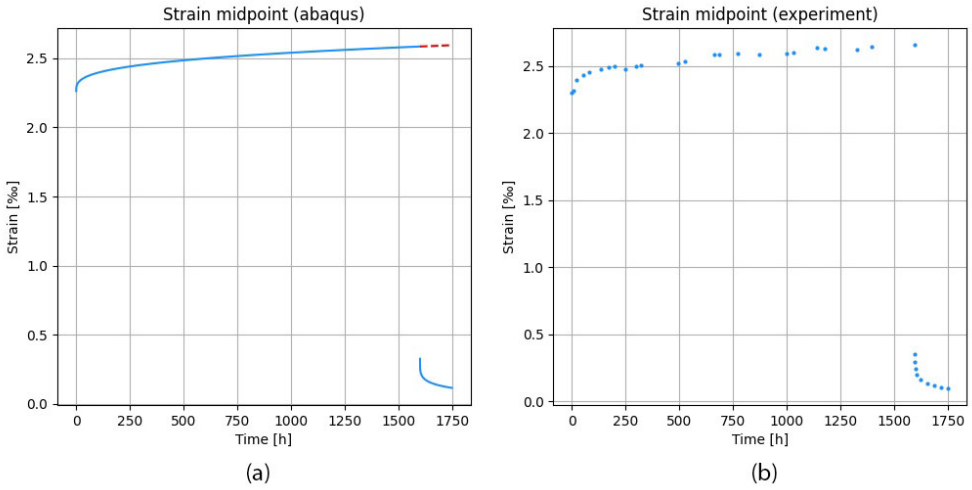

Figure 4-11: Axial strain results Abaqus (a) and strain gauge results from experiments M.Sá (b)

From Figure 4-11 it can be concluded that the model has a very precise prediction of the experimental work. This is partly due to fitted parameters found by M.Sá during the tests for this specific design, load configuration and initial elastic material properties. However, it is still a good and satisfying validation to see that the Abaqus model and the Python post-processing code are working properly. Figure 4-12 and Figure 4-13 show the longitudinal strains in the model at the beginning and the end of the creep cycle respectively.

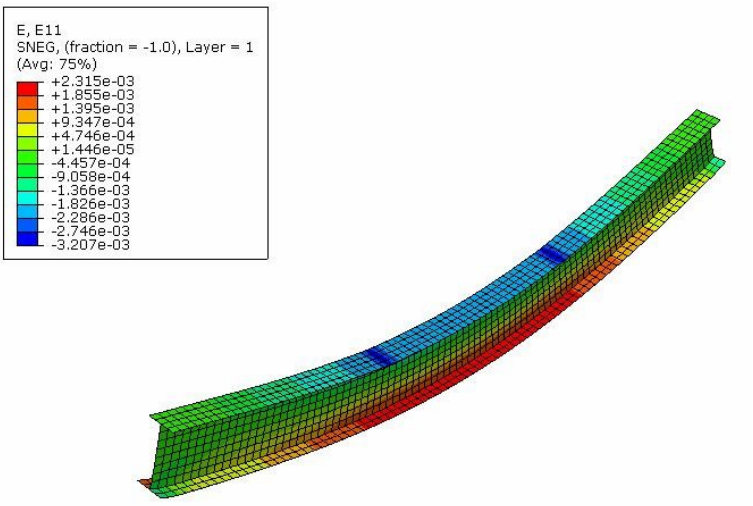

Figure 4-12: Axial strain results Abaqus model at time $t = 0h$

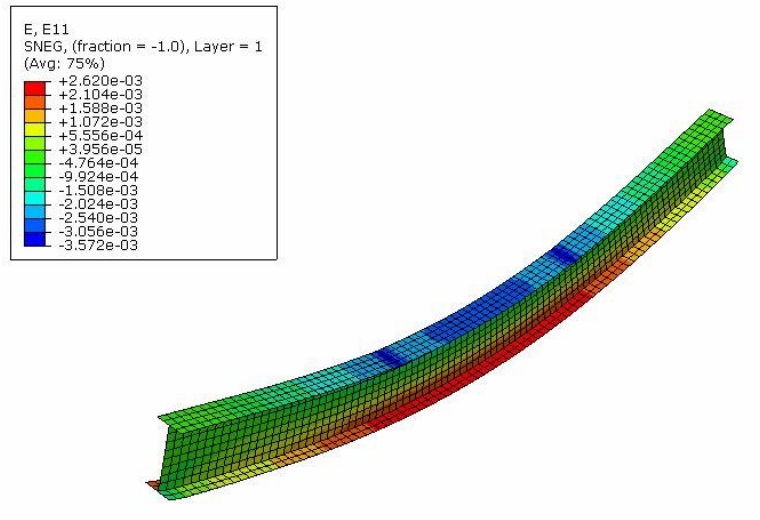

Figure 4-13: Axial strain results Abaqus model at time $t = 1600h$

The high axial compressive strains in the compression zone are located near the concentrated loads and could be neglected for the global analysis of creep in the beam. These higher strains are caused by singularities at the loading locations. The distribution of the forces over a small area will reduce these strains at these locations. Therefore to see what the maximum strains are in the middle of the beam, the maximum tensile strain that occurs gives a reliable value. From Figure 4-12 the maximum creep strain in the middle of the beam is 2.315‰in both the tensile and compression zone. From experiments the axial strain at the top flange in the middle of the beam was almost identical with 2.305‰. The axial strain after 1600 hours in the Abaqus model is calculated at 2.62‰and the outcome of the experiment was 2.65‰. Concluding from these values it could be stated that the numerical model gives very accurate results in the case of using different parameters for both creep and recovery cycles. The deformation of the nodes in the middle of the modelled I-beam are also monitored during the creep analysis for a comparison with the reported experimental results from the experiments done by M.Sá. Figure 4-14 (a) shows the results of the creep deformation of the middle section of the beam calculated by Abaqus and expressed as percentages of the initial elastic strain and Figure 4-14 (b) shows the results from the experiments done.

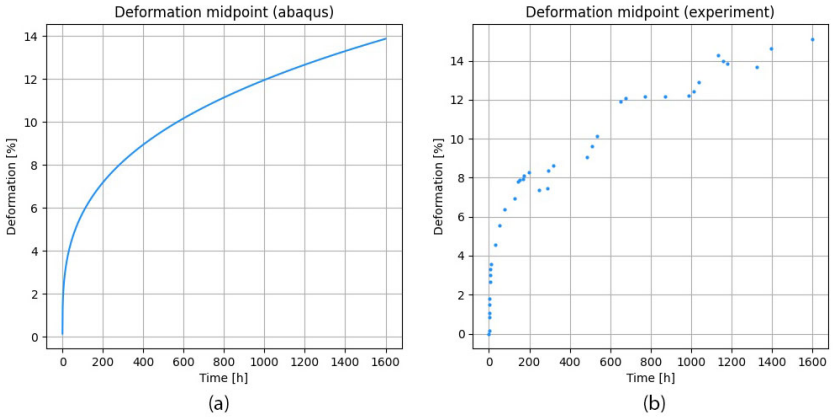

Figure 4-14: Percentage creep strain calculated by Abaqus (a) and from experiments (b)

Concluding from Figure 4-14, it could be stated that the model also has a very accurate prediction for the deformation of the beam provided that the fit parameters correspond well to experimental results. The use of the numerical model for a FRP sandwich deck panel is justified.

4-3 Summarizing and concluding remarks

Figure 4-2 gives a global overview of how the numerical model including Findley and BSP should be combined and implemented into a numerical model including FEA. The rest of Section 4-1 elaborates more on how the UMAT actually looks like and how the findings from Chapter 3 are implemented within the User Subroutine. The model has been validated by remodelling the same experiment that is analysed in Chapter 3. Again, a great correspondence have been found when different parameters are used for the creep and recovery behaviour between the simulation and the experimental results. This validation confirms that both the UMAT and the BSP Python post-processing program are coded correctly. The same code could now be used for the analysis of a sandwich deck panel consisting of different multi-directional laminates for the face sheets and the webs. This is done for a specific case study in Chapter 5.

Chapter 5

Case Study: Pijlebrug, Meppel

The technical committee CEN-TC250, who is responsible for developing the structural Eurocodes, is developing a technical specification (TS19101) as pre-draft for the Eurocode about Fiber-Reinforced Polymer structures. Multiple examples have been made to help engineers understand the TS19101. This case study is about the creep deformation in one of these examples, which was about the design of a FRP sandwich deck panel applied in the Pijlebrug in Meppel (The Netherlands). This bridge has been tested and built in The Netherlands in 2014-2015 and has been in use since then. The provided example should clarify how to correctly determine material properties in preliminary design and how engineers can verify the structural integrity in both ULS and SLS. The authors that constructed this worked example are given in Figure 5-1.

AUTHOR(S)	*Authors:* Liesbeth Tromp[a], Martijn Veltkamp[b], Ane de Boer[c], Johan de Boon[d], Mathieu Koetsier[e] *Contributors:* Georgios Zarifis[f], Sander van Alphen[g], Wouter Claassen[f], Lieuwe Cornelissen[a], Jan Hiddingh[h], Remco Renting[h], Arjen Steenbrink[g], Ward Steijn[i]. a Royal HaskoningDHV b FiberCore Europe c Ane de Boer Consultancy d Rijkswaterstaat e Delft University of Technology f Witteveen+Bos g Movares h Province Groningen i Lantor

Figure 5-1: Authors who constructed and worked on the example about the Pijlebrug

In this chapter the design of the sandwich deck panel will be given and a creep analysis based on the TS19101 will be performed. The same design is going to be used in the Python-Abaqus-Fortran numerical model from Chapter 4. In Chapter 6 the results from bot analyses will be compared to see how much the models differ in deformation and a conclusion could be made for the influence of the traffic load on the creep accumulation.

5-1 General information Pijlebrug

As stated before, the worked example provides the reader of a clarification on the analysis and verifications of both Serviceability Limit States (SLS) and Ultimate Limit States (ULS). However, due to the scope of this thesis, only SLS will be taken into account.

5-1-1 Global design

The Pijlebrug is a regional bridge with a bridge deck that spans 8.3 m, designed for the load models LM1 and LM2. It has a design service life of 100 years and can be classified as a structure of consequence class CC2 and fatigue traffic class 3 [23]. For the purpose of the worked example, the calculation is done on a simplified version of the deck. The simplification lead to the design of a single lane rectangular composite road deck panel, supported at both ends with simple line supports. Torsion in the deck can be neglected due to the fact that the example is a single lane deck. The bridge design is given in Figure 5-2(a) and the deck panel that is used in the worked example and in this case study is given in Figure 5-2(b).

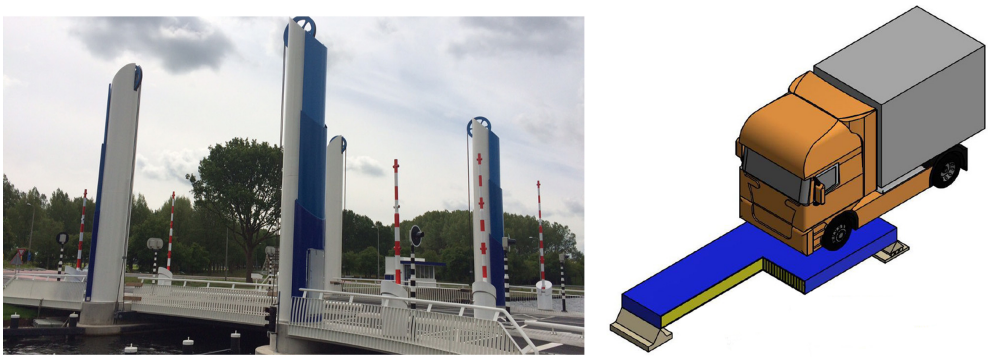

Figure 5-2: The Pijlebrug in Meppel, The Netherlands, (a) and the design of the example (b)

The global design and the dimensions of both the Pijlebrug and the design used in the example are given in Table 5-1. It could be seen that for the example some simplifications were done.

	Pijlebrug produced panel	**Worked example model**
Length	8286 mm	7350 mm
Span	7880 mm	7350 mm
Width	13600 mm	3026 mm
Boundary conditions	Rigidly connected to steel lifting beams	Simply supported by line supports on both ends
Shape in plan	Skew (80°)	Rectangular (90°)
Materials	Composite deck and steel beams	Composite only
Total thickness of the deck	430 mm	430 mm

Table 5-1: Global dimensions and design of the Pijlebrug and the worked example

The simplification of one lane in the example does influence the load transfer of the deck. Calculating one lane deck simply supported by two line supports, will reduce the effects in the transverse direction. However, a wider deck will lead to transverse effects that could not be neglected. Therefore, if the transverse webs and a second lane are added to the design calculation, this will definitely lead to other results and verifications.

5-1-2 Cross-sectional design

The dimensions and design of the bridge deck used in the worked example for the TS19101 are given in Table 5-2. Figure 5-3 shows the corresponding dimensions within the design of the cross-section of the applied web core sandwich deck panel. As stated before, not all the structural elements will be included in the creep analysis of the deck.

Structural element	**Parameters**	**Material and orientation**
Top and bottom face sheet (X_f)	t_f = 25.7 mm	GFRP75 $[0/90/0/0]_s$ V_f = 52%
Longitudinal webs (X_w)	h_w = 404.3 mm t_w = 6.9 mm b_w = 104.1 mm	GFRPQI $[0/90/45/\text{-}45]_s$ V_f = 28%
Transverse webs (X_{tw})	h_{tw} = 404.3 mm t_{tw} = 2.1 mm b_{tw} = 130.0 mm	GFRPQI $[0/90/45/\text{-}45]_s$ V_f = 28%
Endplate (X_{ep})	t_{ep} = 25.7 mm	GFRP75 $[0/90/0/0]_s$ V_f = 52%
Core material (X_c)	t_c = 378.6 d = 404.3 mm	Polyurethane foam, non-structural

Table 5-2: Global dimensions and design of the Pijlebrug and the example

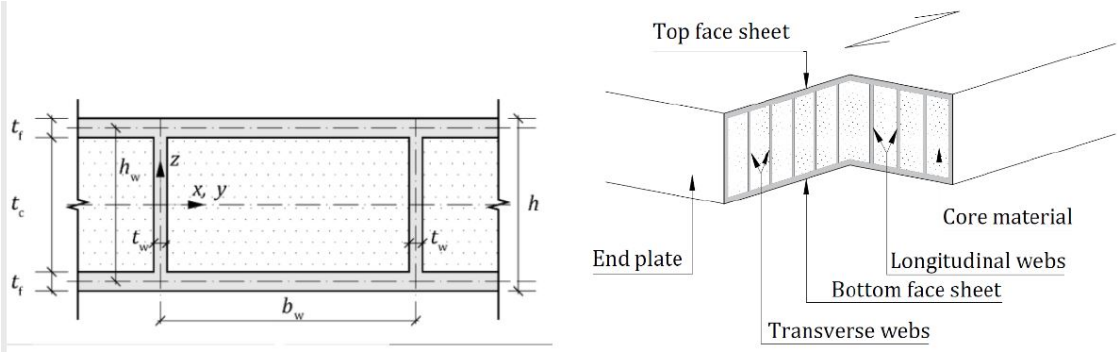

Figure 5-3: Dimensions with corresponding parameters of the web core sandwich deck panel

5-2 Material properties

Table 5-2 gives the different layups of all the structural elements in the beam. However, to describe the material in more detail per structural element, the base materials are elaborated on and listed below.

- **Fiber reinforcement**: E-Glass (Jushi 386 Direct Roving). The glass fibers contain a sizing to optimise the bonding between the fiber and the polyester resin.
- **Resin**: unsaturated DCPD based polyester resin (DSM Synolite 1967-N/X-1).
- **Fiber architecture**: the ply stack is a symmetric and balanced with the following layups:
  - **GFRP75**: $[0/90/0/0]_s$ with 75% of the fiber reinforcement placed in the x-direction of the local coordinate system of the laminate and 25% in the y-direction. The laminate contained a fiber volume fraction of $V_f = 52\%$ and a density of 1880.0 kg/m^3.
  - **GFRPQI**: $[0/90/45/-45]_s$ with 25% of the fiber reinforcement in the x-direction of the local coordinate system of the laminate, 25% in the local y-direction and 50% in the 45°and -45°direction with respect to the local x-axis of the laminate. The laminate contained a fiber volume fraction of $V_f = 28$ % and a density of 1564.0 kg/m^3.
- The production method of the panel is vacuum infusion. The bridge deck structure is entirely produced in one step.

In the example use is made of the conversion factors presented by the TS19101 for the reduction of strength and stiffness properties caused by temperature and moisture effects. To compare the creep deformation due to traffic loads based on both the procedure according to the TS19101 and the procedure of combining Findley and BSP, these conversion factors are neglected. These factors should be included in a verification, but the same reduction must be done in both procedures and will therefore not lead to any differences between the results. Eq. (5-1) shows how the design values of the material properties in verification should be calculated. However, for the values of the elastic moduli and the Poisson's ratios the mean values are used.

$$R_d = \frac{1}{\gamma_{Rd}} \cdot (\eta_{c,i} \cdot \frac{X_k}{\gamma_M}) \tag{5-1}$$

In this equation R_d represents the design value of a material property, γ_{Rd} is a partial factor accounting for the uncertainty in the resistance model, γ_M is a partial factor accounting for unfavourable deviations of the material or product properties. Within the example, use is made of the mechanical properties for the entire laminate retrieved from tests. The creep calculation based on the combination of Findley and BSP together with results from tests done on UD specimens, so the model works for a greater variety of layups. The model from the example is recreated based on UD-plies with the properties retrieved from the TS19101 [42]. Table 5-3 shows the properties that are determined from the TS19101 for the applied sandwich deck panel. How these parameters are determined is given in Appendix E.

Parameter	Flange	Web
E_1	38.9 [GPa]	22.4 [GPa]
E_2	11.5 [GPa]	6.50 [GPa]
G_{12}	3.80 [GPa]	2.87 [GPa]
ν_{12}	0.322	0.358

Table 5-3: Global dimensions and design of the Pijlebrug and the example

The Classical Laminate Theory (CLT) is used to combine the ply properties into one laminate and to find the corresponding elastic properties. The properties presented in Table 5-4 are based on the laminate properties that were presented by the worked example and based on UD-ply properties retrieved from the TS19101.

Parameter		**Worked example**		**TS19101**	
		Flange	Web	Flange	Web
E_1 [MPa]	Tensile	33832.0	11405.0	32268.7	11497.0
	Compression	36619	-	-	-
E_2 [MPa]	Tensile	16042.0	11199.0	18509.3	11497.0
	Compression	20731.0	-	-	-
G_{12} [MPa]	-	4000.0	4400.0	3813.2	4289.9
ν_{12}	-	0.146	0.340	0.201	0.340
ν_{21}	-	0.069	0.340	0.115	0.340

Table 5-4: Stiffness properties of the laminate based on testing and TS19101

It can be seen that most of the stiffness properties that are calculated correspond quite well with the laminate properties retrieved from testing. Only the transverse elastic moduli for both the flange and web contain non-negligible differences between the two procedures. Therefore, a linear elastic analysis is performed and the instantaneous deformations, caused by the permanent loads, are compared. Figure 5-4 (a) shows the deformation due to self-weight, based on the ply properties from TS19101 and calculated by Abaqus. Figure 5-4 (b) shows the self-weight deformation from the worked example based on laminate properties which are retrieved from tests and calculated with the FEA software RFEM.

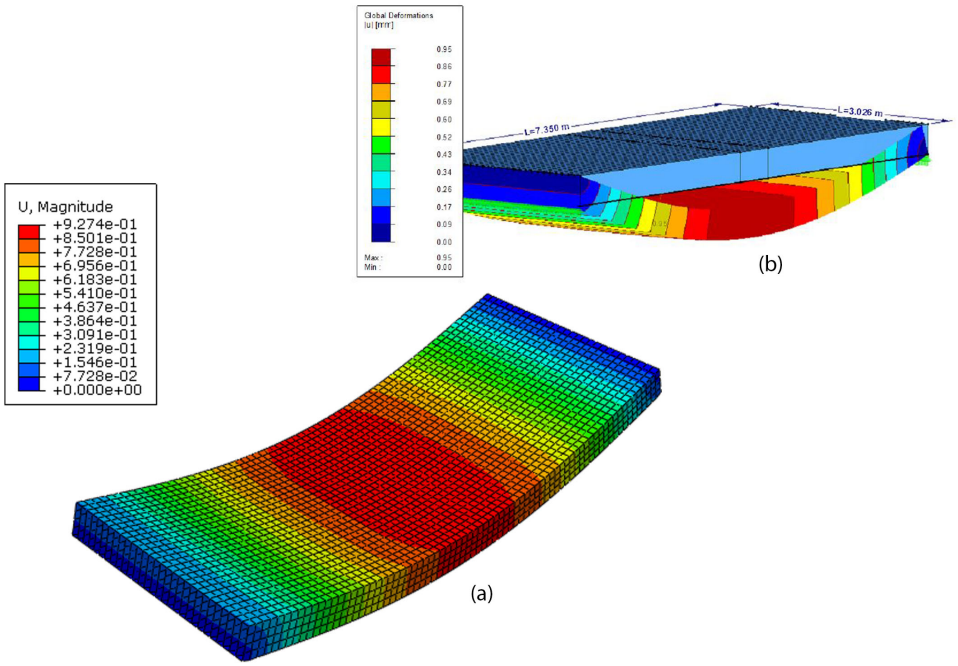

Figure 5-4: Deformation based on properties from TS19101 (a) and from laminate testing (b)

From Figure 5-4 it can be seen that the deformation, based on the UD-ply properties from preliminary design in TS19101, is equal to 0.93 mm. The maximum deformation based on the laminate properties retrieved from the worked example resulted in 0.95 mm. It could be concluded that the deformations are very close and using the UD-ply properties from TS19101 is justified for this case study.

5-3 Actions

The load cases and loading combinations that are of interest are discussed in this section. Appendix F gives more background information on the possible loading combinations and load models. Due to the scope of this thesis, not all loading combinations and verifications are taken into account. The purpose of this analysis is to find the influence of the traffic load on the creep deformation of the structure. Therefore, other loading combinations used for ULS are not considered within this report.

5-3-1 Loads

The two types of loads on the structure could be classified as permanent loads and variable loads. Both of the load types will be taken into account for the creep deformation analysis separately. The following subsections provide the characteristic values of all the permanent and variable loads that are taken into account during the analysis.

Permanent Loads

The permanent loads are largely caused by the self-weight of the structure with some added safety elements like guardrails. The **permanent loads** used in this case study are listed below.

- **Self-weight of the laminates**
  - Top & bottom face sheets — 1880 kg/m^3
  - Longitudinal webs — 1564 kg/m^3
  - Transverse webs — 1564 kg/m^3
  - Endplates — 1880 kg/m^3
- **Self-weight foam core**
  - Density foam — 33 kg/m^3
  - Equivalent UDL — 0.124 kN/m^2
- **Self-weight surfacing**
  - Area weight — 15 kg/m^2
  - Equivalent UDL — 0.15 kN/m^2
- **Self-weight surfacing**
  - UDL — 1.0 kN/m^2

The entire permanent load that is acting on the structure is retrieved from the worked example. The total sum of permanent loads sums up to a final total characteristic distributed permanent load of **1.72 $\mathbf{kN/m^2}$**. This is also the load that is used to compare the elastic instantaneous deformation between the worked example build up from laminate properties and the model used for this case study, build up from UD-ply properties retrieved from the TS19101, in Figure 5-4.

Variable loads

To analyse the final creep deformation, only the vertical variable loads are taken into account. **Load model 1** (LM1) has been chosen as the most appropriate load model for the creep analysis of the sandwich deck panel applied in the Pijlebrug. This load model represents most of the actions caused by heavy trucks and passenger cars. The sandwich deck panel is modelled with a width that corresponds to the width of one driving lane. LM1 presents multiple different distributed loads and axle loads for different lanes. The loads that are placed in the most governing lane are taken into account in this model and multiplied with the correction factors prescribed by the NEN-EN1991-2 [23]. Eq. (5-2) and Eq. (5-3) give both the characteristic values used for the traffic load applied on the sandwich deck panel. Appendix F gives some more background on the load models and elaborates on the correction factors used.

$$\alpha_q q_k = 10.35\ kN/m^2 \tag{5-2}$$

$$\alpha_Q Q_k = 300\ kN \tag{5-3}$$

The 300 kN axle load can be divided over two wheel areas, which means that for each wheel a load of 150 kN needs to be distributed over a surface area of 400x400 mm according to NEN-EN1991-2. Figure F-4 from Appendix F shows the distances between the wheel surface areas. The wheel loads are placed on the sandwich deck panel in such a way that the centre of the wheel loads correspond with the centre of the loaded area. This is the most unfavourable position of the wheel loads and will cause the highest deformation.

5-3-2 Loading combination

In case of (SLS) verifications, in which deformations of a structure are verified, the characteristic load combination should be used. Using the characteristic load combination means that the partial safety factors used for ULS analysis could be neglected. The partial safety factors for SLS are equal to one ($\gamma_i = 1.0$). For SLS verifications including long-term effects such as creep and shrinkage the so-called quasi-permanent load equation must be used. This loading combination differs slightly from the general characteristic load combination. Eq. (5-4) shows the loading combination that needs to be used for the calculation of the long-term deformation at the end of the lifetime of a structure.

$$\sum_{j \geq 1} G_{k,j} + P + \sum_{i \geq 1} \psi_{2,i} Q_{k,i} \tag{5-4}$$

Eq. (5-4) identifies three different types of loading. $G_{k,j}$ represents the permanent loads on the structure, which are present during the entire lifetime. P represents the pre-stress on the structure, if applied. $Q_{k,i}$ represents the variable loading, which in this case study only represents the vertical traffic load according to LM1 with both the distributed load from Eq. (5-2) and the axle load from Eq. (5-3). The NEN-EN1991-1 prescribes a $\psi_{2,i}$ factor of 0.0 for the influence of traffic load on the final creep deformation, which means that no traffic loading is considered in the creep accumulation. However, the Dutch National Annex does prescribe a higher $\psi_{2,i}$ factor of 0.4, which means that 40% of the traffic load is considered in the long-term creep deformation. Due to the scope of this thesis, both the deformation based on the permanent loads and the deformation based on variable loads will be analysed separately. The final long-term creep deformation caused by the permanent loads will be calculated according to the TS19101 and according to the presented Findley model together with the appropriate parameters from Chapter 3. The results of both these analyses will be compared in Section 5-4 as verification of the safety and applicability of the found parameters of Findley.

5-4 Self-weight creep deformation

To validate the creep model of Findley, used for all the creep and recovery cycles in the superposition principle of Boltzmann, a static creep analysis is done according to both the procedures of Findley and TS19101. The aim of this comparison is to validate if the parameters of Findley used in the creep analysis give a deformation, which is in the same range as the deformation that results from the TS19101 procedure. The self-weight of the structural elements and the weight of the wear surface (0.15 kN/m^2) have been taken into account. The sum of both loads result in an area load of 1.72 kN/m^2. The self-weight can be modelled as a uniform distributed load over the entire surface area of the sandwich deck panel. Figure 5-5 gives the load configuration of the permanent loads that act on the sandwich panel.

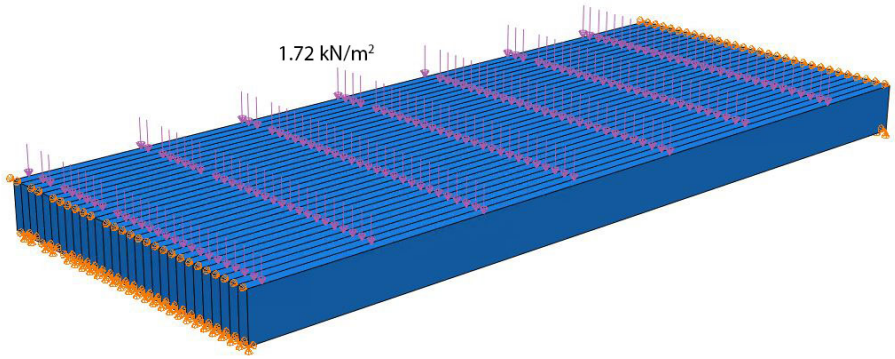

Figure 5-5: Load configuration permanent loads on the structure

The input variables for each analysis and the results corresponding to each of these analyses are discussed in the following subsections. A final comparison is made to validate the use of the parameters of Findley from Section 3-1-4, which are retrieved from literature.

5-4-1 Findley creep permanent loading

The cross-sectional design and material properties used in this analysis can be retrieved from Section 5-1-1 and Section 5-1-2 respectively. The used Findley parameters are given in Table 3-1, but are again given in Table 5-5.

Overview of Findley's parameters		
Parameter	Creep and recovery parameters	Author
E_{1t} (+)	943.0 + 7.5 x σ [GPa]	J. Siccama [14]
E_{1t} (-)	416.5 + 14.7 x σ [GPa]	Y. Choi [19]
E_{2t}	23.0 [GPa]	J. Siccama [14]
G_{12t}	22.8 [GPa]	M. Bottoni [16]
n_1	0.10	J. Siccama [14]
n_2	0.22	J. Siccama [14]
n_{12}	0.25	M. Bottoni [16]

Table 5-5: Findley parameters to be used for multi-directional laminates

Two self-weight creep analyses are done from which one was with both the same Findley parameters for the longitudinal tension and compression elastic moduli. The second analysis was with different Findley parameters for the parts in compression. A clear difference could be found between the final long-term results of the two analyses. Figure 5-6 (a) shows the final deformation after a 100 year service life using the same Findley parameters for the compression and tensile zones. Figure 5-6 (b) shows the results from the same analysis done with different Findley parameters for the compression and tensile elastic moduli.

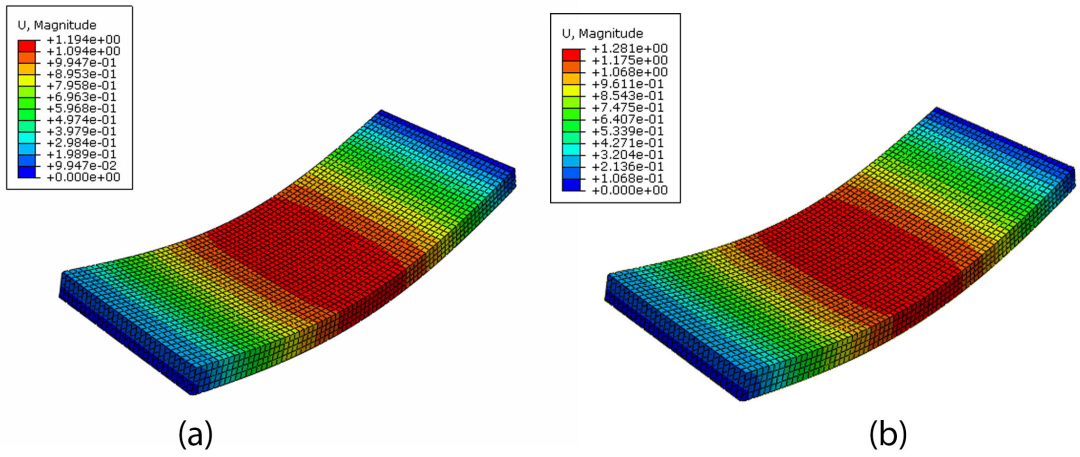

Figure 5-6: Long-term results creep deformation based on Findley parameters from Table 3-1

The results of both analyses will be compared with the results from the TS19101 procedure, to see which one corresponds better with the creep outcome resulting from the TS19101 procedure.

5-4-2 TS19101 creep permanent loading

Section 2-5-3 explains how the technical specification accounts for creep. Basically, it comes down to a simple formula for the reduction of the elastic moduli by using a given creep coefficient or ϕ-factor. Eq. (2-54) gives the general form for the reduction of the elastic and shear moduli. The ϕ-factor is determined from testing and could easily be retrieved from Table A.2 given in the TS19101, shown in Figure 5-7.

Type of reinforcement	Property	Period of time (years)										
		1	5	10	15	20	25	30	40	50	75	100
UD	$E_{x,t}$	0,10	0,11	0,12	0,13	0,13	0,13	0,13	0,14	0,14	0,14	0,15
	$E_{x,c}$	0,15	0,23	0,27	0,30	0,32	0,34	0,36	0,38	0,41	0,45	0,48
	G_{xz}	1,13	1,55	1,78	1,94	2,06	2,16	2,25	2,40	2,52	2,78	2,94
Woven (0/90°)	$E_{x,c}$	0,44	0,53	0,58	0,60	0,62	0,64	0,65	0,67	0,68	0,71	0,73
CSM	$E_{x,t}$, $E_{x,c}$	1,48	1,91	2,12	2,25	2,34	2,42	2,48	2,58	2,67	2,82	2,93

Figure 5-7: Table A.2 from TS19101 with ϕ - factors for the virtual stiffness reduction caused by creep

The instantaneous deformation of the sandwich deck panel is given in Figure 5-8 (a), which corresponds with the deformation from Figure 5-4 (a). From Figure 5-8 it could be seen that the long-term deformation of the sandwich deck panel has better correspondence with the outcome of the Findley analysis, which uses different parameters for the elastic moduli in the tensile and compression zones.

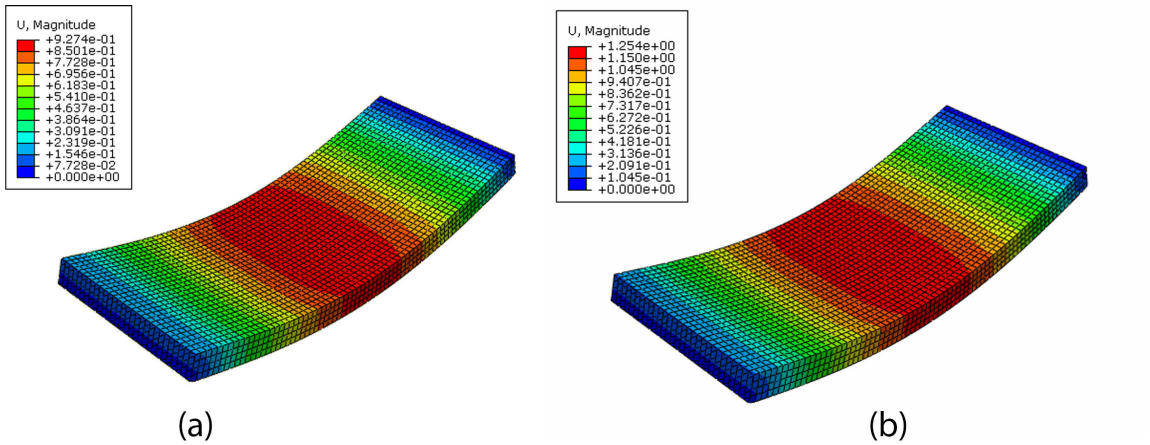

Figure 5-8: Instantaneous deformation (a) and long-term deformation according to TS19101

5-4-3 Comparison Findley and TS19101

To have a better visual comparison, the magnitude of the deformation of the node in the middle of the sandwich deck panel has been monitored during each analysis. Due to the boundary conditions and the loading configuration, the node with the highest deformation is placed exactly in the centre of the panel. Figure 5-9 shows the magnitude of the deformation of that node.

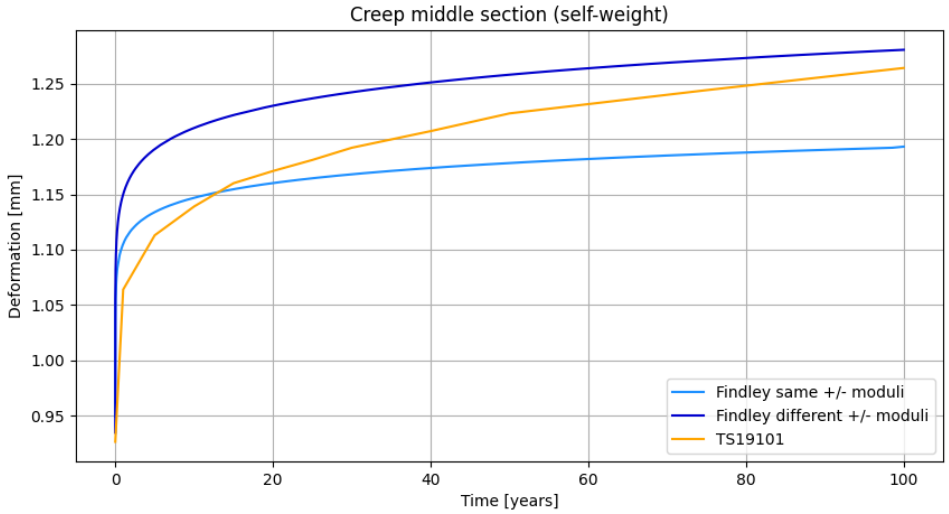

Figure 5-9: Deformation caused by creep during a 100 year life cycle

In Figure 5-9 it could be seen that, by using the formula of Findley, the creep rate will be much higher in the beginning of the lifetime. Although, both the Findley analyses do not match up perfectly with the graph from the TS19101 procedure, the end result from one the Findley analyses corresponds quite well. The outcome of the Findley analysis with different parameters for the tensile and compression zone could be considered as a conservative approach and it is therefore justified to use the corresponding parameters for the variable loading analysis.

5-5 Traffic load creep deformation

In Section 5-4 the permanent loads, including the self-weight and the weight of extra guardrails, were analysed. The results of this analysis justified the use of the Findley parameters found in literature for UD-plies applied in the multi-directional laminate as part of the sandwich deck panel. To find the proportion of the traffic load causing creep that needs to be accounted for in the long-term deformation analysis, load model 1 is used for the load configuration on the sandwich deck panel. Section 5-3-1 explains the loading configuration and the magnitude of the loads used for the traffic loading. Figure 5-10 shows the load configuration based on the findings from Section 5-3-1.

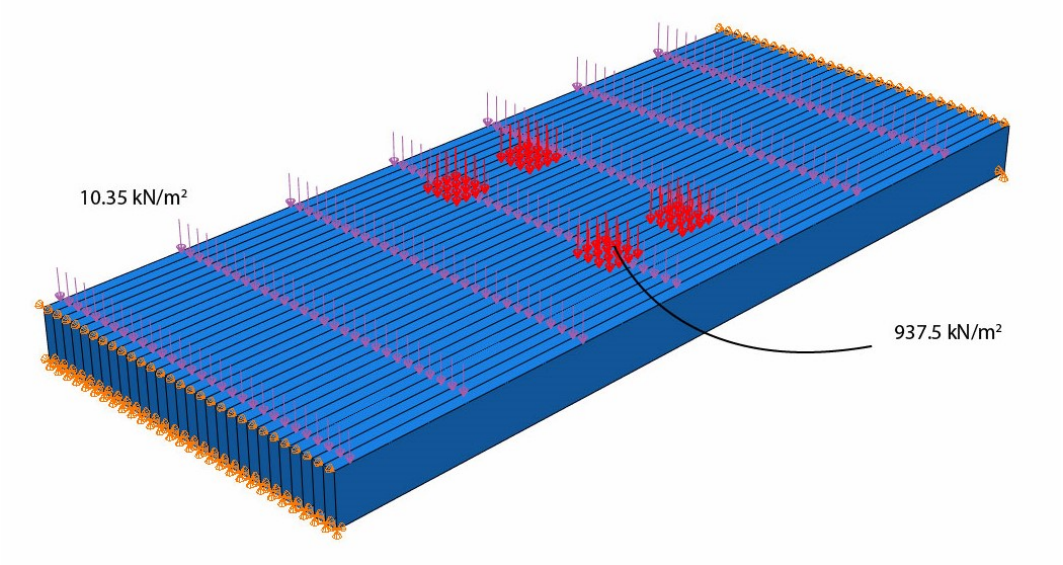

Figure 5-10: Traffic load configuration used in Abaqus

5-5-1 Findley and BSP traffic loading

The procedure of Findley can also be used for the creep deformation caused by the traffic load. However, to account for recovery cycles in between traffic jam hours, use must be made of the Boltzmann superposition principle (BSP). The background of this principle can be found in Section 2-3-2 and the way it could be implemented in a Python script involving Abaqus for the FE calculation is explained in both Chapter 3 and Chapter 4.

Findley creep traffic loading

First, the creep deformation according to the found parameters of Findley and the traffic load configuration must be known. This deformation can easily be calculated in the same way as the deformation calculated in the permanent load analysis. Figure 5-11 (a) gives the instantaneous elastic deformation of the sandwich deck panel loaded according to the configuration shown in Figure 5-10.

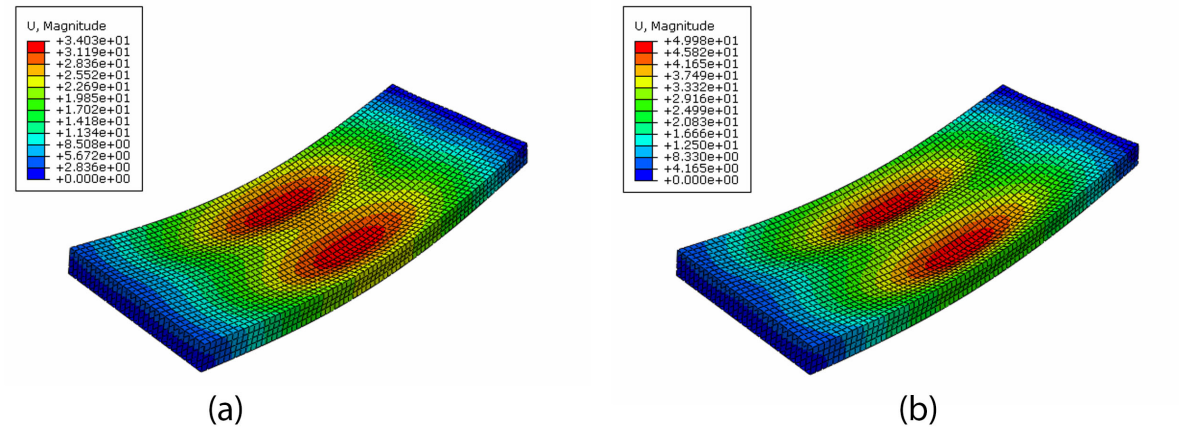

Figure 5-11: Instantaneous traffic load deformation (a) and long-term deformation (b)

Figure 5-11 (b) gives the long-term creep deformation, based on Findley if the entire traffic load without, the $\psi_{2,i}$ reduction, is placed on the deck for the entire service life. Again, the node with the highest magnitude in deformation is monitored during the analysis and used in the superposition principle of Boltzmann. According to the TS19101, the power law of Findley is acceptable to use for long-term permanent loading and the Dutch National Annex prescribes a $\psi_{2,i}$ factor of 0.4 to be used for the traffic loading. Therefore, according to both the TS19101 and the Dutch National Annex 40% of the calculated deformation should be taken as the long-term deformation caused by traffic loading. However, the TS19101 also provides engineers with creep coefficients. Using these within the creep deformation analysis will result in different creep deformation results. All these results are taken and compared within the last paragraph of this section.

BSP creep-recovery traffic loading

When both the creep and the recovery curves for the entire lifetime of the structure are known, the superposition principle of Boltzmann can be used to obtain the creep accumulation in time. For each traffic jam, the corresponding creep cycle is used and shifted horizontally to the right starting point in time and the same is done for each recovery cycle. The following conservative assumptions have been made concerning the duration periods of the traffic jams: every working day two different traffic jams will be located on the bridge and together they will take at least 40% of the entire duration of the day. Therefore, it is conservatively assumed that during every day of the week there will be a rush hour between the times that are listed below (including weekend days).

- Morning traffic jam: **06:00 - 11:00**
- Afternoon/ evening traffic jam: **15:00 - 20:00**

The Royal Dutch Touring Club (ANWB), who is responsible for Dutch traffic information throughout the country, provides the rush hours of the busiest roads in The Netherlands. According to the ANWB, daily rush hours could be between 06:30 - 09:30 in the morning and between 15:30 - 19:00 in the afternoon/evening. Therefore, it could be stated that the assumption for the rush hours is quite conservative. In addition to the selected conservative rush hours, it is also assumed that these traffic rush hours will be located on the bridge during the weekend. How the resulting deformation of these creep and recovery cycles is visualized can be retrieved from Figure 5-12, where for three weeks on each day the traffic jams are placed on the panel. The fourth week is taken as a recovery week to show how the recovery deformation will look like after three weeks of traffic loading and unloading.

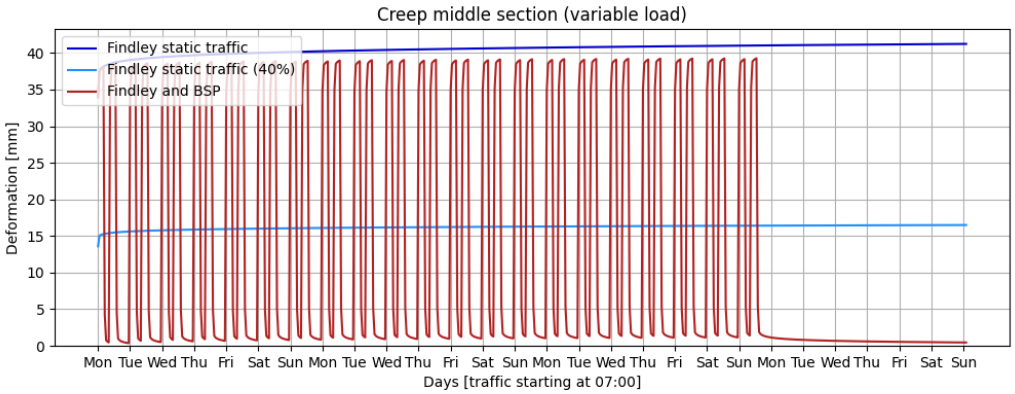

Figure 5-12: First three weeks of traffic loading and one week recovery deformation

The dark red curve represents the total deformation caused by traffic load, which includes both the elastic and the viscoelastic creep-recovery deformation. The dark blue line represents the creep deformation including the elastic deformation caused by a full permanent traffic load prescribed by LM1. The light blue curve represents the creep deformation caused by 40% of a permanent traffic load prescribed by LM1. Due to the scope of this research and the relatively small ratio of viscoelastic creep deformation to elastic deformation, it is useful to subtract the elastic deformation from the total deformation in order to analyse the pure viscoelastic behaviour. Figure 5-13 shows the same results as Figure 5-12, but the elastic deformation of each cycle is subtracted. It gives the pure viscoelastic deformation caused by traffic loading.

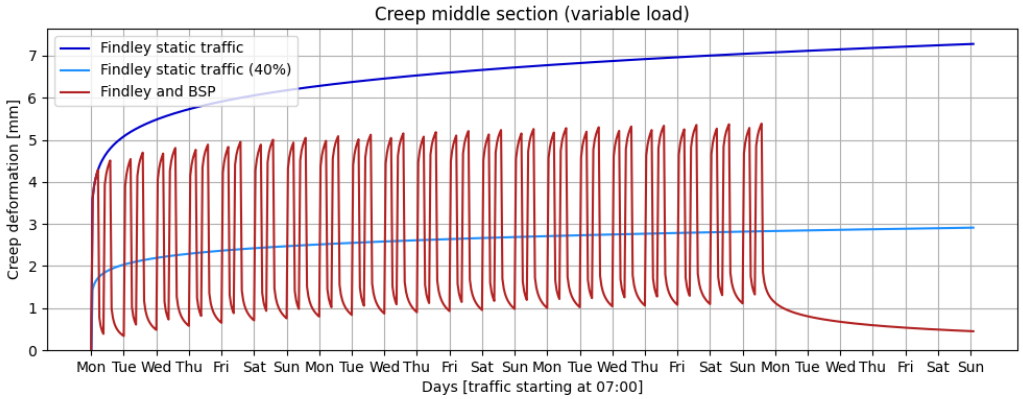

Figure 5-13: First three weeks of traffic loading and one week recovery without elastic deformation

To find the residual deformation after the entire lifetime of a structure, the same graph needs to be continued for a long time. Note that the recovery week included in the graph only is added to show how the recovery at the end of a lifetime will look like. This recovery week is not included at each four weeks during the entire lifetime of a structure. How the graph looks like for the last three weeks at the end of 100 years is given in Figure 5-16. Again, one week of recovery is added to the entire lifetime of the structure as visualization of its recovery behaviour.

5-5-2 TS19101 creep traffic loading

To calculate the creep deformation according to the TS19101, the same procedure could be used as the one used for the permanent load. The creep coefficients from Table A.2 from the TS19101, given in Figure 5-7, can also be used for the creep calculation containing a virtual static 40% of the traffic load. Figure 5-14 (a) gives the resulted instantaneous elastic deformation, caused by 40% of the traffic load. Figure 5-14 (b) gives the long-term creep deformation according to the TS19101 procedure.

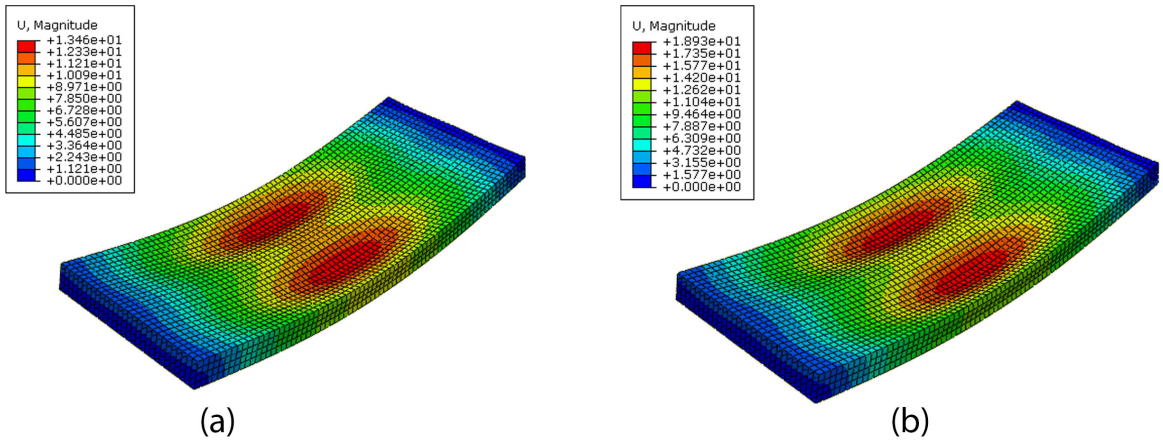

Figure 5-14: TS19101 instantaneous elastic deformation (a) and long-term creep deformation (b)

The magnitude of the deformation differs greatly compared to the results from the Findley analysis shown in Figure 5-11. This is mainly caused by the difference in elastic deformation. In the Findley analysis the entire traffic load is used and in the TS19101 analysis just 40% of the traffic load is used. However, in the next subsection the results of both procedures will be compared excluding the effects of elastic deformation.

5-5-3 Comparison Findley + BSP and TS19101

Figure 5-12 and Figure 5-13 show how Findley and BSP can simulate the viscoelastic deformation throughout the first three weeks of creep-recovery cycling. However, to verify the long-term creep deformation at the end of the lifetime of a structure, the last weeks should be evaluated. Figure 5-15 shows the viscoelastic creep deformation, assuming the entire traffic load is placed on the structure for one plot and assuming 40% of the traffic load placed for the other, both for each procedures. A linear function has been plotted through the results corresponding to 50 years and 100 years in time retrieved from the TS19101 procedure. In this way the creep accumulation according to the TS19101 could

be plotted on a smaller timescale at the end-of-life. From Figure 5-15 it is again verified that using the power law of Findley is a conservative approach on calculating the long-term deformation. The creep-recovery plot that is created by combining Findley and BSP from Figure 5-13 is not given within this figure, due to the difficulty in graphical representation on this timescale. However, by evaluating the deformations at the start of each morning traffic creep cycle, a creep curve could be created. This curve is represented in Figure 5-15 with a black colour.

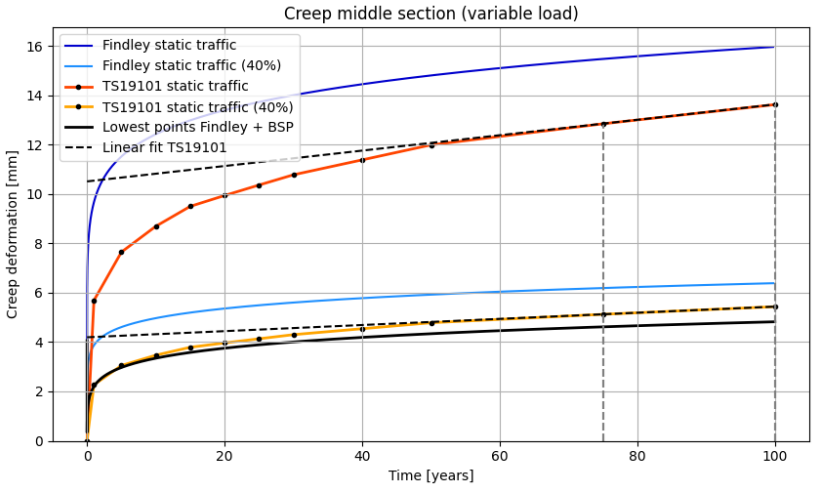

Figure 5-15: Creep deformation 100 years according to Findley+BSP and TS19101

From Figure 5-15 it could be concluded that under the very conservative assumptions the final creep deformation calculated with Findley and BSP is already lower than results from the TS19101 will give. Figure 5-16 shows the deformation of the last three weeks at the end of a 100 year lifetime of the structure. The colors of the graphs correspond with the colors used in Figure 5-15, but are now plotted on a much smaller timescale. All the single creep cycle approaches, including Findley and the use of the creep coefficients, are plotted horizontally. This is caused by the effect of a constant creep rate during the secondary creep stage on the 100 year lifetime scale. At the end of the lifetime, the deformation continues to grow very slowly and could be constant for weeks. However, using both Findley and BSP will not lead to such a constant creep deformation, because it considers each traffic jam as a new creep input cycle.

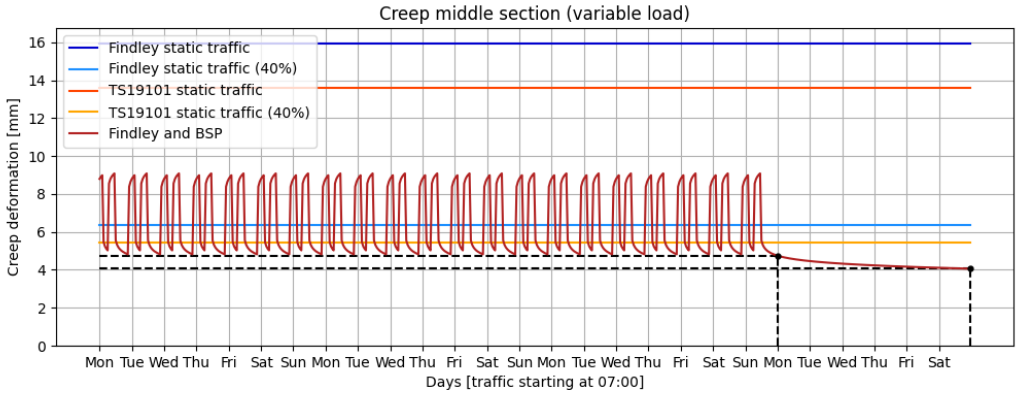

Figure 5-16: Last three weeks viscoelastic residual deformation after 100 years

Figure 5-16 shows that after on week of recovery the residual deformation curve slightly starts to flatten a little. However, due to the fact that the same Findley parameters needed to be used for both creep and recovery cycles a much longer recovery period eventually should go asymptotically back to zero. In reality this is most likely not the case and therefore the residual deformation after one week of recovery is taken and compared to the creep deformation results from the other approaches. Section 3-1-4 elaborates more on this final recovery behaviour and explains the conservative assumptions done in more detail.

Creep analysis	**LM1**	**Analysis description**	**Residual deformation**	
			Monday	Sunday
Power law of Findley	100%	Power law analysis based on Findley parameters from literature	15.96 mm	15.96 mm
Power law of Findley	40%	Power law analysis based on Findley parameters from literature	6.38 mm	6.38 mm
TS19101	100%	Analysis based on the ϕ-factors for elastic reduction from TS19101	13.62 mm	13.62 mm
TS19101	40%	Analysis based on the ϕ-factors for elastic reduction from TS19101	5.43 mm	5.43 mm
Findley and BSP	100%	Creep-recovery analysis based on both Findley and BSP	4.75 mm	4.06 mm

Table 5-6: Long-term deformation results based on different creep approaches

The two black markers in Figure 5-16 are two points in time for which the residual deformation is evaluated. The points represent the moments at 07:00 on Monday morning and Sunday morning including a one week recovery. The presented creep analysis for variable traffic loading had been computed for multiple scenario's in which differences are made in load and recovery durations. The most conservative computation is presented in this chapter. However, the results of other approaches including weekend recovery durations and shorter loading durations that correspond better with the rush hours provided by the ANWB, are presented in Appendix G. The results from this most conservative analysis are taken as final results. These results are analysed and an interpretation of these results is given in Section 6-1.

5-6 Summarizing and concluding remarks

To find how much of the traffic load should be accounted for in the calculation of long-term creep deformation, a case study has been done. The design and loading scenarios are taken from an example that is presented by the European Technical Committee CEN-TC250, who is responsible for developing the structural Eurocodes. In the example the Dutch road traffic bridge The Pijlebrug, located in Meppel (The Netherlands), was used as an example to clarify calculations and verifications for future engineers that will work with FRP. The entire FRP web core sandwich deck panel applied was simplified to a single lane rectangular composite sandwich deck panel.

The material properties used in the example were based on laminate testing. The numerical model presented in Chapter 3 and Chapter 4 calculates the long-term deformation based on UD-ply properties. A good correspondence was found between the instantaneous elastic deformation based preliminary

material design parameters from the TS19101 (see Appendix E) and the deformation calculated in the worked example using the laminate properties. The results of both the analyses are given in Figure 5-4 and it could be concluded that using the UD-ply properties from the TS19101 resulted in a accurate instantaneous elastic deformation.

The TS19101 provides engineers with multiple creep coefficients for varying elastic moduli. For example it prescribes different creep coefficients for both axial tensile and compression elastic moduli. It is impossible to find equivalent creep coefficients that need to be used for traffic loading, due to the fact that it is unknown how much each creep coefficient will contribute to the overall deformation. Therefore, the influence of the variable traffic load is sought in the $\psi_{2,i}$ factor, which represents the combination value for variable loading within the quasi-permanent loading combination. As stated before, according to the Dutch National Annex this value is 0.4 and therefore accounts for 40% of the traffic load as permanent load for long-term deformations.

Two load cases have been analysed separately. First the long-term deformation caused by the permanent load on the structure have been analysed according to TS19101 procedure and with the numerical model containing Findley and BSP. The use of the numerical model with the Findley parameters has been validated by comparing the results with the results obtained by the procedure prescribed by TS19101. Figure 5-9 shows that using the numerical model with the power law of Findley results in conservative long-term creep deformation results. Therefore, the use of the Findley parameters found in literature is justified for the variable traffic load analysis.

The same parameters of Findley are used to determine the long-term deformation after a 100 year lifetime, caused by variable traffic loading. Figure 5-16 shows a plot with the residual deformation of the last three weeks at the end of lifetime. The results that are plotted are based on a static load analysis done with the Findley parameters and a static analysis based on the creep coefficients from the TS19101 considering 40% of the traffic load as a permanent load. The results from the numerical model consisting of both Findley and BSP in which the full traffic load has been taken into account are plotted as well. The results for the residual deformation after a 100 year lifetime including one week of recovery at the end are calculated for each creep analysis and given in Table 5-6. The discussion of the results is given in Chapter 6, in which these results will be elaborated and a certain interpretation will be assigned to these results.

Chapter 6

Discussion

6-1 Interpretation of the results

The results found by comparing the multiple creep deformation analyses indicate that the creep deformation based on procedures provided by current design recommendations are too conservative. According to the Dutch National Annex NEN-EN1990, 40% of the variable traffic loading should be considered as a static load on the bridge. This part of the traffic load together with the entire permanent load should be taken into account when calculating the long-term deformation, largely caused by creep. Both these different load cases are incorporated within the **quasi-permanent load combination** for long-term serviceability limit states (SLS). This load combination is represented by Eq. (5-4), where the $\psi_{2,i}$ represents the reduction factor for variable loading and is equal to 0.4 for the traffic loading. The technical specification TS19101, created by the European Technical Committee CEN-TC250, provides engineers with certain creep coefficients in Table A.2 of the TS19101. These creep coefficients could be used for the virtual reduction of certain stiffness properties. Engineers can implement the reduced stiffness properties to calculate the final long-term deformation. However, using analytical formulas for creep deformation caused by variable loading, retrieved from literature, results in smaller creep deformations. Based on the results presented in Table 5-6 from Chapter 5, it could be concluded that the $\psi_{2,i}$ factor for the traffic load could be lower than the 0.4 currently prescribed by the Dutch National Annex. Based on the results from Chapter 5 and the results from the other analyses presented in Appendix G, Table 6-1 could be made.

Creep analysis	**Weekend Recovery**	**Rush hours**		**$\psi_{2,i}$ factor**	
		Start	End	Monday	Sunday
Least conservative	Yes	06:00	10:00	0.19	0.17
		15:00	19:00		
Conservative	Yes	05:00	10:00	0.23	0.21
		15:00	20:00		
Most conservative	No	05:00	10:00	**0.35**	0.30
		15:00	20:00		

Table 6-1: $\psi_{2,i}$ factors based on Findley and BSP for different rush hour periods

The residual deformation changes over time when the sandwich deck panel is recovering at the end of the lifetime. To visualize how residual deformations will accumulate, two moments within one week after the last creep cycle are evaluated: Monday morning, the night after the last creep cycle, and Sunday morning one week after the last creep cycle. To be most conservative, it is assumed that the sandwich deck panel only will recover over one night before the deformation is evaluated. This means that the $\psi_{2,i}$ factor could **at least** be reduced to **0.35**. Figure 5-15 shows that the long-term deformations based on TS19101 calculations (yellow line) are more conservative than the residual deformations calculated by the presented numerical model (black line). This result originates from the numerical simulations and calculations based on Findley and BSP together with several assumptions for the parameters, loading durations and simplifications. The conservative statements related to the assumptions that were made are listed below.

- **Use of Findley parameters found in literature.**
  The Findley parameters from literature were found during specific test conditions. To find out if these parameters are safe to use, multiple static analyses have been done for both a permanent self-weight load and a permanent traffic load. These results are given in Figure 5-9 and Figure 5-15, which show that the use of the found Findley parameters results in higher deformations than the deformations that result from the TS19101 procedure.
- **Use of the same Findley parameters for both creep and recovery behaviour.**
  The recovery behaviour is usually much faster than the creep behaviour and using the same parameters results in a much slower recovery behaviour than the behaviour that could be found from experiments. Section 3-1-4 explains that using the same Findley parameters for creep and recovery behaviour resulted in a recovery time of almost 7.5 times slower to eventually get to the same residual axial strain measured in experiments.
- **Assumptions made for the number of the traffic jams and the duration of each traffic jam.**
  Multiple simulations have been done considering different rush hour times and including or excluding weekend recovery times. Each of the analyses used conservative rush hours during the week compared to the rush hours provided by the ANWB. However, the most conservative analysis has been used for the recommendation about lowering the $\psi_{2,i}$ factor. This analysis considered that the entire LM1 load will be placed on the deck for 40% of the time, which results in serious conservative rush hour times (see Section 5-5-1).
- **Use of the entire LM1 load, heaviest lane with truck wheel loads in the center of the panel.**
  The case study used, simplified The Pijlebrug to a one lane sandwich deck panel. It is assumed that for each traffic jam the **entire** load of LM1 will be placed on the structure, instead of the 40% of the traffic load prescribed by the Dutch National Annex NEN1990-1. Summing up the UDL traffic load and the local wheel loads leads to a total weight of more than 80 tons. According to a research done by the Dutch research institute TNO, the weight of a medium loaded truck is 11.4 ton and the weight of a heavy loaded truck is around 19.6 ton [76]. This means that in the conservative analysis it is assumed that each morning and evening, including the weekend, there will be a load on the relative small sandwich deck panel that is equivalent to a minimum of four heavy loaded trucks. No further argumentation is needed to state that this is very conservative.

6-2 Implications and limitations

The used formulas for the numerical prediction of the creep behaviour are based on theories and experimental results retrieved from literature. The numerical calculation of the long-term deformation

results rests on the reliability of the findings in literature. Results from this research showed that by incorporating the recovery behaviour of FRP in the long-term SLS analysis, the creep deformation should be lower than calculations according to current design recommendations will give. By making use of the User Subroutine module in Abaqus and Python post-processing automation, a model has been created that implements these analytical formulas to predict both the creep and recovery behaviour for a certain design input. This model can serve as starting point for future researchers to analyse creep behaviour of FRP composites under variable loading. Many aspects such as the duration of each traffic jam, a more detailed description of the creep-recovery behaviour and considering nonlinear material behaviour could extend the model for a more precise prediction of long-term deformations. For now the current model has its limitations, on which further research should be done. The limitations are elaborated in the following subsections.

6-2-1 Same Findley parameters for creep and recovery

As stated before, when it comes down to experimental creep results of UD-specimens and the recovery behaviour of FRP in general, the literature is very limited. Important parameters retrieved from literature could be identified for the reader as the so-called Findley parameters within this report. These parameters are found in multiple studies for some variety in initial design and material properties. During this research most of the used theories and formulas have been validated trough the remodelling of experimental work. For one of the experiments a deformation fit using different parameters for creep and recovery resulted in a accurate prediction of both creep and recovery behaviour. However, using these different parameters for a relatively short load and long recovery duration resulted in weird outcomes for the residual deformation. These results are illustrated in Figure 3-8 and Figure 3-9 in Chapter 3. Based on these results, it could be concluded that using the power law of Findley with different parameters for creep and recovery, to describe the creep compliance function is not compatible with the superposition principle of Boltzmann on the long-term. Using the same parameters resulted in a residual deformation that looks more like one would expect. As Figure 3-9 shows, a relatively short creep and long recovery cycle will result in an ongoing recovery behaviour towards the initial state of the element.

6-2-2 Power law of Findley versus other models

The applicability of Findley's power law is found in its simplicity, using a few parameters will give a broadband approximation to a creep master curve rather than the more accurate generalized Maxwell or Kelvin models. It sacrifices accuracy in representation over the entire time scale from short-term (glassy) behaviour to long time (rubbery) behaviour. Figure 6-1 shows the compliance data of creep tests done on a epoxy resin specimen, which is often used as the polymer matrix within a FRP composite. It shows that fitting the power law on short-term data points will lead to an under prediction of the long-term behaviour. Also it shows that fitting the power law to a longer time compliance slope (fitlong curve), the quality of the short-term is sacrificed. Note that the power law is unable to fit the long time rubbery plateau of the material response as the mathematical form ensures an ever increasing compliance value in time. However, the fit using the Prony series predicts the creep behaviour more accurately [7].

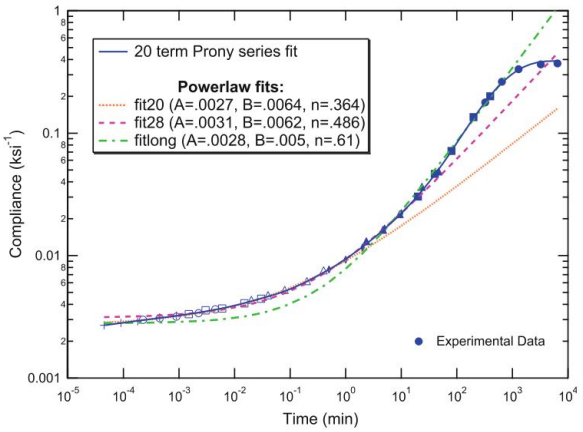

Figure 6-1: Fits on compliance data of creep epoxy resin tests [7]

6-2-3 Nonlinear material behaviour

According to the background document of the TS19101, the creep coefficients (ϕ-factors) given in table A.2 of the TS19101, are valid provided that linear viscoelastiscity applies. This means that the stress is proportional to the strain at a given time and the linear superposition principle of Boltzmann holds. The TS19101 gives certain boundary values for external factors that can have an influence on this principle of linear viscoelasticity. Table A.2 from the TS19101 prescribes the creep coefficients and presents minimum values of 35% for the fiber volume fraction, a maximum service temperature of 25°C and a maximum relative humidity of 65%. In addition to those limiting values, some researches found evidence that stresses up to 45% of the ultimate strength will not cause the start of the tertiary creep stage [77]. Stresses higher than this percentage will definitely cause nonlinear material behaviour and BSP will no longer be valid. However, due to the fact that deformation (SLS) and stability (ULS) criteria are often governing when it comes to FRP structures, the stress ranges are often far below the ultimate strength of the material. To incorporate nonlinear effects caused by temperature, physical ageing, moisture and stress level, BSP should be replaced with the Schapery single-integral nonlinear model presented and explained in Section 2-3-2.

6-2-4 Fiber-truss effect

Section 2-2-2 explains in general how creep could be accounted for in a FRP composite. CLT can be extended to describe the time-dependent behaviour of a multi-directional laminate. However, predictions for laminates with more than two fiber orientations seem to overestimate the final creep deformation. Provided CLT and FSDT, the numerical procedure to obtain time-dependent strains assumes that the normals through the laminate remain straight and normal. These assumptions imply that, in case of three or more applied fiber directions, the fibers act as pinned trusses and form a vast network of triangular truss elements. This is what is called the fiber-truss effect and it ensures an increased stiffness and strength. For long-term durability, it has been demonstrated that specimens with three or more fiber orientations have dramatically less creep than laminates consisting of only two different fiber directions [49]. Although the fiber-truss effect might lead to different results than simple implementation of time-dependent moduli properties, the numerical calculation could be seen as conservative.

Chapter 7

Conclusions and recommendations

7-1 Conclusions

This study tried to quantify the accumulation of creep caused by variable loads, based on a scientific approach. Analytical formulas combined with experimental results are often used to extend and predict the behaviour of certain Glass Fiber-Reinforced Polymer (GFRP) specimens. However, implementing such scientific approaches in practical design scenarios is not often done. During this research multiple of these analytical formulas together with experimental work are analysed and some are used for the long-term creep prediction of a specific practical design scenario. These analytical formulas together with experimental results retrieved from literature were implemented in a numerical model. The use of the User Subroutine module UMAT within Abaqus enabled an approach for creep accumulation within a multi-directional laminated sandwich deck panel. The results from Abaqus are then post-processed by using Python programming. The UMAT and the post-processing were validated by remodelling experimental work and then used for a case study which consisted of one single lane FRP web core sandwich deck panel. The sub-questions presented in Section 1-3-2 are listed below and each answer on it will support the answer to the main research question.

Sub-questions

How can the mechanism of creep (in FRP) best be explained and accounted for?

- Creep is the time-dependent deformation of a material subjected to an applied load over an extended period of time. The creep deformation of a material can be characterized by three different creep stages. The first stage is referred to as the transient or primary creep stage in which the creep rate increases quickly and eventually decelerates as transition to its second creep stage . The second stage is identified with a more constant creep rate and is in most cases the longest stage of the three stages. In the last tertiary creep stage the creep rate starts to accelerate and often leads to the phenomenon called creep rupture.

- Creep behaviour in FRP is mainly caused by the polymeric matrix around the fibers. Polymers can be characterized as amorphous materials, which means that there is no clear molecular crystalline structure. On micro-scale, stress gradients or temperature differences ensure diffusion of molecules controlled by free volume within the molecular structure of the polymer.

How do temperature effects, moisture effects and physical ageing of the composite influence the long-term creep behaviour?

- Creep deformation of a material is caused by differences in stress gradient or differences in temperature on micro-scale within the material. Polymers have a relatively low glass transition temperature T_g, which means that in practical applications a relative low stress gradient can cause the material to creep. How both these influences could be incorporated in long-term creep deformation predictions is explained in Section 2-4.
- Moisture can influence the long-term creep behaviour of polymers with a process which is referred to as chemical ageing. Chemical ageing is a collective term describing changes in the oxidation, density and molecular weight. An increase in moisture concentration will lead to oxidation and subsequently to a lower T_g. As discussed before, the T_g of the polymer dictates the resistance against creep caused by differences in temperature or stress gradient.
- Physical ageing is a manifestation of a a polymer that is slowly getting to its thermodynamic equilibrium. This manifestation ensures that the properties of a polymer can vary over time due to a change in molecular structure, which can happen without any applied stress. Long-term theoretical predictions can be made by using the effective time theory. How this could be implemented within the given analytical creep models is described in Section 2-4-4.

Which models describe the creep behaviour of composites and how do these models differ from each other?

- Multiple models have been presented in Section 2-3-2, some which describe the material response under a constant load over time. The description of the models focuses on the constitutive relation between stresses and strains through the creep compliance function. The creep compliance functions is usually time-dependent, but nonlinear parameters could be added. Some of these compliance functions are derived from phenomenological mechanical models, which could be created by combining both Hookean springs with Newtonian dash-pots as representation for the constitutive relation between stresses and strains. Models such as the Bürger model and both the generalized Maxwell and Kelvin models seem to have a very accurate correspondence with experimental results. Unfortunately, these models are not often used as starting point for experimental analysis due to the complexity in finding their parameters. Section 2-3-2 contains a more extensive elaboration on these models.
- To describe the viscoelastic behaviour of FRP composites, the power law of Findley is used more often due to its simplicity. Two different parts of the power law can be characterised: the elastic instantaneous part and the transient part. The transient part is dependent on time containing an exponent n and multiplied by a parameter m, which can both be determined from creep testing. The power law is used to predict long-term strains for specific loading scenarios. However, it could be rewritten in the form of a creep compliance, which is the inverse of the time-dependent elastic moduli.
- The models discussed above try to describe how a viscoelastic material will behave in time given a constant stress state. However, this research tries to quantify how creep deformation will

accumulate caused by variable traffic loading. Therefore, models are needed that can describe the strain or deformation output based on a variable stress or loading input. The superposition principle of Boltzmann or BSP is one of the most fundamental theories of viscoelasticity and it enables the calculation of strains or deformations with a variable stress or load inputs. It states that the sum of the time-dependent strain outputs resulting from each component of the stress input is the same as the strain output resulting from the combined stress inputs. In literature other models based on BSP have been proposed, in which nonlinear effects are accounted for. Schapery's integral procedure is likely the most widely used technique to represent the nonlinear time-dependent behaviour of (Fiber-Reinforced) Polymers.

How could such analytical models be implemented in a numerical model including Finite Element Analysis to determine long-term creep deformation?

- Most commercial FEA software packages have implemented features to define viscoelastic material behaviour modules for isotropic materials. However, FRP sandwich deck panels containing laminates consisting of multiple layers that are oriented differently are not isotropic. Although the entire laminate could be considered as anisotropic, each ply within the laminate has orthotropic properties. Therefore, the time-dependent viscoelastic stiffness properties must be implemented in multiple directions per ply. How the analytical formulas for predicting creep can be implemented in the stiffness matrix for each ply is based on CLT. Section 3-2-2 elaborates in more depth how both the power law of Findley together with BSP could be implemented within the stiffness matrix that describes the constitutive relation between stresses and strains.
- Although most of the FEA software packages do not provide the user with the possibility to implement viscoelastic behaviour for anisotropic or orthotropic materials, Abaqus does in some matter. Abaqus provides a feature called the User Subroutine, which enables the user to implement a Fortran code that is used during the Finite Element Analysis. In the case of describing personalized material behaviour, the so-called UMAT (user material) subroutine should be used. The description of the material behaviour presented in Section 3-2-2 is implemented in such a User Subroutine, which is explained in more detail in Section 4-1-2.
- The deformation in time, based on the creep and recovery cycles, is retrieved from Abaqus and post-processed using Python. Some assumptions have been made on the durations of the creep cycles that represent the morning and evening traffic jams. All these durations are used in a loop together with BSP to find the final residual deformation at the end of lifetime of the structure.

How do current standards treat creep compliance in the long-term deformation verifications (SLS) and how does the TS19101 (Eurocode proposal) deviate from it?

- Current standards provide a great variety in creep strategies. Not all standards take into account the use of UD-ply properties, but are more focused on pultruded GFRP elements or randomly laid laminates. Both the Dutch standard CUR96 and the JRC make use of creep conversion factors, which can simply be seen as the inverse of the creep coefficients often described in this report as ϕ-factors and used in the TS19101. Section 2-5 explains in more depth how creep should be accounted for according to these current standards.
- The TS19101 makes use of tabulated creep coefficients that can be used for the reduction of elastic moduli. It distinguishes the properties for axial tensile, axial compression and shear moduli for UD-, woven and randomly oriented plies (Figure 5-7).

Main research question

How much creep deformation is build up in GFRP web core sandwich deck panels applied in road traffic bridges, due to traffic load?

The Dutch National Annex of the Eurocode NEN-EN1990-1 prescribes that 40% of the traffic load should be accounted for in the quasi-permanent loading combination. However, this value is based on a very conservative assumption that finds origin in the experience with current concrete bridges. Using such a large fraction of the traffic load for the long-term deformation of GFRP structural elements placed in bridges forces engineers to design FRP structures more conservatively. Long-term SLS verifications are more often governing when it comes to FRP structures compared to concrete structures. This research presents a detailed numerical approach on the calculation of long-term creep deformation caused by variable loading and based on scientific experimental results and analytical formulas. In contrast to the approach prescribed by codes and design recommendations, the numerical model has taken into account the recovery behaviour of FRP. Figure 5-16 shows the resulted residual creep deformation resulting from several approaches of creep calculation. From this figure it can be concluded that incorporating all the conservative assumptions in the numerical model will still lead to a lower creep deformation caused by traffic loading over a 100 year structure lifetime. According to the Findley and BSP approach within this numerical model, the $\psi_{2,i}$ factor prescribed by the Dutch National Annex of the Eurocode NEN-EN1990-1 could be at least be reduced to $\psi_{\mathbf{2,i}} = \mathbf{0.35}$. It is expected that this factor could even be taken lower considering the very conservative assumptions done for simplifying the analysis and the lack of experimental data in literature. Figure 5-15 shows the accumulation of creep over 100 years according to the TS19101 approach and the numerical model. It could be seen that the creep deformation over the years calculated by the numerical model deviates from the results calculated by using the TS19101 approach.

7-2 Recommendations and further research

Section 6-2 already laid down the implications and limitations of this research. In addition, this section will provide the reader of some recommendations, which can be categorized into two different aspects: recommendations regarding knowledge and experimental input and recommendations regarding the improvement and extension of numerical models capable of predicting long-term creep deformations.

7-2-1 Recommendations for future experimental work

As stated quite often in this report, literature containing experimental results of long-term creep experiments are scarce. For an accurate prediction of long-term creep behaviour of FRP a lot of experimental work still needs to be done and possibly with other approaches than the ones used in current researches. Important aspects that need to be taken into account for future experimental work are listed below.

- Large part of the researches about creep in FRP is about pultruded sections. The only experimental results found in literature for UD-plies are from J.Siccama and these were only about the axial viscoelastic moduli for the longitudinal and transverse direction. In addition, the results from this research for the transverse viscoelastic properties were very poor.

Experimental results that determine the viscoelastic shear moduli for UD-plies were not found through a thorough literature research. Therefore, the properties for the viscoelastic shear behaviour are retrieved from tests done on pultruded specimens and it is assumed that these parameters are also applicable to UD-plies. Due to the increase in use of multi-directional laminates applied in a growing amount of FRP structural elements produced by VARTM, more experimental work should define these viscoelastic properties of UD-plies. These properties can easily be implemented into a numerical model using CLT or FEA to accurately predict long-term deformations.

- Many of the creep researches done, use the power law of Findley to predict long-term viscoelastic material behaviour. However, experimental results done on epoxy resins show that compliance functions based on phenomenological mechanical models such as the **Prony series** can predict the short-term and long-term deformation caused by creep significantly better. Given a creep master curve over time, it is more challenging to find the Prony parameters τ_i and E_i for providing a good fit than it would be by using the power law of Findley. This problem has been addressed by a number of methods in literature including Procedure X by Tobolsky and Murakami, the collocation method by Schapery, the multidata method by Cost and Becker and the windowing method by Emri and Tschoegl [78, 79, 80, 81].
- In addition to the different approaches and types of testing, a lot of experimental work needs to be done concerning the recovery behaviour of FRP. Not only is the amount of recovery tests very scarce in general, but there is no experimental work on the recovery behaviour of UD-plies.
- Only when experimental work succeeds in identifying viscoelastic parameters for more accurate prediction models than the power law of Findley, the focus could be more on the nonlinear parameters from the Schapery integral procedure. This integral is given in Eq. (2-30) and in Eq. (7-1).

$$\varepsilon(t) = g_0 D_0 \sigma + g_1 \int_0^t D_t(\psi - \psi') \frac{d}{d\tau}[g_2 \sigma(\tau)]\, d\tau \tag{7-1}$$

The parameters g_0, g_1, g_2 and a_σ from the Schapery integral, given in Eq. (7-1), should be determined from experimental testing to account for an entire nonlinear description of the FRP viscoelastic material behaviour. The parameters used in this integral could be dependent on the stress level, temperature differences and physical ageing.

7-2-2 Recommendations for the improvement of a numerical model

During this research a numerical model was created that implemented scientific experimental creep results to predict long-term deformation in a FRP sandwich deck panel. How this numerical model is build up is explained in Chapter 4. The model makes use of the FEA software Abaqus and its programmable feature the User Subroutine together with Python pre-processing and post-processing. The numerical model can be seen as a starting point for future numerical models that try to predict long-term viscoelastic behaviour of FRP sandwich deck panels. Some recommendations regarding possible optimization of the numerical model are listed below.

- The numerical model includes the long-term permanent load creep and recovery cycle calculation with Abaqus based on the power law of Findley. Python is then used to post-process the results and applying BSP. Although, it is a clumsy way of combining the power law of Findley together with BSP into one numerical model, it is quite effective for the calculation of the residual deformation. However, the User Subroutine module from Abaqus enables to program certain loading inputs as well in the module called DLOAD. Using both the User Subroutine modules

DLOAD and UMAT enables the user to program the load and recovery cycles within the Abaqus calculation. This means that BSP is not used for the superpositioning of the deformation results, but is implemented directly and evaluated at each step in the Abaqus FE calculation. Eq. (7-2) shows the constitutive relation based on BSP that could be implemented within a combined User Subroutine model.

$$\begin{bmatrix} \varepsilon_1(t) \\ \varepsilon_2(t) \\ \gamma_{12}(t) \end{bmatrix} = \begin{bmatrix} S_{11} & S_{12} & 0 \\ S_{12} & S_{22} & 0 \\ 0 & 0 & S_{66} \end{bmatrix} \begin{bmatrix} \sigma_1(t) \\ \sigma_2(t) \\ \tau_{12}(t) \end{bmatrix} + \begin{bmatrix} \int_0^t \Delta S_{11}(t-\tau)\frac{d\sigma(\tau)}{d\tau}d\tau \\ \int_0^t \Delta S_{22}(t-\tau)\frac{d\sigma(\tau)}{d\tau}d\tau \\ \int_0^t \Delta S_{66}(t-\tau)\frac{d\sigma(\tau)}{d\tau}d\tau \end{bmatrix} \tag{7-2}$$

- The numerical model incorporating BSP at each time step could also be extended so that nonlinear effects caused by caused by stress, temperature differences or physical ageing, are accounted for. The integral of Schapery together with future experimental work on the yet unknown parameters in this model, could replace BSP in the constitutive relationship presented in Eq. (7-2). The new Fortran code should include multiple User Subroutine modules to account for variable loading, temperature changes and the material behaviour in time. The User Subroutine modules that can be used for this are: DLOAD, UTEMP and UMAT. The stiffness matrix from Eq. (7-2) will change to the matrix shown in Eq. (7-3).

$$\begin{bmatrix} S_{11} & S_{12} & 0 \\ S_{12} & g_{0,22}S_{0,22} & 0 \\ 0 & 0 & g_{0,66}S_{0,66} \end{bmatrix} \tag{7-3}$$

The additional time- and temperature dependent matrix containing the viscoelastic part of the deformation should be changed as well to account for time, temperature and physical ageing of the material. The additional matrix presented in Eq. (7-2) needs to be changed to the one presented in Eq. (7-4)

$$\begin{bmatrix} g_{1,11}\int_0^t \Delta S_{11}(\chi-\chi')\frac{d(g_{2,11}\sigma_{22}(\tau))}{d\tau}d\tau \\ g_{1,22}\int_0^t \Delta S_{22}(\psi-\psi')\frac{d(g_{2,22}\sigma_{22}(\tau))}{d\tau}d\tau \\ g_{1,66}\int_0^t \Delta S_{11}(\phi-\phi')\frac{d(g_{2,66}\sigma_{12}(\tau))}{d\tau}d\tau \end{bmatrix} \tag{7-4}$$

Section 2-3-2 elaborates more on the parameters that account for nonlinear behaviour based on stress and temperature differences.

Appendix A

Mechanisms of creep

Different phenomena in the micro-structure of a material can lead to the macroscopic behaviour that one can call creep. The different creep mechanisms distinguished in material science are presented here [82].

- Nabarro-Herring creep
- Coble creep
- Harper-Dorn creep

} Diffusion creep

- Dislocation slip
- Dislocation climb

} Dislocation creep

- Grain boundary sliding

They are related to different microstructural mechanisms, which each depend on differences in temperature and stress levels. Depending on the microstructural mechanisms, various equations are suggested for the description of creep [83]. In order to compare the different creep processes it is convenient to express the steady-state creep rate through the standard relationship given in Eq. (A-1).

$$\dot{\varepsilon}_{ss} = \frac{ADG\mathbf{b}}{kT}\left(\frac{\mathbf{b}}{d}\right)^{p}\left(\frac{\sigma}{G}\right)^{n} \tag{A-1}$$

$$D = D_0 \exp\left(-\frac{Q_d}{\bar{R}T}\right) \tag{A-2}$$

In which D is the diffusion coefficient (Eq. (A-2)), where D_0 is the frequency factor, Q_d is is the activation energy for diffusion, $\bar{R}$ is the gas constant, T is the absolute temperature, G is the shear modulus , $\mathbf{b}$ is the Burgers vector, k is the Boltzmann constant, d is the grain size, σ is the applied stress, p and n are the exponents of the inverse grain size and the stress, respectively and A is a dimensionless constant. Thus, the individual creep mechanisms may be identified from the values for D, n and p since all remaining terms in Eq. (A-1) depend only upon the material and the testing conditions [12]. Each of the different mechanisms will be described shortly in the following subsections.

Diffusion creep

According to suggestion of Nabarro, any crystal can change it shape by self-diffusion in such way as to yield to an applied stress [84]. This phenomena can cause the macroscopic behaviour of a poly-crystalline solid to be like that of a viscous fluid [85]. To find out what diffusion creep exactly is, it is useful to formulate a definition of what the phenomenon diffusion itself actually is. **Diffusion** is the spontaneous intermixing of atoms over time, which is often said to be thermally activated. It can be seen as the flow of vacancies through the structure of the material. Diffusion could be driven by a varying concentrations of atoms which is represented by a so called concentration gradient. However, diffusion could be driven by other types of gradients as well. A stress gradient drives diffusional flow and power-law creep. Also a temperature gradient can drive diffusion of matter as well as diffusion of heat [3]. Diffusion creep refers to the stress-directed flow of vacancies that takes place in other to restore equilibrium. In Figure A-1 (a) it is illustrated how this flow of vacancies happens, where Figure A-1 (b) shows the build up of particles on longitudinal boundaries and the formation of denuded zones on transverse boundaries.

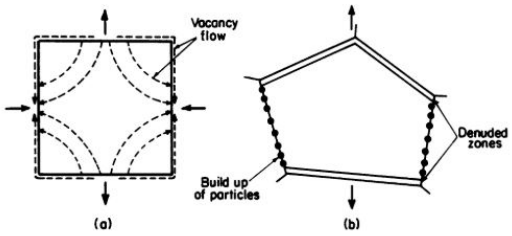

Figure A-1: Principle of diffusion creep [12]

As illustrated in Figure A-1 (a), there are two possible ways for vacancies to flow to transverse boundaries. The flow through the lattice is what is called **Nabarro-Herring diffusion creep** and the flow along the grain boundaries is what is called **Coble diffusion creep**. Experimental results from Harper and Dorn showed that when the temperature is near to the melting point of the material the Nabarro-Herring creep model does not predict the creep accurately anymore. This suggested the occurrence of another creep mechanism, which is called the **Harper-Dorn creep**. In Table A-1 the different parameters that can be used in Eq. (A-1), according to their creep mechanism, are given. D_l and $D_g b$ are the coefficients for lattice self-diffusion (Nabarro-Herring) and grain boundary diffusion (Coble), respectively.

Creep parameters per creep mechanism			
Type of creep mechanism	p inverse grain size	n inverse stress	D diffusion constant
Nabarro-Herring	2	1	D_l
Coble	3	1	D_{gb}
Harper-Dorn	0	1	D_l

Table A-1: Creep parameters belonging to each diffusion mechanism [12]

Dislocation creep

Defects in the crystalline structure of metals and ceramics play a key role in diffusion, creep and sintering. Dislocations are such defects in the crystalline structure of metals and ceramics and they distort the lattice. It is dislocations that make metals soft and ductile [3]. At high stresses, creep is controlled by the movement of such dislocations. Dislocation creep is strongly influenced by the applied stress [83]. Two types of creep can be distinguished under the general heading of dislocation creep, these two types are: **slip-** and **climb dislocation creep**. Creep takes place as a result of dislocation motion in a crystalline specimen by movement known as slip or glide. One part of the dislocation moves one lattice point along a plane known as the slip plane, relative to the rest of the crystal. For dislocation motion to occur, the bonds between the atoms (ions, in case of nonmetallic materials) must be broken during the deformation. Creep by dislocation glide occurs over the entire range of temperatures, although the temperature influences the rate of this motion. The stress needed to drive dislocation slip are on the order of a tenth the theoretical shear strength. Glide-by-slip strengthens the material as they deform. During dislocation motion, the creep rate is limited by the obstacles resisting dislocation motion [45]. The creep rate is lower at lower stress levels and becomes limited by the rate at which the dislocations can climb over obstacles by means of vacancy diffusion.

Grain boundary sliding

Grain boundary sliding is creep process in which the grains are not elongated, like with diffusion creep, but they become displaced with respect to each other. In this way a there is a net increase in their number lying along the tensile axis. This behaviour is often referred to as Rachinger [86] sliding and it occurs both under conditions of high temperature creep when the grain size is reasonably large and in super-plasticity when the grain size is small. In practice the grains of a poly-crystalline matrix cannot become displaced with respect to each other without the accommodation process in the form of some limited dislocation slip within the grains [12]. The values that can be used in Eq. (A-1) are given in Table A-2.

Creep parameters grain boundary sliding			
Type of creep mechanism	p inverse grain size	n inverse stress	D diffusion constant
Small grain size	2	2	D_{gb}
Large grain size	1	3	D_l

Table A-2: Creep parameters belonging to grain boundary sliding [12]

Appendix B

Findley parameters from literature

Creep behavior of pultruded GFRP elements [9, 13]

This research is done by M.Sá, A. Gomes and J. Correia and the paper is published in two parts in 2011 . It presents both an analytical and experimental study about the viscoelastic time-dependent creep behaviour of pultruded GFRP elements made of polyester and E-glass fibers. The pultruded I-profiles used in the experimental study had a height of 150 mm, a width of 75 mm and an equal web and flange thickness of 8 mm. The pultruded profile is made of an isophthalic polyester matrix reinforced by alternate layers of E-glass rovings and mats. The fiber-volume fraction (V_f) in the web was 61.5% and the V_f in the flange was 63%. A set of coupons specimens, extracted from the original profile, were tested in 3-point bending and a full-section profile was tested in 4-point bending, in order to characterise the long-term mechanical and structural behaviour of the GFRP pultruded material at two different scales (laminate- and beam element scale). The specimens were tested for a duration of 1200h and at different load levels ranging from 20% till 60% of the maximum stress (110 - 330 MPa). **Findley's power law** is as an fit for the data. The parameters found for Findley's power law are given in Figure B-1.

Findley's law parameters predicted from laminated coupons and I-section profile tests [4].

Member	σ/σ_u (%)	ε_0 (‰)	m (‰)	n (–)	R^2 (–)	E_0 (GPa)	E_t (GPa)	β (–1)
Web coupons								
W-20	20	4.64	0.179	0.21	0.95	22.7	587.1	25.9
W-30	30	6.01	0.189	0.21	0.94	26.3	834.9	31.7
W-40	40	8.97	0.184	0.22	0.97	24.8	1144.4	46.1
Flange coupons								
F-20	20	4.27	0.071	0.33	0.97	25.8	1551.5	60.1
F-30	30	6.64	0.061	0.31	0.92	24.9	2710.8	108.9
F-40	40	9.40	0.092	0.34	0.98	23.4	2402.7	102.6
F-50	50	12.59	0.182	0.36	0.97	21.9	1509.4	69.0
F-60	60	16.50	0.210	0.36	0.91	20.0	1573.4	78.5
I-Profile	33	2.305	0.036	0.31	0.99	28.4	1809.2	63.6

Figure B-1: Findley's parameters from test results on pultruded I-section [9, 13]

M. Sá et al. present a modified form of Findley's power law. This modified form makes use of the vertical and horizontal shift factors a_v and a_h. These shift factors could also be determined from tests and the shift factors for the stresses of 20%, 30% and 40% are given in Figure B-2.

Shifting factors values of the characterization technique TSSP, for a reference stress of 20%.σ_u.

	Stress level–σ/σ_u	20%-ref.	30%	40%
Shifting factors	$a_{v(\text{vertical})}$	1.000	1.556	2.204
	$a_{h(\text{horizontal})}$	1.000	6.040	5.044

Figure B-2: Modified Findley shift factors determined from test results on pultruded I-section [9, 13]

An experimental research into the creep behavior of glass fiber reinforced polyester [14]

This research is done by J. Siccama and is published as a Master Thesis in the repository of the Delft University of Technology in 2016. The test specimens were cut from a vacuum infused plate into strips of 25x215 mm. The thickness of the UD-specimens are made up of three plies of glass fibers with an approximate total thickness of 2.7 mm. The thickness of the cross-laminate needed to be higher due to the layers with 90 degrees. The approximate total thickness of these laminates was 5.4 mm. The measured fiber volume fraction had an average of 55.6% with an deviation of 0.5%. To simplify this and be on the conservative side the upper bound of this standard deviation will be rounded and used, which gives a fiber volume fraction of 56.%. Both short-term tensile tests with the duration of a couple of days and long-term tensile tests with the duration of more than a month were performed. By using the TSSP, creep compliances for even longer are approximated. J. Siccama also made use of **Findley's power law** to fit a curve on the test results. The instantaneous creep compliance D_0 can be taken as the inverse of $0.9 \times E_{chord}$, which can be taken from Figure B-3.

Laminate	E_{chord}[GPa]	ν [ratio]	n	s[GPa]
UD0	44.3	0.27	11	2.4
UD90	16.9	0.11	8	5.2
UD90 (6MPa)	20.6	0.11	3	5.9
UD90 (14MPa)	12.1	0.10	3	0.6
UD90 (20MPa)	18.5	0.10	2	1.6

E_{chord} = chord modulus.
n = number of specimens .
s = standard deviation moduls.

Figure B-3: Chord modulus of recorded data during load application of creep tests [14]

The transient creep compliance $D_t(t)$ in Findley's power law model has two unknowns: m and n. However, the m fit parameter is dependent on the stress level and the temperature: $m(\sigma, T)$. J. Siccama proposed a linear relation between the influences of the temperature and stress on this m parameter, but noted that this not proven and a better relationship might exist. The relation between these factors and the transient creep compliance $D_t(t)$ is given in Eq. (B-1). The fit parameters belonging to the given UD-ply properties are shown in Figure B-4.

$$D_t(t) = [m_0 + C_\sigma \sigma + C_T T]t^n \tag{B-1}$$

Fit parameter	Estimate $[MPa^{-1}]$	Standard error $[MPa^{-1}]$	tStat	pValue
m_0	7.87E-07	6.88E-09	114.4	1.46E-244
C_σ	-2.70E-09	4.05E-11	-66.725	8.09E-179
C_T	6.31E-09	2.04E-10	30.952	3.33E-94
n	0.10	4.41E-15	2.35E+13	0 (incalculable)

Figure B-4: Power law model fit results of UD0 ply [14]

Unfortunately there was insufficient data to determine the model parameters for the UD90 plies within the laminate. So, the creep behaviour of the transverse direction could not entirely be described with the given data.

Deflection Creep of Pultruded Composite Sheet Piling [15]

This research is done by Y. Shao and J. Shanmugam and was published in 2004 and contains the creep test data on composite sheet piling. The design of the sheet piling is given in Figure B-5. The pultruded section was made of an isopthalic polyester matrix reinforced by E-glass rovings and mats. The tensile modulus of elasticity and the shear modulus were determined from tests: $E_0 = 29.9GPa$ and $G_0 = 3.1GPa$ respectively.

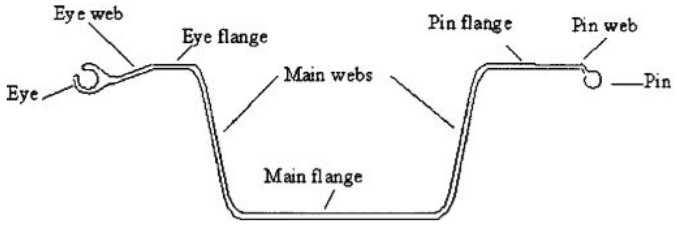

Figure B-5: Cross-sectional view of the composite sheet pile [15]

The time-dependent creep tests were carried out in equally spaced three point bending test. The span of the sheet was $6.1m$. The constant load applied in each test was 50% (2.2 kN) and 25% (1.1 kN) of the maximum load. During the tests the tensile, shear and deflection creep strain were monitored with the duration of 1 year (9,000 h). During the entire test, the temperature varied from 19 to 28 °C and the relative humidity ranged from 22% to 62%. For this research Y. Shao also made use of **Findley's power law** and the parameters were both found for tensile and shear creep. The found fit parameters are given in Figure B-6.

Tensile Creep Parameters

Beam	P/P_{max}	ε_0 $(\times 10^{-6})$	$(\varepsilon_{creep})_{9,000\ h}$ $(\times 10^{-6})$	n_e	m_e $(\times 10^{-6})$	r^2	E_t (GPa)
1	50%	750	165	0.35	5.33	0.87	4,207
2	25%	365	105	0.37	3.35	0.81	3,257
Average	—	—	—	0.36	—	—	3,732

Shear Creep Parameters

Beam	P/P_{max}	γ_0 $(\times 10^{-6})$	$(\gamma_{creep})_{9,000\ h}$ $(\times 10^{-6})$	n_g	m_g $(\times 10^{-6})$	r^2	G_t (GPa)
1	50%	600	365	0.36	14.60	0.93	126
2	25%	265	155	0.32	9.17	0.91	89
Average	—	—	—	0.34	—	—	107

Figure B-6: Findley's creep parameters determined by Y. Shao [15]

Creep tests on pultruded specimens subjected to traction or shear [16]

In thi research M. Bottoni, C. Mazzotti and M. Savoia did experimental long-term tests on pultruded GFRP specimens made of E-glass fibers in combination with a polyester matrix. The specimens have been subjected to constant traction and shear forces for about 760 days (18240 h). The tests have been performed under a controlled temperature of 20 °C and a humidity of 60% inside a climatic room. the specimens under traction have been cut from the flanges of a wide flange GFRP pultruded beam. The shear specimens are cut from the web of the same beam. Some specimens have been externally strengthened by bonding carbon fibres sheets, in order to increase their stiffness. For the web ±45° layers of CFRP are added and in the flange in some specimens UD-layers of CFRP are added. Four unstiffened specimens have been taken from the flange from which two have the dimensions of $46 \times 245mm$ and two others have the dimensions of $65 \times 335mm$. In this way the length/width ratio for the four specimens is the same. The differences in width allows for some more insight in how different stress levels can affect the creep strain evolution. The thickness of the beam flange is $9.53mm$. The long-term shear creep tests are done on four different specimens with the dimensions of $120 \times 220mm$, from which two are strengthened with ±45° CFRP layers. The axial stress of the narrow unstiffened specimens was $20.7MPa$ or 15% of the tensile strength of the plate. The larger specimens are designed in order to see the effects of a lower stress level, these specimens experienced a axial tensile stress of $14.7MPa$. The latter was used as the reference stress σ'. The plates cut from the web used for shear testing experienced a shear stress of $4.11MPa$, which was the only stress measured and therefore there was no difference between the reference stress and the applied stress. M. Bottoni also made use of **Findley's power law** for both the aixal and shear tests. The fit parameters belonging to this creep model are given in Figure B-7 and Figure B-8.

Summary of the calibrated Findley parameters in traction ($\sigma' = 14.69$ MPa).

	$10^6\ m$	$10^6\ m'$	α (–)	R^2
TWP7	128.73	128.73	0.249	0.997
TWP8	134.06	134.06	0.243	0.996
TNP5	245.74	173.89	0.211	0.993
TNP6	241.67	171.75	0.212	0.993
Average TWP	131.40	131.40	0.246	–
Average TNP	243.71	172.82	0.212	–

Figure B-7: Findley's axial creep parameters determined by M. Bottoni [16]

Summary of the calibrated Findley parameters for shear ($\tau' = \tau_0 = 4.11$ MPa).

	$10^6\ m = 10^6\ m'$	α (–)	R^2
SP5	179.97	0.206	0.997
SP6	170.26	0.208	0.997
SP7	177.16	0.211	0.997
SP8	194.65	0.196	0.994

Figure B-8: Findley's shear creep parameters determined by M. Bottoni [16]

Creep and failure of a full-size fiber-reinforced plastic pultruded frame [75]

In this research L. Bank and A Mosallam investigated the long-term creep and short-term failure of a portal frame entirely made of pultruded FRP components both experimentally and analytically. The components were made of glass/ vinylester pultruded beams. The cross-section of the beam had an I-profile with the following cross sectional properties: $I = 41.28 \times 10^6\ mm^4$ and $A = 5632\ mm^4$. Creep data up to 5 months (10,000 h) is reported in this paper. L. Bank also made use of **Findley's power law** to fit a curve on the data results from the tests. The specimens are subjected to a constant stress of: $\sigma = 12.1$ MPa, which resulted to the Findley parameters given below. Both the axial and shear strains resulted into different fit parameters.

Axial:

$$m_E = 9.46 \times 10^{-}6$$

$$n_E = 0.33$$

Shear:

$$m_G = 21.525 \times 10^{-}6$$

$$n_G = 0.338$$

The elastic parameters found in the short term tests were: $E_0 = 16.2$ GPa and $G_0 = 0.372$ GPa.

Creep and creep buckling of pultruded glass-reinforced polymer members [17]

In this research K. Harries, Q. Guo and D. Cardoso investigated the flexural creep and creep buckling behaviour of pultruded glass fiber reinforced polymer plate specimens. The flexural creep tests had a duration of 1000 h and were conducted at three different load levels. The temperature was around 21 °C and the relative humidity during the test was 53 ± 5% and were both determined through continuous monitoring. The specimens had the following dimensions: 38 × 350 mm with a plate thickness of 6.4 mm. The plate fiber architecture contained three layers of unidirectional glass fibers separated by four layers of continuous strand mat and two surfacing veils in an isophthalic polyester resin matrix. K. Harries also made use of **Findley's power law** and found an average value of $n = 0.18$ for the fit parameter. The m fit parameter changes with the given stress range, as is shown in Figure B-9. The Young's modulus is determined from shot-term tests and is estimated on: $E_0 = 20.9$ GPa.

Flexural creep specimen details and results.

	Specimen	A	B	C	D	E	G
1	Width, b (mm)	38.99	39.05	38.74	38.83	38.69	38.83
2	Thickness, t (mm)	6.26	6.17	6.19	6.21	6.16	6.15
3	Applied load, F (N)	227	227	450	450	672	672
4	Extreme fiber stress (MPa)	52	54	106	105	160	160
		$0.12f_u$	$0.13f_u$	$0.25f_u$	$0.25f_u$	$0.38f_u$	$0.38f_u$
		Measured midspan strains					
5	0 h tension strain, ε_{t0} (με)	2613	2420	5173	5207	7923	8304
6	0 h compression strain, ε_{c0} (με)	−2535	−2593	−5107	−5276	−7332	−8055
7	1000 h tension strain, ε_{t1000} (με)	3015	2779	6056	6202	9075	9431
8	1000 h compression strain, ε_{c1000} (με)	−2835	−2956	−5895	−6312	−8222	−9164
9	Tension creepocity = $(\varepsilon_{t1000} - \varepsilon_{t0})/\varepsilon_{t0}$	0.15	0.15	0.17	0.19	0.15	0.14
10	Compression creepocity = $(\varepsilon_{t1000} - \varepsilon_{t0})/\varepsilon_{t0}$	0.12	0.14	0.15	0.20	0.12	0.14
		Measured midspan deflections					
11	0 h deflection, Δ_0 (mm)	8.32	8.60	14.68	14.01	22.34	24.05
12	1000 h deflection, Δ_{1000} (mm)	9.87	10.23	17.05	16.99	25.57	27.62
13	$(\Delta_{1000} - \Delta_0)/\Delta_0$	0.19	0.19	0.17	0.21	0.14	0.15
		Neutral axis location (measured from tension face)					
14	0 h neutral axis location	$0.508t$	$0.483t$	$0.503t$	$0.497t$	$0.519t$	$0.508t$
15	1000 h neutral axis location	$0.515t$	$0.485t$	$0.507t$	$0.496t$	$0.525t$	$0.507t$
16	Neutral axis shift (mm)	+0.04	+0.01	+0.02	−0.01	+0.05	−0.01
		Modulus					
17	0 h modulus, E_0 (MPa)	21,000	21,500	21,100	20,500	21,200	20,100
18	1000 h modulus, E_{1000} (MPa)	18,105	19,000	17,900	16,800	18,600	17,200
		Findley Power Law parameters (1000 h data)					
19	n	0.176	0.184	0.187	0.178	0.084	0.076
20	m (με)	92.3	104	224	304	488	634
21	$E_t = \sigma/m$ (MPa)	56,3380	51,9231	47,3214	34,5395	32,7869	25,2366
22	Coefficient of determination, R^2	0.998	0.994	0.984	0.993	0.984	0.989
		Findley Power Law parameters (first 10 h data)					
23	n	0.193	0.148	0.309	0.257	0.115	0.092
24	m (με)	90.4	109	189	274	473	636
25	$E_t = \sigma/m$ (MPa)	575,221	495,413	560,847	383,212	338,266	251,572
26	Coefficient of determination, R^2	0.975	0.739	0.979	0.986	0.978	0.987
		Findley Power Law parameters (first 24 h data)					
27	n	0.188	0.173	0.257	0.218	0.089	0.075
28	m (με)	91.8	106	200	286	487	648
29	$E_t = \sigma/m$ (MPa)	566,449	509,434	530,000	367,133	328,542	246,914
30	Coefficient of determination, R^2	0.981	0.900	0.951	0.962	0.917	0.950
		Findley Power Law parameters (first 194 h data)					
31	n	0.179	0.181	0.208	0.185	0.077	0.068
32	m (με)	91.8	105	215	300	495	653
33	$E_t = \sigma/m$ (MPa)	56,6449	51,4286	493,023	350,000	323,232	245,023
34	Coefficient of determination, R^2	0.996	0.979	0.967	0.978	0.957	0.977

Figure B-9: Findley's flexural creep parameters determined by K. Harries [17]

Short- and long-term structural properties of pultruded beam assemblies using adhesive bonding [18]

In this reasearch J. Mottram investigated the long-term properties of pultruded beam assemblies. The test configuration was a three-point bending test. Accelerated creep test data were used to determine long-term behaviour using **Findley's power law** model. The design of the assembled cross section is given in Figure B-10.

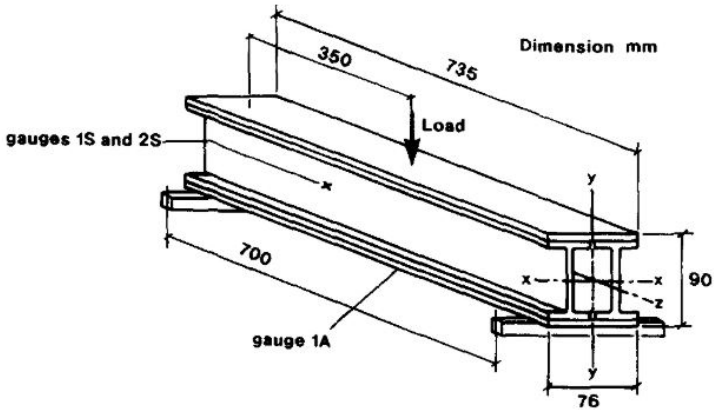

Figure B-10: Assembled FRP beam used for testing axial and shear strains [18]

The E-glass fiber reinforcement is continuous filament mat to impart transverse properties and unidirectional roving bundles. The resin is an isophthalic polyester, mixed with 10-15 parts per weight of filler to form the matrix. Each assembly had the dimensions $735 \times 76 \times 90$ mm, as shown in Figure B-10. The purpose of the long-term tests was to determine the creep behaviour of the assemblies under normal laboratory conditions. The temperature during the tests was 22±2 °C and a relative humidity of 50±5 %. It can be expected that for exterior applications of FRP this conditions will be more severe. With a span of 700 mm, the specimen was loaded to 22.8 kN at a constant rate of 0.2 $\frac{kN}{s}$. The axial surface strains were measured in the top and bottom plates and the shear strains were measured in the middle of the web, see Figure B-10. Findley's creep parameters were found for both shear conditions and axial compression/ tensile conditions. The initial elastic- and shear modulus that were measured at $t = 0$ were the following: $E_0 = 29.2$ GPa and $G_0 = 3.15$ GPa.

Axial:

$$m_E = 135 \times 10^{-}6$$

$$n_E = 0.22$$

Shear:

$$m_G = 180 \times 10^{-}5$$

$$n_G = 0.24$$

Compression Creep of Pultruded E-Glass-Reinforced-Plastic Angles [10]

In this research an experimental study was done on E-glass pultruded angle sections. This research was done by G. McClure and Y. Mohammadi. Compression tests were carried out on three 152 mm angle stubs made of isophthalic polyester resin with 53 - 59% E-glass fibers in weight. Both coupon ans stub tests were performed simultaneously and results of the two series of tests were compared to validate the use of coupon tests to predict creep behaviour of the full-size members. The total duration of the tests 2500 h followed by 250 h creep recovery test. G. McClure also made use of **Findley's power law** with creep parameters determined from both the coupon and stub tests. The average predictions based on Findley's law fitted on both the results of the coupon and stub tests agreed with one another. This indicated that there is no real benefit in making detailed creep-strain measurements on the stubs.

The dimensions of the angle stubs were: $152.4 \times 50.8 \times 50.8$ mm with a thickness of 6.35 mm. The dimensions of the coupons were: 12.7×31.75 mm with a thickness of 6.35 mm. The temperature during the entire test was around 24 °C and a relative humidity of 25 %. The applied average stress on the stubs was 44 MPa. The applied stress to the coupons was 146 MPa, which corresponded to 45% of the ultimate compressive stress and 3.3 times stress that was applied on the stubs. In Figure B-11 and Figure B-12, the determined Findley parameters belonging to the experimental results of both the stubs and coupons respectively are given.

Leg number (1)	Creep Parameters[a]		Average Creep Strain at Time t h (με)			
	m (με) (2)	n (3)	$t=1$ (4)	$t=500$ (5)	$t=1{,}000$ (6)	$t=2{,}500$ (7)
(*a*) Predictions using Findley's model						
1	84.2 ± 13%	0.171 ± 5%	84 ± 13%	245 ± 15%	277 ± 15%	323 ± 16%
2	84.9 ± 13%	0.170 ± 8%	85 ± 13%	245 ± 16%	277 ± 16%	323 ± 17%
(*b*) Experimental measurements						
1	—	—	84 ± 14%	246 ± 15%	277 ± 16%	321 ± 16%
2	—	—	89 ± 16%	250 ± 15%	279 ± 17%	324 ± 17%

[a]Average of 15 results.

Figure B-11: Findley's parameters stub determined by G. McClure and comparison to experimental results [10]

Coupon number (1)	Creep Parameters		Average Creep Strain at Time t h (με)			
	m (με) (2)	n (3)	$t=1$ (4)	$t=500$ (5)	$t=1{,}000$ (6)	$t=2{,}500$ (7)
(*a*) Predictions using Findley's model						
1	129.8	0.255	131	646	763	960
2	127.9	0.250	129	616	726	908
3	122.4	0.256	123	610	721	906
Average	127 ± 7%	0.254 ± 3%	128 ± 7%	624 ± 10%	737 ± 11%	925 ± 11%
(*b*) Experimental measurements						
1	—	—	129	642	759	958
2	—	—	122	614	720	919
3	—	—	138	634	737	889
Average	—	—	130 ± 9%	630 ± 11%	739 ± 11%	922 ± 11%

Figure B-12: Findley's parameters coupon determined by G. McClure and comparison to experimental results [10]

The strain recovery was predicted using Findley's power law and by using the superposition principle of Boltzmann. Agreement was also made with the obtained recovery data and the prediction done by Findley's power law and Boltzmann's superposition principle. The results of the predictive model for the creep-recovery tests for the stub and coupon are given in Figure B-13 (a) and Figure B-13 (b) respectively.

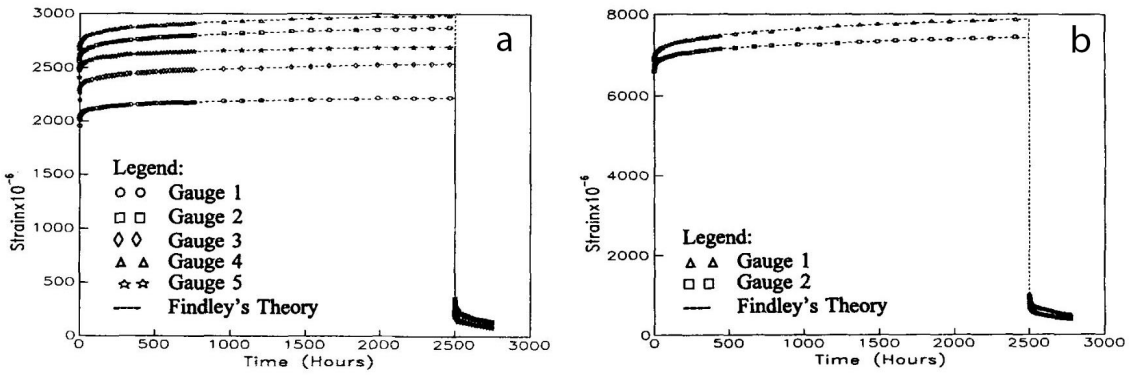

Figure B-13: Creep-recovery strains experimental and predictive results [10]

Time-Dependent Deformation of Pultruded Fiber Reinforced Polymer Composite Columns [19]

In this paper Y. Choi and L. Yuan investigated the time-dependent deformation of pultruded glass fiber reinforced polymer composite columns under axial-compressive loading. Tests were conducted on both closed and open cross section types. The columns were 1200 mm in length and had gross cross sectional dimensions of 102 × 102 mm with a wall thickness of 6.4 mm. The columns have been tested on different stress levels of: 20, 30, 40 and 50% of the ultimate compressive strength that was retrieved from shot-term column tests. The experiments were conducted with a duration of 2500 h. The fibers took 45 - 75% of the nominal weight of the entire column formed the composite together with a high performance grade of polyester resin. All the creep tests were carried out in an environmental room with a temperature 23 ± 0.5 °C and a relative humidity of 50 ± 1.5 %. Also Y. Choi made use of **Findley's power law** to fit a curve on the found experimental parameters. For both the wide flange I-section and the box cross section, the Findley parameters are determined. These parameters are given for different stress levels in Figure B-14.

Section type	Loading level (%)	ε_0 ($\mu\varepsilon$)	m ($\mu\varepsilon$)	n
Wide flange	20	1,180	45	0.148
	30	1,875	50	0.170
	40	2,150	70	0.137
	50	2,850	95	0.133
Box	20	1,253	30	0.195
	30	1,935	43	0.196
	40	2,340	47	0.178

Figure B-14: Findley's parameters determined by Y. Choi [19]

Findley's power law: $\varepsilon(t) = \varepsilon_0 + m \cdot t^n$ or $D(t) = D_0 + D_t \cdot t^n$ or $E(t) = (E_0 \cdot E_t) / (E_t + E_0 \cdot t^n)$																			
Authors	Year	Test type	Specimen	Material	Duration (h	Measurement type	Creep/recove	Vf (%)	σ [MPa]	σ/σu (%)	T (°C)	ε0 or γ0 (‰)	m (‰)	E0 (GPa)	Et (GPa)	G0 (GPa)	Gt (GPa)	n	
M. Sá	2011	Flexural	FRP Pultruded I-section	Glass/ polyester	1600	Web coupon	Creep		61,5	-	20	-	4,64	0,179	22,7	587,1	-	-	0,21
M. Sá	2011	Flexural	FRP Pultruded I-section	Glass/ polyester	1600	Web coupon	Creep		61,5	-	30	-	6,01	0,189	26,3	834,9	-	-	0,21
M. Sá	2011	Flexural	FRP Pultruded I-section	Glass/ polyester	1600	Web coupon	Creep		61,5	-	40	-	8,97	0,184	24,8	1144,4	-	-	0,22
M. Sá	2011	Flexural	FRP Pultruded I-section	Glass/ polyester	1600	Flange coupon	Creep		63	-	20	-	4,27	0,071	25,8	1551,5	-	-	0,33
M. Sá	2011	Flexural	FRP Pultruded I-section	Glass/ polyester	1600	Flange coupon	for		63	-	30	-	6,64	0,061	24,9	2710,8	-	-	0,31
M. Sá	2011	Flexural	FRP Pultruded I-section	Glass/ polyester	1600	Flange coupon	Creep		63	-	40	-	9,4	0,092	23,4	2402,7	-	-	0,34
M. Sá	2011	Flexural	FRP Pultruded I-section	Glass/ polyester	1600	Flange coupon	Creep		63	-	50	-	12,59	0,182	21,9	1509,4	-	-	0,36
M. Sá	2011	Flexural	FRP Pultruded I-section	Glass/ polyester	1600	Flange coupon	Creep		63	-	60	-	16,5	0,21	20	1573,4	-	-	0,36
M. Sá	2011	Flexural	FRP Pultruded I-section	Glass/ polyester	1600	I-section	Creep		-	-	33	-	2,305	0,036	28,4	1809,2	-	-	0,31
J.Siccama	2016	Tensile	UD Laminate	Glass/ polyester		Centre strain gauge [0]	Creep		55,6	63	-	21	-	-	42,19	1383,1	-	-	0,10
J.Siccama	2016	Tensile	UD Laminate	Glass/ polyester		Centre strain gauge [0]	Creep		55,6	88	-	39	-	-	47,17	1222,5	-	-	0,11
J.Siccama	2016	Tensile	UD Laminate	Glass/ polyester		Centre strain gauge [0]	Creep		55,6	212	-	39	-	-	45,7	2320,2	-	-	0,11
J.Siccama	2016	Tensile	UD Laminate	Glass/ polyester		Centre strain gauge [0]	Creep		55,6	211	-	59	-	-	41,3	1700,7	-	-	0,11
J.Siccama	2016	Tensile	UD Laminate	Glass/ polyester		Centre strain gauge [0]	Creep		55,6	210	-	22	-	-	42,2	25316	-	-	0,09
J.Siccama	2016	Tensile	UD Laminate	Glass/ polyester		Centre strain gauge [0]	Creep		55,6	85	-	21	-	-	42,9	1634	-	-	0,10
J.Siccama	2016	Tensile	Cross ply laminate	Glass/ polyester		Centre strain gauge [90]	Creep		55,6	20	-	23	-	-	1,56	3,6	-	-	0,01
J.Siccama	2016	Tensile	Cross ply laminate	Glass/ polyester		Centre strain gauge [90]	Creep		55,6	20		39	-	-	6,2	2,53	-	-	0,45
J.Siccama	2016	Tensile	Cross ply laminate	Glass/ polyester		Centre strain gauge [90]	Creep		55,6	14		23	-	-	11,46	23,24	-	-	0,44
J.Siccama	2016	Tensile	Cross ply laminate	Glass/ polyester		Centre strain gauge [90]	Creep		55,6	14		59	-	-	1,68	1,12	-	-	0,05
J.Siccama	2016	Tensile	Cross ply laminate	Glass/ polyester		Centre strain gauge [90]	Creep		55,6	7		59	-	-	18,3	23	-	-	0,22
J.Siccama	2016	Tensile	Cross ply laminate	Glass/ polyester		Centre strain gauge [90]	Creep		55,6	6		39	-	-	25	32,57	-	-	0,15
J.Siccama	2016	Tensile	Cross ply laminate	Glass/ polyester		Centre strain gauge [90]	Creep		55,6	14		14	-	-	6,67	2,64	-	-	0,09
Y. Shao	2004	Flexural	FRP Pultruded sheet pile	Glass/ polyester	9000	Flange coupon	Creep		-	-	25	21	0,365	0,0034	29,9	3257	-	-	0,37
Y. Shao	2004	Flexural	FRP Pultruded sheet pile	Glass/ polyester	9000	Flange coupon	Creep		-	-	50	21	0,75	0,0053	29,9	4207	-	-	0,35
Y. Shao	2004	Flexural	FRP Pultruded sheet pile	Glass/ polyester	9000	Web strain gauge	Creep		-	-	25	21	0,265	0,0092	-	-	3,1	89	0,32
Y. Shao	2004	Flexural	FRP Pultruded sheet pile	Glass/ polyester	9000	Web strain gauge	Creep		-	-	50	21	0,6	0,0146	-	-	3,1	126	0,36
M. Bottoni	2014	Tensile	FRP Pultruded w/ beams	-	18240	Flange coupon	Creep		-	-	10,5	20	-	0,131	-	111,8	-	-	0,25
M. Bottoni	2014	Tensile	FRP Pultruded w/ beams	-	18240	Flange coupon	Creep		-	-	15	20	-	0,244	-	85,2	-	-	0,21
M. Bottoni	2014	Shear	FRP Pultruded w/ beams	-	18240	Web coupon	Creep		-	4,1	10,5	20	-	0,181	-	-	3,4	22,8	0,25
L. Bank	1932	Flexural	FRP Pultruded I-section	Glass/ vinylester	10000	Flange strain gauge	Creep		-	-	-	-	0,746	0,0095	16,2	1277,7	-	-	0,33
L. Bank	1932	Flexural	FRP Pultruded I-section	Glass/ vinylester	10000	Web strain gauge	Creep		-	-	-	-	1,178	0,0215	-	-	3,7	203,5	0,34
K. Harries	2017	Flexural	FRP Pultruded plate	-	1000	Flange strain gauge	Creep		-	-	13	21	2,52	0,0384	19,9	54,04	-	-	0,18
K. Harries	2017	Flexural	FRP Pultruded plate	-	1000	Flange strain gauge	Creep		-	-	25	21	5,19	0,0258	19,9	421,51	-	-	0,20
K. Harries	2017	Flexural	FRP Pultruded plate	-	1000	Flange strain gauge	Creep		-	-	38	21	8,11	0,58	19,9	284,13	-	-	0,04
J. Mottram	1993	Flexural	FRP Pultruded double I-sec	Glass/ polyester	24	Flange strain gauge	Creep		-	-	38	22	3,02	0,135	23,2	533,2	-	-	0,22
J. Mottram	1993	Flexural	FRP Pultruded double I-sec	Glass/ polyester	24	Web strain gauge	Creep		-	-	38	22	-	0,18	-	-	3,15	27,86	0,24
G. McClure	1995	Compressic	Angle stubs	Glass/ polyester	2500	Coupon	Creep		-	-	45	24	-	0,1267	21,8	1140,4	-	-	0,25
Y. Choi	2003	Compressic	FRP Pultruded w/ columns	-	2500	Flange strain gauge	Creep		30	-	20	23	1,18	0,045	26,4	688,9	-	-	0,148
Y. Choi	2003	Compressic	FRP Pultruded w/ columns	-	2500	Flange strain gauge	Creep		30	-	30	23	1,875	0,05	26,4	930	-	-	0,17
Y. Choi	2003	Compressic	FRP Pultruded w/ columns	-	2500	Flange strain gauge	Creep		30	-	40	23	2,15	0,07	26,4	885,7	-	-	0,14
Y. Choi	2003	Compressic	FRP Pultruded w/ columns	-	2500	Flange strain gauge	Creep		30	-	50	23	2,85	0,095	26,4	815,8	-	-	0,13

Figure B-15: Overview of foudn Parameters of Findley

Appendix C

Tables used for creep from design recommendations

Toetsaspect							
Conversiefactor	**Sterkte (UGT)**	**Stabiliteit (UGT)**	**Vermoeiing (UGT)**	**Vervorming onder quasi-blijvende belasting (BGT)**	**Vervorming onder kortdurende belasting (BGT) (1)**	**Comfort (trillingen) (BGT) (2)**	**Schade (BGT)(6)**
η_{ct}	✓	✓	✓	✓	✓	✓	✓
η_{cm}	✓	✓	✓	✓	✓	✓	✓
η_{cv} (3)	✓	✓ (4)		✓			✓
η_{cf} (5)		✓		✓	✓	✓	✓

(1) De conversiefactoren hoeven niet toegepast te worden voor het bepalen van vervormingen door thermische belasting;
(2) De bruikbaarheidsgrenstoestand comfort moet worden getoetst zowel met als zonder de conversiefactoren voor effecten door temperatuur, water(damp) en vermoeiing;
(3) De conversiefactor voor kruipeffecten hoeft alleen te worden toegepast voor het langeduur gedeelte van de belasting, (zie 6.1.1). Bij de toets op kruipbreuk (zie 6.7) hoeft de conversiefactor voor kruip niet te worden toegepast;
(4) De conversiefactor voor kruipeffecten voor de toets op stabiliteit moet worden toegepast voor het bepalen van de excentriciteit in de vervormde toestand;
(5) De conversiefactor voor vermoeiingseffecten hoeft alleen te worden toegepast voor stijfheidgerelateerde grenstoestanden indien er sprake is van een vermoeiingsbelasting;
(6) Met schade wordt bijvoorbeeld bedoeld eerste scheurvorming.

Figure C-1: Table 2-6 from CUR96, an overview of conversion factors [2]

	Aspect being verified						
Influencing factor	Strength (ULS)	Stability (ULS)	Fatigue (ULS)	Creep (SLS)	Momentary deformation (SLS)	Comfort (vibrations) (SLS)	Damage (SLS)
η_{ct}	√	√	√	√	√	√	√
η_{cm}	√	√	√	√	√	√	√
η_{cv}	√	√		√			√
η_{cf}		√		√	√	√	√

Figure C-2: Table 2.4 from JRC, an overview of conversion factors[20]

Type of material	$\eta_{cv,20}$					
Random laid laminate RLM	0,63					
Mixed laminate ML	$1/(2,0 - \delta)$					
Filament wound laminate FWL parallel to the direction of winding	$1/(1,8 - \delta)$					
Filament wound laminate FWL vertical to the direction of winding	FWL 1	FWL 2	FWL 3	FWL 4	FWL 5	FWL 6
	0,56	0,47	0,36	0,59	0,5	0,42
with $\varepsilon_z > 0,2\%$	0,42	0,34	0,26	0,48	0,38	0,36
Pultrusion profiles P parallel to the direction of pultrusion	$1/(1,8 - \delta)$					
Pultrusion profiles P vertical to the direction of pultrusion	0,53					
Pultrusion profiles P parallel to the direction of pultrusion with $\varepsilon_z > 0,2\%$	0,50					
Pultrusion profiles P vertical to the direction of pultrusion with $\varepsilon_z > 0,2\%$	0,33					

Figure C-3: Table 10.1 from JRC, conversion factors for strength reduction in 20 years[20]

Type of material	$\eta_{cv,20}$ for Elasticity and Strain					
Random laid laminate RLM	Cured			Not Cured		
	$1/(2,4-2\delta)$			$1/(2,6-2\delta)$		
Mixed laminate ML	Cured			Not Cured		
	$1/(2,3-2\delta)$			$1/(2,5-2\delta)$		
Filament wound laminate FWL parallel to the direction of winding	Normal force			Bending		
	$1/(1,75-\delta)$			$1/(1,85-\delta)$		
Filament wound laminate FWL vertical to the direction of winding	FWL 1	FWL 2	FWL 3	FWL 4	FWL 5	FWL 6
	$1/(2,2-\delta)$	$1/(2,45-\delta)$	$1/(3,0-\delta)$	$1/(2,15-\delta)$	$1/(2,3-\delta)$	$1/(3,2-2\delta)$
with $\varepsilon_z > 0,2\%$	$1/(2,7-\delta)$	$1/(3,1-\delta)$	$1/(4,1-\delta)$	$1/(2,6-\delta)$	$1/(2,8-\delta)$	$1/(4,0-2\delta)$
Pultrusion profiles P parallel to the direction of pultrusion	Normal force			Bending		
	$1/(1,75-\delta)$			$1/(1,85-\delta)$		
Pultrusion profiles P vertical to the direction of pultrusion	Normal force			Bending		
	0,57			0,54		
Pultrusion profiles P vertical to the direction of pultrusion with $\varepsilon_z > 0,2\%$	Normal force			Bending		
	0,5			0,4		

Figure C-4: Table 10.2 from JRC, conversion factors for stiffness reduction in 20 years[20]

The quantity δ accounts for the mass portion of fibers in the direction of interest and ε_z is the strain in tension perpendicular to the winding direction.

Appendix D

Creep model Maple validation

Material and test properties

> $F := 22.8E3 : F\_half := \frac{F}{2} :$

> $L\_span := 1800 : l1 := \frac{L\_span}{3} : l2 := \frac{2 \cdot L\_span}{3} :$

> $E\_0 := 27.3E3 :$
$D0\_E := \frac{1}{E\_0} :$
$E\_t := 1809.2E3 :$
$Dt\_E := \frac{1}{E\_t} :$
$n\_flexural := 0.31 :$

> $D0\_E\_rec := \frac{1}{E\_0} :$
$Dt\_E\_rec := 3.017 \cdot Dt\_E :$
$n\_recovery := 0.5846 \cdot n\_flexural :$

Determining the cross sectional properties

> $b\_w := 150 : t\_w := 8 :$
$b\_f := 75 : t\_f := 8 :$

> $A\_tot\_cs := (b\_w - t\_f) \cdot (t\_w) + 2 \cdot (t\_f \cdot b\_f) :$
$A\_eff\_cs := b\_w \cdot t\_w :$

> $Iyy\_cs := evalf\left(\frac{1}{12} \cdot b\_f \cdot (b\_w + t\_f)^3 - \frac{1}{12} \cdot (b\_f - t\_w) \cdot (b\_w - t\_f)^3 \right) :$

Determining the elastic modulus on time t is done with Findley's power law model.

> $E\_compliance(t) := \frac{1}{D0\_E + Dt\_E \cdot t^{n\_flexural}};$

$$E\_compliance := t \mapsto \frac{1}{D0\_E + Dt\_E \cdot t^{n\_flexural}}$$

> $E\_compliance\_recovery(t) := \frac{1}{D0\_E\_rec + Dt\_E\_rec \cdot t^{n\_recovery}};$

$$E\_compliance\_recovery := t \mapsto \frac{1}{D0\_E\_rec + Dt\_E\_rec \cdot t^{n\_recovery}}$$

EulerBernoulli FourPointBending

```
> q1 := F_half·Dirac(x − l1) : q2 := F_half·Dirac(x − l2) :
> ODE1 := −E·Iyy·diff(w1(x), x$4) = −(q1 + q2) :
> sol := dsolve(ODE1, w1(x)) : assign(sol) :
> w1 := w1(x) :
> phi1 := −diff(w1, x) : kappa1 := diff(phi1, x) : M1 := E·Iyy·kappa1 : V1 := diff(M1, x) :
> x := 0 : eq1 := w1 = 0 : eq2 := M1 = 0 :
```

```
  x := L_span : eq3 := w1 = 0 : eq4 := M1 = 0 :
> sol := solve({eq1, eq2, eq3, eq4}, {_C1, _C2, _C3, _C4}) : assign(sol) :
> x :='x':
> E := E_compliance(0) : Iyy := Iyy_cs :
> pltEuler := plot(−w1, x = 0..L_span, color = "DarkRed") :
> w1_init := w1 :
> x := L_span/2 : w1_mid_init := w1;
```

$$w1\_mid\_init := 9.975416049$$

```
> sigma_bend := M1·(1/2·b_w + 1/2·t_w)/Iyy;
```

$$sigma\_bend := 62.35936176$$

```
> x :='x': E :='E': Iyy :='Iyy':
```

Results and plots (static and creep)

At time t=0 the static displacement only depends on the initial elastic modulus both Timoshenko's deflection and Euler's deflection are given in the figure below.

```
> display({pltEuler}, legendstyle = [location = bottom], gridlines = true, labels
      = ["Location along beam [mm]", "Deflection [mm]"]);
```

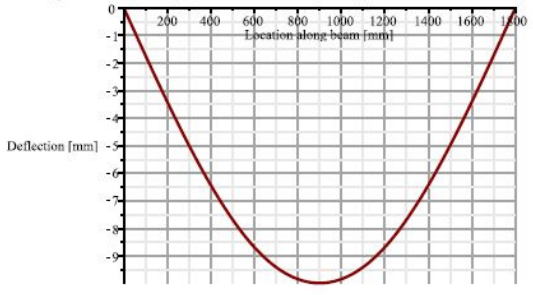

To see how creep influences the final deflection at time t the midpoint of the beam is concerned and evaluated

```
> x := L_span/2 : t_begin := 0 : t_end := 1600 : t :='t':
> E := E_compliance(t) : Iyy := Iyy_cs : A := A_eff_cs :
> plot(w1, t = t_begin..t_end, color = "DarkRed", gridlines = true, labels = ["Time [hours]",
      "Deflection [mm]"]);
```

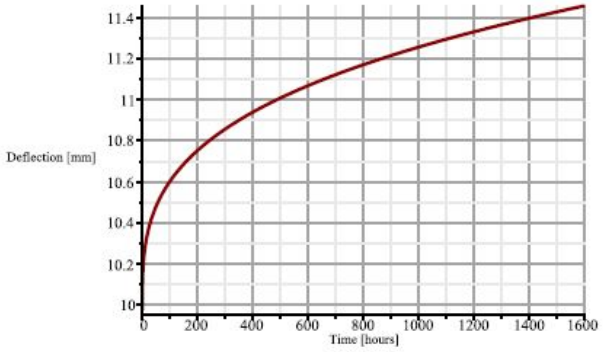

> $pltEuler\_mid\_time := plot\left(\left(\frac{w1}{w1\_mid\_init} - 1\right)\cdot 100,\ t = t\_begin..t\_end,\ color = \text{"DarkRed"}\right):$

> $display(\{pltEuler\_mid\_time\},\ title = \text{"Creep percentage of elastic deformation"},\ legendstyle = [location = bottom],\ gridlines = true,\ labels = [\text{"Time [hours]"}, \text{"δ[%]"}]);$

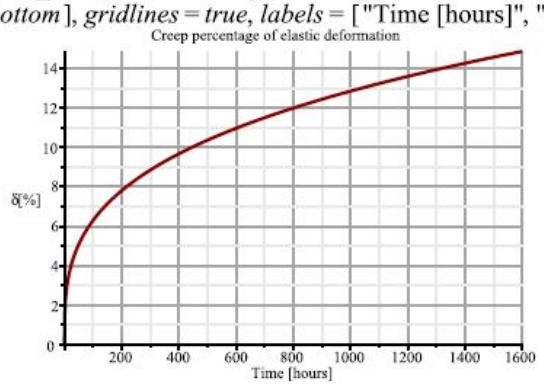

>

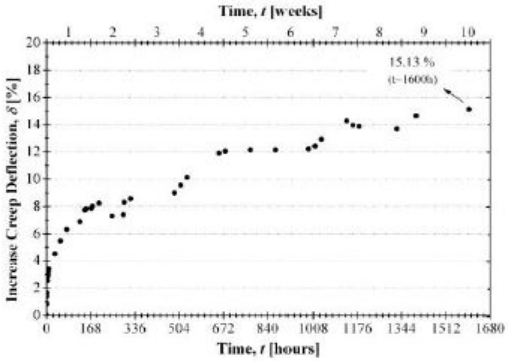

> $t := 1600 : def\_1600 := \left(\frac{w1}{w1\_mid\_init} - 1\right)\cdot 100;$

$def\_1600 := 14.8577574$

> $t := 't':$

In the results given below the axial strain of the flange at midpoint is evaluated, the same is done in

> $z\_top := \frac{(b\_w + t\_f)}{2} : z\_bottom := z\_top :$

```
> epsilonEuler_creep := kappa1·z_top :
> pltEuler_creepstrain_midpoint := plot(epsilonEuler_creep·1000, t = 0 ..1600, color
      = "DarkRed", thickness = 2) :
> display({pltEuler_creepstrain_midpoint}, gridlines = true, legendstyle = [location = bottom],
      labels = ["Time[hours]", "ε[‰]"])
```

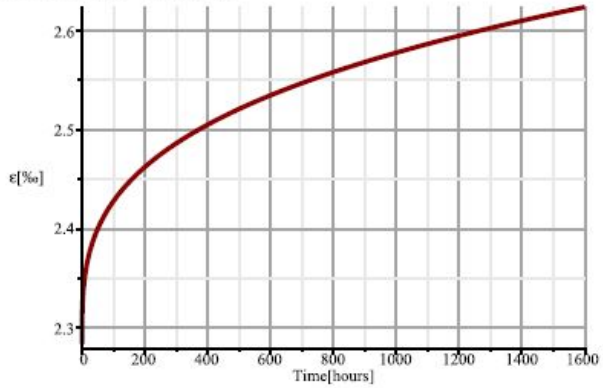


```
> E := E_compliance_recovery(t);
```

$$E := \frac{1}{0.00003663003663 + 1.667587884\ 10^{-6}\ t^{0.181226}}$$

```
> kappa1_func := unapply(kappa1, t);
```

$$kappa1\_func := t \mapsto 0.00002891424945 + 1.316325521\ 10^{-6} \cdot t^{0.181226}$$

```
> t_unload := 1600 :
> epsilonEuler_recovery := -kappa1_func(t - t_unload)·z_top :
> pltEuler_recoverystrain_midpoint := plot(epsilonEuler_recovery·1000, t = 0 ..2000, color
      = "DarkRed", legend = "Euler", thickness = 2) :
> epsilonEuler_residualstrain_midpoint := epsilonEuler_creep + epsilonEuler_recovery :
> pltEuler_residualstrain_midpoint := plot(epsilonEuler_residualstrain_midpoint·1000, t = 0
      ..1748, color = "DarkRed", thickness = 2) :
```

```
> display({pltEuler_creepstrain_midpoint, pltEuler_residualstrain_midpoint}, title
      = "Axial creep strain outer flange", gridlines = true, legendstyle = [location = bottom], labels
      = ["Time[hours]", "ε[‰]"])
```

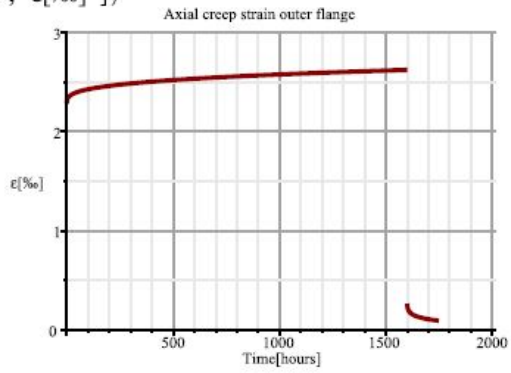

The results given in the paper of Mário F. Sá are analysed on two point in time: creep strain at t = 1600h and residual strain at t = 1748h given in the picture below

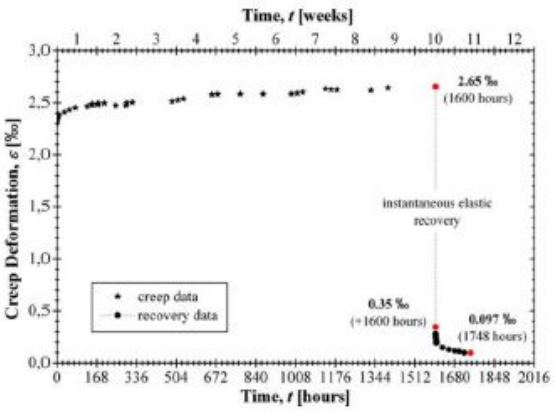

$t := 0 : epsiloncreep\_0 := epsilonEuler\_creep \cdot 1000;$

$$epsiloncreep\_0 := 2.284225707$$

$t := 1600 : epsiloncreep\_1600 := epsilonEuler\_creep \cdot 1000;$

$$epsiloncreep\_1600 := 2.623610421$$

$t := 1600 : epsilonresidual\_1600 := epsilonEuler\_residualstrain\_midpoint \cdot 1000;$

$$epsilonresidual\_1600 := 0.3393847136$$

$t := 1748 : epsilon\_1748 := epsilonEuler\_residualstrain\_midpoint \cdot 1000;$

$$epsilon\_1748 := 0.09160508740$$

Appendix E

Material properties Pijlebrug deck

Stiffness properties of UD plies

Equations to calculate the averaged stiffness properties of the lamina

> $E1 := (Er + (Ef1 - Er)\cdot Vf)\cdot phi\_UD;$

$$E1 := (Er + (Ef1 - Er)\ Vf)\ phi\_UD$$

> $E2 := \left(\frac{(1 + xi\_2\cdot eta\_2\cdot Vf)}{(1 - eta\_2\cdot Vf)}\cdot Er\right)\cdot phi\_UD;$

$$E2 := \frac{(xi\_2\ eta\_2\ Vf + 1)\ Er\ phi\_UD}{-eta\_2\ Vf + 1}$$

> $G12 := \left(\frac{(1 + xi\_G\cdot eta\_G\cdot Vf)}{(1 - eta\_G\cdot Vf)}\cdot Gr\right)\cdot phi\_UD;$

$$G12 := \frac{(xi\_G\ eta\_G\ Vf + 1)\ Gr\ phi\_UD}{-eta\_G\ Vf + 1}$$

> $nu12 := nu\_r - (nu\_r - nu\_f)\cdot Vf;$

$$\nu 12 := nu\_r - (nu\_r - nu\_f)\ Vf$$

Stiffness properties of the base materials

E_1, E_2 is de elasticiteitsmodulus van de lamel in de materiaalhoofdrichtingen (respectievelijk 1 en 2) in het vlak van de lamel;
G_{12} is de glijdingsmodulus van de lamel in het vlak van de lamel;
ν_{12} is de dwarscontractiecoëfficiënt in de materiaalhoofdrichtingen (1 en 2) in het vlak de lamel;
ν_r is de dwarscontractiecoëfficiënt van de hars in de materiaalhoofdrichtingen (1 en 2);
ν_f is de dwarscontractiecoëfficiënt van de vezel in het vlak van de vezel in de materiaalhoofdrichtingen (1 en 2);
ϕ_{UD} is een empirische reductiefactor gelijk aan 0.97;
E_r is de elasticiteitsmodulus van de hars;
E_{f1}, E_{f2} is de elasticiteitsmodulus van de vezel in de vezelhoofdrichtingen (respectievelijk 1 en 2);
G_r is de glijdingsmodulus van de hars;
V_f is het vezelvolumepercentage van het lamel.

E-Glass fibers, values retrieved from the TS19101 CEN-TC250

> $Ef1 := 74E3 : \#MPa$
$Ef2 := 74E3 : \#MPa$
> $Gf := 30E3 : \#MPa$
> $nu\_f := 0.25 :$

Polyester matrix, values retrieved from TS19101 CEN-TC250

> $Er := 3.4E3 : \#MPa$
> $Gr := 1.4E3 : \#MPa$
> $nu\_r := 0.40 :$

Other factors needed for the calclation of the correct stiffness properties

> $phi\_UD := 0.97 :$
> $xi\_2 := 2.0 :$
$xi\_G := 1.0 :$

> $eta\_2 := \dfrac{\left(\frac{Ef2}{Er} - 1.0\right)}{\left(\frac{Ef2}{Er} + xi\_2\right)};$

$eta\_2 := 0.8737623762$

> $eta\_G := \dfrac{\left(\frac{Gf}{Gr} - 1.0\right)}{\left(\frac{Gf}{Gr} + xi\_G\right)};$

$eta\_G := 0.9108280255$

Stiffness parameters for the plies in the flange

> $Vf := 0.52;$

$$Vf := 0.52$$

> $E1\_flange := \frac{E1}{1000}; \#GPa$

$E2\_flange := \frac{E2}{1000}; \#GPa$

$G12\_flange := \frac{G12}{1000}; \#GPa$

$nu12\_flange := nu12;$

$$E1\_flange := 38.90864000$$
$$E2\_flange := 11.53671638$$
$$G12\_flange := 3.801874152$$
$$nu12\_flange := 0.3220$$

>

Stiffness parameters for the plies in the web

> $Vf := 0.28;$

$$Vf := 0.28$$

> $E1\_web := \frac{E1}{1000}; \#GPa$

$E2\_web := \frac{E2}{1000}; \#GPa$

$G12\_web := \frac{G12}{1000}; \#GPa$

$nu12\_web := nu12;$

$$E1\_web := 22.47296000$$
$$E2\_web := 6.502623674$$
$$G12\_web := 2.287793433$$
$$nu12\_web := 0.3580$$

>

ABD and equivalent laminate parameters for the flange

```
> t_f := 25.7;
```

$$t\_f := 25.7$$

```
> layup_half_f := [0, 90, 0, 0] :
  p_per_layer_f := 0.25 :
> t_per_layer_half := 1/2 · t_f · p_per_layer_f;
```

$$t\_per\_layer\_half := 3.212500000$$

```
> AAf := 10^5 · [ 8.49  0.98  0.0
                  0.98  4.87  0.0
                  0.0   0.0   0.98 ] :
  BBf := [ 0.0  0.0  0.0
           0.0  0.0  0.0
           0.0  0.0  0.0 ] :
  DDf := 10^7 · [ 4.48  0.54  0.0
                  0.54  2.86  0.0
                  0.0   0.0   0.54 ] :
> E1f := 1/t_f · ( AAf[1, 1] − AAf[1, 2]^2 / AAf[2, 2] ); #MPa
  E2f := 1/t_f · ( AAf[2, 2] − AAf[1, 2]^2 / AAf[1, 1] ); #MPa
```

$$E1f := 32267.6755195823$$

$$E2f := 18509.2555689477$$

```
> G12f := 1/t_f · AAf[3, 3];
```

$$G12f := 3813.22957232000$$

```
> v_12f := AAf[1, 2] / AAf[2, 2];
  v_21f := AAf[1, 2] / AAf[1, 1];
```

$$v\_12f := 0.201232032854209$$

$$v\_21f := 0.115429917550059$$

ABD and equivalent laminate parameters for the web

> $t\_w := 6.9;$

$$t\_w := 6.9$$

> $layup\_half\_w := [0, 90, 45, -45]:$
> $p\_per\_layer\_w := 0.25:$

> $t\_per\_layer\_half := \frac{1}{2} \cdot t\_w \cdot p\_per\_layer\_w;$

$$t\_per\_layer\_half := 0.8625000000$$

> $AAw := 10^4 \cdot \begin{bmatrix} 8.97 & 3.05 & 0.0 \\ 3.05 & 8.97 & 0.0 \\ 0.0 & 0.0 & 2.96 \end{bmatrix}:$

$$BBw := \begin{bmatrix} 0.0 & 0.0 & 0.0 \\ 0.0 & 0.0 & 0.0 \\ 0.0 & 0.0 & 0.0 \end{bmatrix}:$$

$$DDw := 10^5 \cdot \begin{bmatrix} 4.58 & 0.79 & 0.0 \\ 0.79 & 3.32 & 0.0 \\ 0.0 & 0.0 & 0.76 \end{bmatrix}:$$

> $E1w := \frac{1}{t\_w} \cdot \left(AAw[1,1] - \frac{AAw[1,2]^2}{AAw[2,2]} \right); \#MPa$

$$E2w := \frac{1}{t\_w} \cdot \left(AAw[2,2] - \frac{AAw[1,2]^2}{AAw[1,1]} \right); \#MPa$$

$$E1w := 11497.0028895586$$

$$E2w := 11497.0028895586$$

> $G12w := \frac{1}{t\_w} \cdot AAw[3,3];$

$$G12w := 4289.85507152000$$

> $\nu\_12w := \frac{AAw[1,2]}{AAw[2,2]};$

$$\nu\_21w := \frac{AAw[1,2]}{AAw[1,1]};$$

$$\nu\_12w := 0.340022296544036$$

$$\nu\_21w := 0.340022296544036$$

>

Appendix F

Load actions

F-1 Load combination

According to NEN-EN1990, the **characteristic load** combination should be used in case of irreversible serviceability limit states [21]. This load combination is given by Eq. (F-1), where G is the permanent loading, P is the pre-stress load and Q is the variable loading. The $\psi_{0,i}$ factor determines the combination value of the variable loads in the characteristic loading combination.

$$\sum_{j\geq 1} G_{k,j} + P + Q_{k,1} + \sum_{i\geq 1} \psi_{0,i} Q_{k,i} \tag{F-1}$$

One can speak of irreversible serviceability limit state when somewhere in the construction the yield stress is reached and a irreversible strain has left when the loading is removed. However, a different load combination can be used in the case of reversible serviceability limit state. In such a case the so-called **frequent load** combination could be applied, given in Eq. (F-2). To use this load combination, one need to verify the yield stress is not reached [87]. The $\psi_{1,i}$ factor determines the combination value for the variable loads in the frequent loading combination.

$$\sum_{j\geq 1} G_{k,j} + P + \psi_{1,1} Q_{k,1} + \sum_{i\geq 1} \psi_{1,i} Q_{k,i} \tag{F-2}$$

Beside the characteristic and the frequent load combination another SLS load combination is possible as well. This load combination is called the **quasi-permanent** load combination and is used to verify the long-term effects like **creep** and **shrinkage**. This load combination is given by Eq. (F-3) [87]. The $\psi_{2,i}$ factor determines the combination value of the variable loads in the quasi-permanent loading combination.

$$\sum_{j\geq 1} G_{k,j} + P + \sum_{i\geq 1} \psi_{2,i} Q_{k,i} \tag{F-3}$$

The given load parameters for the permanent, pre-stress and variable loading are the characteristic values. To use these values in design, a partial safety factor is needed. However, this partial safety

factor is equal to one ($\gamma_i = 1.0$) in the analysed serviceability limit state. This means the characteristic load combination could directly be used for design as well. Each of the given load combinations contains different ψ-factors, which incorporates the chance of multiple variable loads being combined. The combined values for variable loading are the given in the list below [87].

- $\psi_0 Q_k$ is the combination value for irreversible SLS
- $\psi_1 Q_k$ is the combination value for reversible SLS
- $\psi_2 Q_k$ is the combination value for irreversible SLS based on long-term effects

These ψ-factors Eurocode NEN-EN1990 [21]. The ψ-factors for traffic loads, wind loads, thermal loads and other loads on bridges used for traffic are given in table A2.1 of the NEN-EN1990. The table is also shown in Figure F-1. These ψ-factors for The Netherlands are given in the National Annex of the Eurocode NEN-EN1990 [22].

Belasting	**Symbool**		ψ_0	ψ_1	ψ_2
Verkeersbelastingen (zie EN 1991-2, tabel 4.4)	gr1a (LM1+voetgangers- of fietspadbelastingen) [1]	TS	0,75	0,75	0
		UDL	0,40	0,40	0
		Voetgangers- +fietspadbelastingen [2]	0,40	0,40	0
	gr1b (enkele as)		0	0,75	0
	gr2 (horizontale krachten)		0	0	0
	gr3 (voetgangersbelastingen)		0	0,40	0
	gr4 (LM4 – belasting door een menigte)		0	–	0
	gr5 (LM3 – speciale voertuigen)		0	–	0
Windkrachten	F_{wk} – blijvende ontwerpsituaties		0,6	0,2	0
	– uitvoering		0,8	–	0
	F_W^*		1,0	–	–
Thermische belastingen	T_k		0,6 [3]	0,6	0,5
Sneeuwbelastingen	$Q_{Sn,k}$ (tijdens de uitvoering)		0,8	–	0
Belastingen tijdens de bouw	Qc		1,0	–	1,0

Figure F-1: ψ-factors for bridges used for traffic loads Eurocode [21]

The ψ-factors for traffic loads, windloads, thermal loads and other loads on bridges used for traffic are given in table NB.9 of the Dutch National Annex. The table is also shown in Figure F-2. Most of the differences are found in rounding the ψ-factors differently. However, when the ψ_2 factor is considered a significant difference is noticed. In The Netherlands, when load model 1 is considered, 40% of the characteristic load is included in the calculation of deformation with respect to long-term effects. |

Belasting	Symbool		ψ_0	ψ_1	ψ_2
Verkeersbelastingen (zie NEN-EN 1991-2+C1, tabel 4.4)	gr1a (LM1 + voetgangers- of fietspad-belastingen)	TS	0,8	0,8	0,4
		UDL		0,8	
		Horizontale belasting		0,8	
		voetgangers- + fietspad-belastingen		0,8 [d]	
	gr1b (enkele as)		0	0,8 [b]	0
	gr2 (horizontale krachten dominant)		0,8	0,8 [c]	0
	gr3 (voetgangersbelastingen)		0	0,8 [b]	0
	gr4 (LM4 – belasting door een menigte)		0	0,8 [b]	0
	gr5 (LM3 – speciale voertuigen)	TS	0	0,8 [b]	0
		UDL		0,8 [b]	
		Horizontale belastingen		0,8 [b]	
		Speciaal voertuig		1,0 [b]	
Windkrachten	F_{Wk}	blijvende ontwerpsituatie	0,3	0,6 [b]	0
		uitvoering	0,8	0	0
	F_W*		1,0	0	–
Thermische belastingen	T_k		0,3	0,8 [b]	0,3 [a]
Sneeuwbelastingen	$Q_{Sn,k}$	blijvende ontwerpsituatie	0	0	0
		uitvoering	0,6	0	0
Belastingen tijdens de bouw	Q_c		1,0	0	1,0

[a] In de uiterste grenstoestand mag voor ψ_2 voor thermische belasting de waarde 0 zijn aangehouden.

[b] Voor aanrijding op of onder de brug en aanvaring is $\psi_1 = 0$.

[c] Voor scheurvomingsberekeningen van beton zijn de verschillende waarden van ψ_1 gelijk aan de waarden behorend bij gr1a.

[d] Voor scheurvormingsberekeningen van beton moet $\psi_1 = 0,4$ zijn aangehouden.

OPMERKING Groepen verkeersbelastingen hoeven niet met elkaar te zijn gecombineerd.

Figure F-2: ψ-factors for bridges used for traffic loads National Annex [22]

F-2 Load models

To quantify the traffic load, use is made of the NEN-EN1991-2 section 4.3 about vertical actions. the characteristic values of traffic loading could be divided into 4 different load models, which are listed below. The fatigue load models are ignored, due to the fact that these can only be used for fatigue verifications and not for creep verifications.

- **Load Model 1** or LM1 contains both concentrated axle loads and a distributed area load, which represents most the actions caused by heavy trucks and passenger cars. This model needs to be

used for the global and local verifications.

- **Load Model 2** or LM2 contains one concentrated axle load with specific contact areas of the wheels, which covers the dynamical effect of usual traffic on compact structural elements.
- **Load model 3** or LM3 contains a system of axle loads, that represent unique vehicles that take routes for which unique loading conditions are provided.
- **Load Model 4** or LM4 represents the load of a crowd, only used for global verifications

Based on the application of the case study in Chapter 5 and the multiple given load models above, only LM1 will be considered for the creep deformation analysis. LM1 consists of two systems of load: concentrated double axle loads and uniform distributed loads. Figure F-3 gives the table from NEN-EN1990-2 that shows the distributed loads and the concentrated axles loads.

Positie	Tandemstelsel *TS*	Gelijkmatig verdeelde belasting (GVB)
	Aslast Q_{ik} (kN)	q_{ik} (of q_{rk}) (kN/m^2)
Rijstrook nummer 1	300	9
Rijstrook nummer 2	200	2,5
Rijstrook nummer 3	100	2,5
Overige rijstroken	0	2,5
Resterende oppervlakte (q_{rk})	0	2,5

Figure F-3: Loads according to load model 1 from NEN-EN1990-1 [23]

The distributed loads from Figure F-3 are per driving lane and the axle loads represent the concentrated loads caused by two wheels. The distance between the axle loads could be retrieved from Figure F-4.

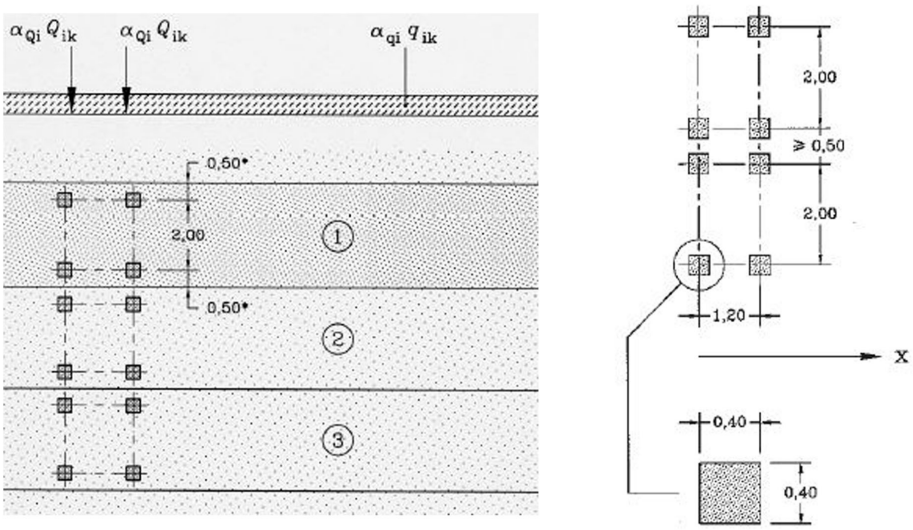

Figure F-4: Locations of the wheel loads and lane numbering [23]

The correction factors α_q and α_Q can be retrieved from the National Annex NEN-EN1991-2 [24]. A heavy traffic lane an α factor is proposed of $\alpha_\mathbf{q}$ **= 1.15** and the α_Q factor could be retrieved from table NB.1 given in Figure F-5.

Aantal vrachtwagens per jaar per rijstrook voor zwaar verkeer N_{obs} [a]	α_{Q1} en α_{q1}				α_{qr}
	Lengte van de overspanning of invloedslengte (L)				
	20 m	50 m	100 m	≥ 200 m	
≥ 2 000 000	1,0	1,0	1,0	1,0	
200 000	0,97	0,97	0,95	0,95	0,90
20 000	0,95	0,94	0,89	0,88	0,80
2 000	0,91	0,91	0,82	0,81	0,70
200	0,88	0,87	0,75	0,74	0,60
[a] Tussengelegen waarden mogen worden geïnterpoleerd.					

Figure F-5: Correction factors α for traffic load LM1 [24]

Appendix G

Results BSP simulations

The Royal Dutch Touring Club ANWB (Figure G-1), who is responsible for the traffic information in The Netherlands, provides the rush hour times during a work week. These times are based on the busiest highways in The Netherlands and they provide times in which the chance of a traffic jam is higher. The times provided by the ANWB are listed below.

- Morning traffic jam: **06:30 - 09:30**
- Afternoon/ evening traffic jam: **15:30 - 19:00**

Figure G-1: Well known ANWB logo

Three different analyses have been done with multiple assumptions for the rush hour times with inclusion of weekend recovery or not. During each analysis it is assumed that at the given rush hour times there will be a 100% chance of a traffic jam. In other words, without a doubt there will be a traffic jam at the assumed conservative traffic jam hours.

Analysis 1 (least conservative): in this analysis it is assumed that during the weekends there will be no rush hours, due to the fact that there will be no commuting traffic. The conservative assumption for the rush hours used in this analysis are listed below.

- Morning traffic jam: **06:00 - 10:00**
- Afternoon/ evening traffic jam: **15:00 - 19:00**

The results from the analysis for the first weeks are given in Figure G-2 and Figure G-3 and the results for the last three weeks after a 100 year lifetime are given in Figure G-4.

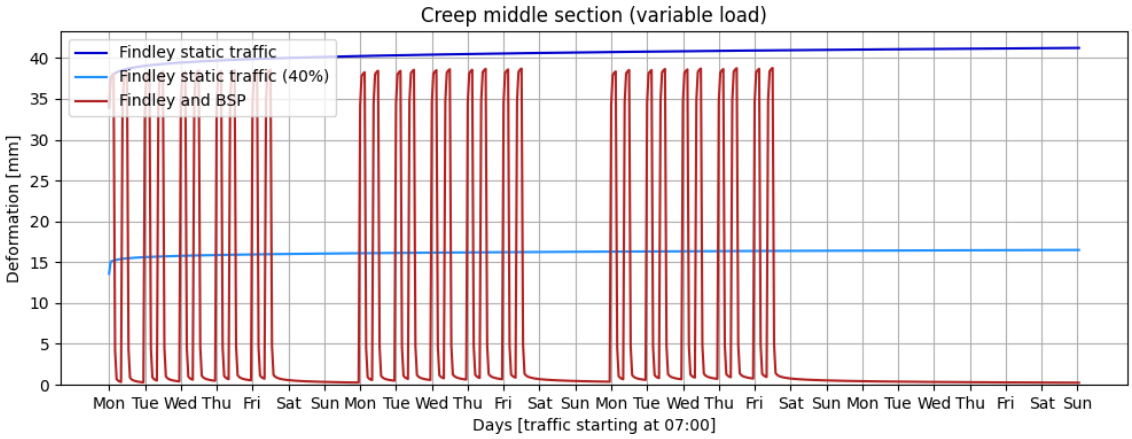

Figure G-2: Results first three weeks with both elastic and viscoelastic deformation

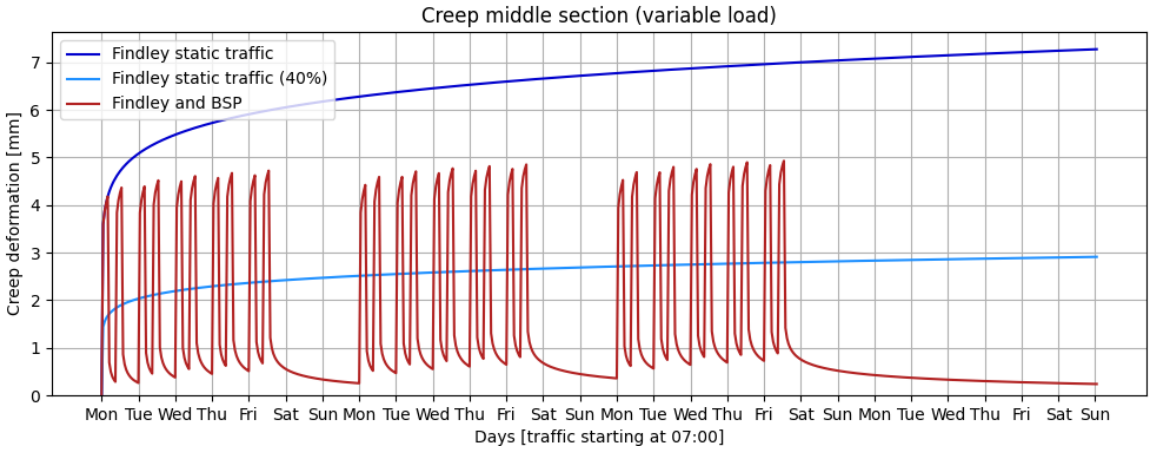

Figure G-3: Results first three weeks with just viscoelastic deformation

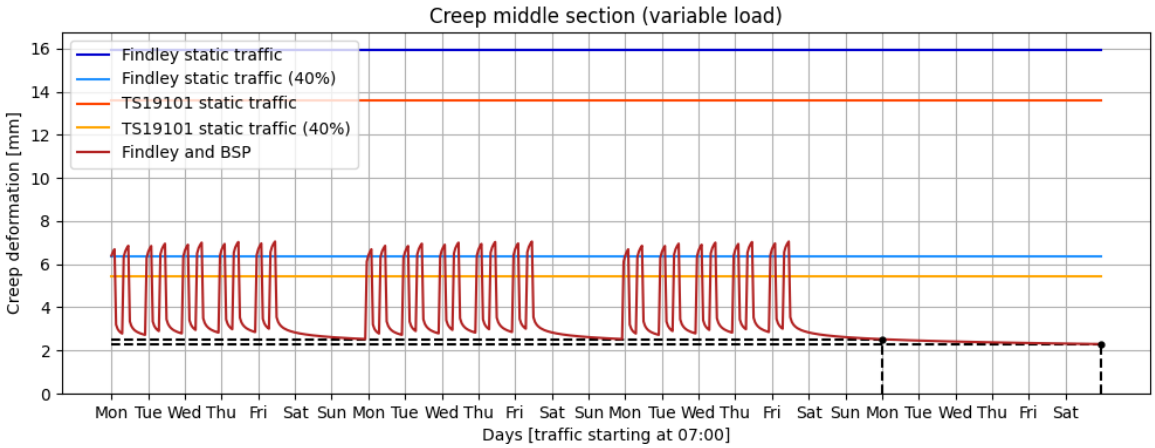

Figure G-4: Results last three weeks with just viscoelastic deformation

Analysis 2 (conservative): in this analysis it is assumed that during the weekends there will be no rush hours, due to the fact that there will be no commuting traffic. The conservative assumption for the rush hours used in this analysis are listed below.

- Morning traffic jam: **05:00 - 10:00**
- Afternoon/ evening traffic jam: **15:00 - 20:00**

The results from the analysis for the first weeks are given in Figure G-5 and Figure G-7 and the results for the last three weeks after a 100 year lifetime are given in Figure **??**.

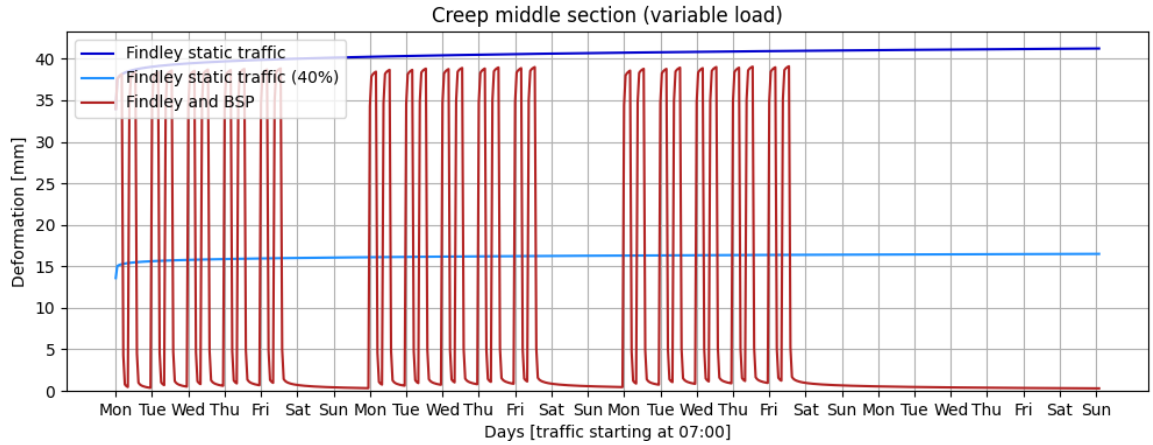

Figure G-5: Results first three weeks with both elastic and viscoelastic deformation

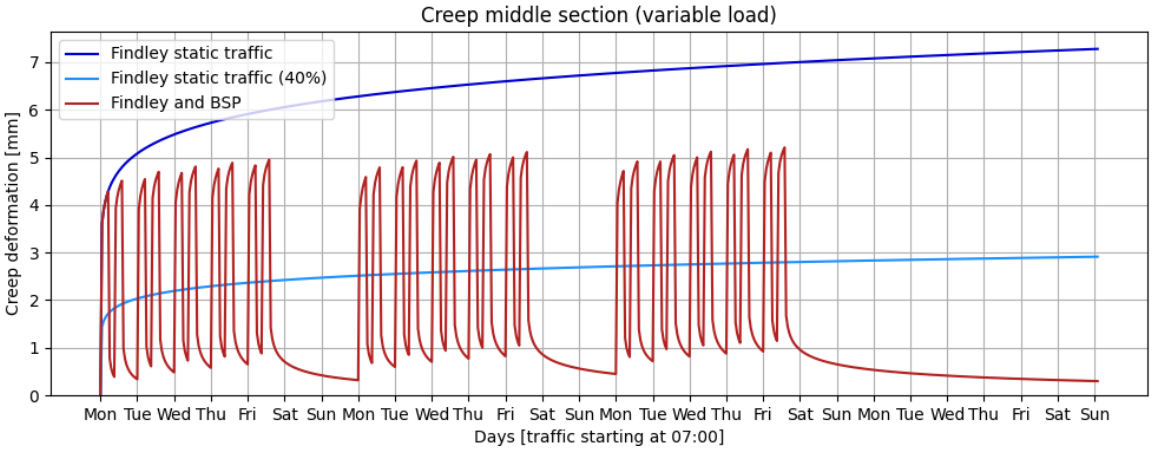

Figure G-6: Results first three weeks with just viscoelastic deformation

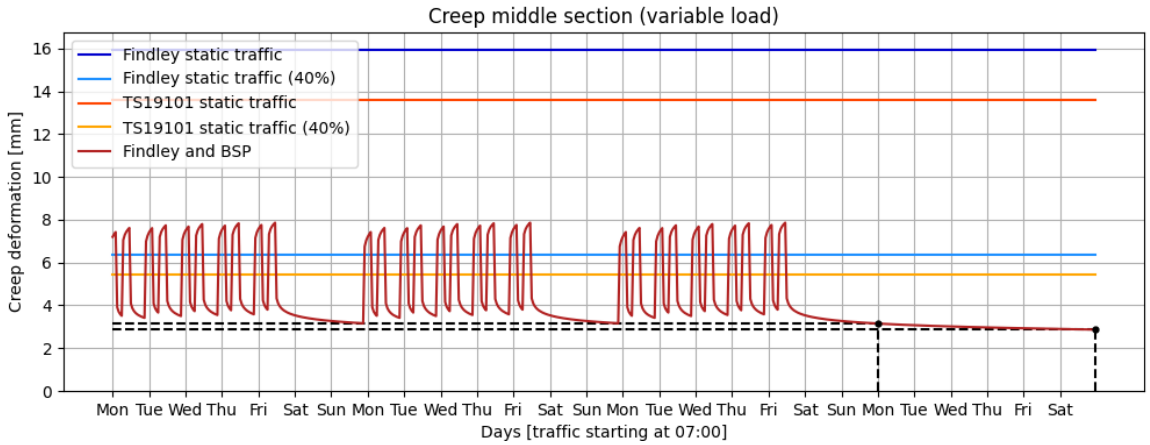

Figure G-7: Results last three weeks with just viscoelastic deformation

Analysis 3 (most conservative): in this analysis it is assumed that during the weekends there will be rush hours, so that the total traffic loading time adds up to more than 40%. The conservative assumption for the rush hours used in this analysis are listed below.

- Morning traffic jam: **05:00 - 10:00**
- Afternoon/ evening traffic jam: **15:00 - 20:00**

The results from the analysis for the first weeks are given in Figure G-8 and Figure G-10 and the results for the last three weeks after a 100 year lifetime are given in Figure **??**.

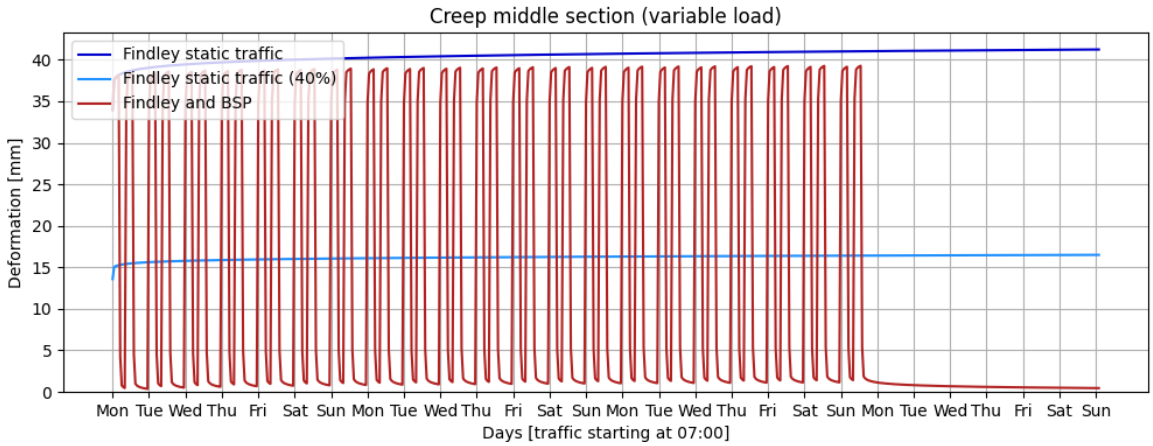

Figure G-8: Results first three weeks with both elastic and viscoelastic deformation

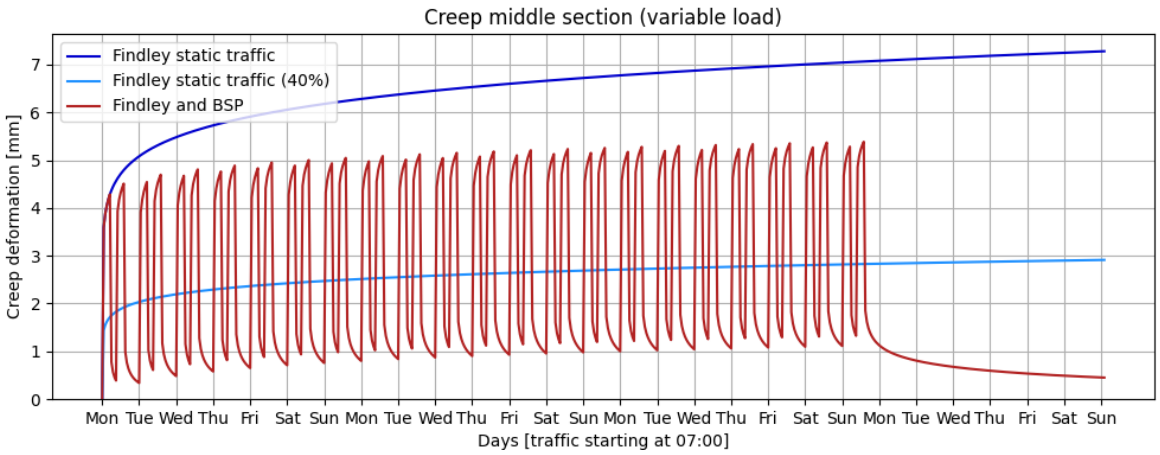

Figure G-9: Results first three weeks with just viscoelastic deformation

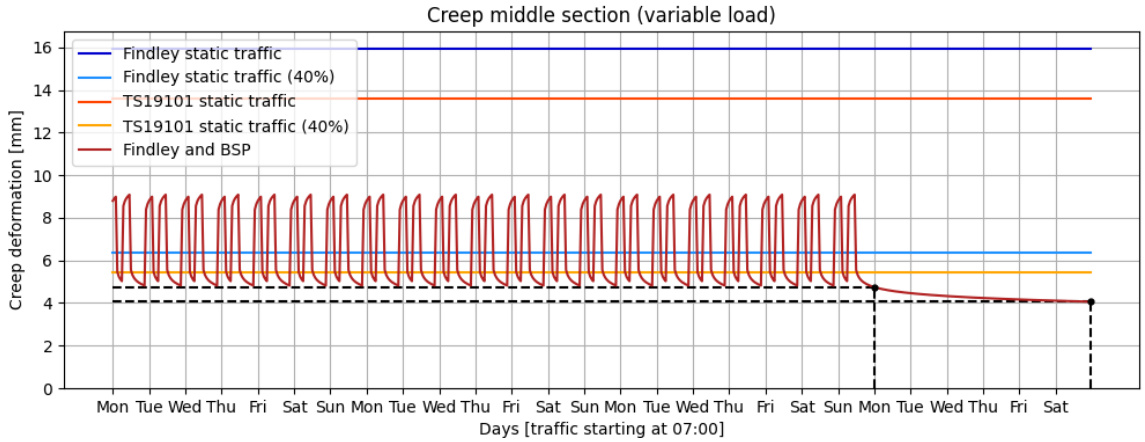

Figure G-10: Results last three weeks with just viscoelastic deformation

Bibliography

[1] F. Irgens, *Continuum mechanics*. No. November, Springer, 2014.

[2] CROW-commissie 1850, "CROW-CUR Aanbeveling 96:2019 Vezelversterkte kunstoffen in bouwkundige en civiel-technische draagconstructies," tech. rep., 2019.

[3] M. Ashby, H. Shercliff, and D. Cebon, *Materials engineering, science, processing and design*. Butterworth-Heinemann, 2007.

[4] M. Nakada, Y. Miyano, H. Cai, and M. Kasamori, "Prediction of long-term viscoelastic behavior of amorphous resin based on the time-temperature superposition principle," *Mechanics of Time-Dependent Materials*, vol. 15, no. 3, pp. 309–316, 2011.

[5] R. Gibson, S. Hwang, G. Kathawate, and C. Sheppard, "Measurement of compressive creep behavior of glassi pps composites using the frequencyltime transformation methods," in *Advanced materials/affordable processes, Proc. 23rd SAMPE Technical Conference, Kiamesha Lake, New York*, pp. 208–18, 1991.

[6] R. A. Shenoi, H. G. Allen, and S. D. Clark, "Cyclic creep and creep-fatigue interaction in sandwich beams," *Journal of Strain Analysis for Engineering Design*, vol. 32, no. 1, pp. 1–18, 1997.

[7] H. F. Brinson and L. C. Brinson, *Polymer engineering science and viscoelasticity: An introduction, Second edition*. 2015.

[8] R. Mohan and D. F. Adams, "Nonlinear creep-recovery response of a polymer matrix and its composites," *Experimental Mechanics*, vol. 25, no. 3, pp. 262–271, 1985.

[9] M. F. Sá, A. M. Gomes, J. R. Correia, and N. Silvestre, "Creep behavior of pultruded GFRP elements - Part 1: Literature review and experimental study," *Composite Structures*, vol. 93, no. 10, pp. 2450–2459, 2011.

[10] G. McClure and Y. Mohammadi, "Compression Creep of Pultruded E-Glass-Reinforced-Plastic Angles," *Journal of Materials in Civil Engineering*, vol. 7, no. 4, pp. 269–276, 1995.

[11] E. J. Barbero, *Finite element analysis of composite materials using Abaqus*. 2013.

[12] T. G. Langdon, "Identifiying creep mechanisms at low stresses," *Materials Science and Engineering A*, vol. 283, no. 1-2, pp. 266–273, 2000.

[13] M. F. Sá, A. M. Gomes, J. R. Correia, and N. Silvestre, "Creep behavior of pultruded GFRP elements - Part 2: Analytical study," *Composite Structures*, vol. 93, no. 9, pp. 2409–2418, 2011.

[14] J. Siccama, "Masters Thesis: An experimental research into the creep behavior of glass fiber reinforced polyester," 2016.

[15] Y. Shao and J. Shanmugam, "Deflection Creep of Pultruded Composite Sheet Piling," *Journal of Composites for Construction*, vol. 8, no. 5, pp. 471–479, 2004.

[16] M. Bottoni, C. Mazzotti, and M. Savoia, "Creep tests on GFRP pultruded specimens subjected to traction or shear," *Composite Structures*, vol. 108, no. 1, pp. 514–523, 2014.

[17] K. A. Harries, Q. Guo, and D. Cardoso, "Creep and creep buckling of pultruded glass-reinforced polymer members," *Composite Structures*, vol. 181, pp. 315–324, 2017.

[18] J. T. Mottram, "Short- and long-term structural properties of pultruded beam assemblies fabricated using adhesive bonding," *Composite Structures*, vol. 25, no. 1-4, pp. 387–395, 1993.

[19] Y. Choi and R. L. Yuan, "Time-Dependent Deformation of Pultruded Fiber Reinforced Polymer Composite Columns," *Journal of Composites for Construction*, vol. 7, no. 4, pp. 356–362, 2003.

[20] L. Ascione, J. Caron, P. Godonou, K. van Ijselmuijden, J. Knippers, T. Mottram, and L. Tromp, "Prospect for New Guidance in the design of FRP," Tech. Rep. january, 2016.

[21] NEN-EN, "NEN-EN 1990+A1+A1C2," 2011.

[22] NEN-EN, "NEN-EN 1990+A1+A1C2 (National Annex)," 2011.

[23] NEN-EN, "NEN-EN 1991-1-2 + C1," vol. 2002, no. december 2011, 2017.

[24] NEN-EN, "NEN-EN 1991-2 + C1 / NB," no. december 2011, 2017.

[25] M. Koetsier, *Virtual fatigue verification of Glass Fibre-Reinforced Polymer components for civil engineering applications*. PhD thesis, 2021.

[26] M. S. v. H.-M. Geesteranus, "Vaststelling van de begrotingsstaten van het Ministerie van Infrastructuur en Milieu (XII) voor het jaar 2017," 2016.

[27] J. Smits, "Fiber-Reinforced Polymer Bridge Design in the Netherlands: Architectural Challenges toward Innovative, Sustainable, and Durable Bridges," *Engineering*, vol. 2, no. 4, pp. 518–527, 2016.

[28] T. Siwowski, D. Kaleta, and M. Rajchel, "Structural behaviour of an all-composite road bridge," *Composite Structures*, vol. 192, no. January, pp. 555–567, 2018.

[29] L. Tromp and A. De Boer, "Developments in Dutch FRP design guidance for FRP in infrastructure," *Engineering for Progress, Nature and People*, pp. 2215–2222, 2014.

[30] Y. J. Kim, "State of the practice of FRP composites in highway bridges," *Engineering Structures*, vol. 179, no. October 2018, pp. 1–8, 2019.

[31] D. W. Scott, J. S. Lai, and A.-H. Zureick, "Creep Behavior of Fiber-Reinforced Polymeric Composites: A Review of the Technical Literature," *Reinforced Plastics and Composites*, p. 30, 1995.

[32] L. S. Lee, "Creep and time-dependent response of composites," in *Durability of Composites for Civil Structural Applications*, ch. 8, Woodhead Publishing, 2007.

[33] L. Ascione, V. P. Berardi, and A. D'Aponte, "Creep phenomena in FRP materials," *Mechanics Research Communications*, vol. 43, pp. 15–21, 2012.

[34] C. M. Howard and L. Hollaway, "The characterization of the non-linear viscoelastic properties of a randomly orientated fibre/matrix composite," *Composites*, vol. 18, no. 4, pp. 317–323, 1987.

[35] G. Boscato, C. Casalegno, and S. Russo, "Creep Effects in Pultruded FRP Beams," *Mechanics of Composite Materials*, vol. 52, no. 1, pp. 27–42, 2016.

[36] T. Dijk van, "Barsten in de brug," *Journalistic platform TU Delft*, 2015.

[37] R. Lassche and R. Rook, *Renovatie stalen brugdekken met een VVK sandwichconstructie*. PhD thesis, 2018.

[38] M. Kulpa and T. Siwowski, "Stiffness and strength evaluation of a novel FRP sandwich panel for bridge redecking," *Composites Part B: Engineering*, vol. 167, no. September 2018, pp. 207–220, 2019.

[39] T. Sakai and S. Somiya, "Analysis of creep behavior in thermoplastics based on visco-elastic theory," *Mechanics of Time-Dependent Materials*, vol. 15, no. 3, pp. 293–308, 2011.

[40] R. Miranda Guedes, J. J. Morais, A. T. Marques, and A. H. Cardon, "Prediction of long-term behaviour of composite materials," *Computers and Structures*, vol. 76, no. 1, pp. 183–194, 2000.

[41] M. Pavlovic, "Options for Finite Element Analysis of FRP composite structures," Tech. Rep. September, 2018.

[42] Technical Committee CEN/TC250, "CEN-TC250 Design of Fibre-Polymer Composite Structures Second Draft-20200430," 2020.

[43] M. F. Sá and J. R. Correia, "Background Report TS CEN-TC250 sub-clause creep," 2020.

[44] E. N. D. C. Andrade, "On the viscous flow in metals, and allied phenomena," *Proceedings of the Royal Society of London. Series A, Containing Papers of a Mathematical and Physical Character*, vol. 84, no. 567, pp. 1–12, 1910.

[45] J. Pelleg, *Solid Mechanics and Its Applications: Creep in Ceramics*. Springer, 2017.

[46] B. Josef, *Creep mechanics*, vol. 53. Springer, 2019.

[47] W. K. Goertzen and M. R. Kessler, "Creep behavior of carbon fiber/epoxy matrix composites," *Materials Science and Engineering A*, vol. 421, no. 1-2, pp. 217–225, 2006.

[48] F. Campbell, *2.1 Fiber Terminology*. ASM International, 2010.

[49] D. A. Dillard, K. C. Gramoll, and H. F. Brinson, "The implications of the fiber truss concept for creep properties of laminated composites," *Composite Structures*, vol. 11, no. 2, pp. 85–100, 1989.

[50] J. Aboudi and G. Cederbaum, "Analysis of viscoelastic laminated composite plates," *Composite Structures*, vol. 12, no. 4, pp. 243–256, 1989.

[51] J. L. Sullivan, "Creep and physical aging of composites," *Composites Science and Technology*, vol. 39, no. 3, pp. 207–232, 1990.

[52] Y. Miyano, M. Kanemitsu, T. Kunio, and H. A. Kuhn, "Role of Matrix Resin on Fracture Strengths of Unidirectional CFRP," *Journal of Composite Materials*, vol. 20, no. 6, pp. 520–538, 1986.

[53] Y. T. Yeow, D. H. Morris, and H. F. Brinson, "A new experimental method for the accelerated characterization of composite materials," p. 395, 1978.

[54] L. Brinson and T. Gates, *Viscoelasticity and Aging of Polymer Matrix Composites: Polymer and Elastomer Matrix Composites*, vol. 2, pp. 333–368. Elsevier Science, 2000.

[55] S. C. Yen and D. H. Morris, "Accelerated characterization of a chopped fiber composite using a strain energy failure criterion," *Polymer Composites*, vol. 10, no. 4, pp. 249–255, 1989.

[56] H. Brinson, D. Morris, and Y. Yeow, "A New Experimental Method for the Accelerated Characterization of Composite Materials," p. 395, 1978.

[57] D. A. Dillard, D. H. Morris, and H. F. Brinson, "Predicting Viscoelastic Response and Delayed Failures in General Laminated Composites.," *ASTM Special Technical Publication*, pp. 357–370, 1982.

[58] K. C. Gramoll, D. A. Dillard, and H. F. Brinson, "Thermoviscoelastic Characterization and Prediction of Kevlar/Epoxy Composite Laminates," in *Composite Materials: Testing and Design (Ninth Volume)* (S. P. Garbo, ed.), pp. 477–493, West Conshohocken, PA: ASTM International, jan 1990.

[59] S. C. Yen and F. L. Williamson, "Accelerated characterization of creep response of an off-axis composite material," *Composites Science and Technology*, vol. 38, no. 2, pp. 103–118, 1990.

[60] R. F. Gibson and G. R. Kathawate, "Rapid screening of creep susceptibility of structural polymer composites," in *Plastics and Plastic Composites: Material Properties, Part Performance, and Process Simulation: Presented at the Winter Annual Meeting of the American Society of Mechanical Engineers, Atlanta, Georgia, December 1-6, 1991*, vol. 29, p. 161, Amer Society of Mechanical, 1991.

[61] N. Findley, S. Lai, James, and K. Onaran, *Creep Relaxation of Nonlinear Viscoelastic Materials - With an Introduction to Linear Viscoelasticity*. Dover Publications, 1976.

[62] D. Weissman-Berman, *Sandwich Constructions 2*. Engineering Materials Advisory Services, 1992.

[63] K. Yamaguchi, A. G. Thomas, and J. J. Busfield, "Stress relaxation, creep and set recovery of elastomers," *International Journal of Non-Linear Mechanics*, vol. 68, pp. 66–70, 2015.

[64] H. Leaderman, *Elastic and creep properties of filamentous materials*. PhD thesis, 1941.

[65] N. Findley, "26-Year Creep and Recovery of Poly(Vinyl Chloride) and Polyethylene," *Journal of Chemical Information and Modeling*, vol. 53, no. 9, pp. 1689–1699, 2013.

[66] R. A. Schapery, "On the characterization of nonlinear viscoelastic materials," *Polymer Engineering & Science*, vol. 9, no. 4, pp. 295–310, 1969.

[67] E. P. Najafabadi, M. Bazli, H. Ashrafi, and A. V. Oskouei, "Effect of applied stress and bar characteristics on the short-term creep behavior of FRP bars," *Construction and Building Materials*, vol. 171, pp. 960–968, 2018.

[68] D. W. Scott and A. H. Zureick, "Compression creep of a pultruded e-glass/vinylester composite," *Composites Science and Technology*, vol. 58, no. 8, pp. 1361–1369, 1998.

[69] M. Garrido, J. R. Correia, and T. Keller, "Effect of service temperature on the flexural creep of vacuum infused GFRP laminates used in sandwich floor panels," *Composites Part B: Engineering*, vol. 90, pp. 160–171, 2016.

[70] L. C. Bank, T. R. Gentry, and A. Barkatt, "Accelerated Test Methods to Determine the Long-Term Behavior of FRP Composite Structures: Environmental Effects," 1995.

[71] A. Apicella, C. Migliaresi, L. Nicodemo, L. Nicolais, L. Iaccarino, and S. Roccotelli, "Water sorption and mechanical properties of a glass-reinforced polyester resin," *Composites*, vol. 13, no. 4, pp. 406–410, 1982.

[72] V. Panasyuk, M. Delyavskii, and L. T. Berezhnitskii, "Creep of unidirectional glass-reinforced plastics under the effect of liquid media and elevated temperatures," *Plenum Publishing Corporation*, no. 5, pp. 654–658, 1988.

[73] J. L. Sullivan, E. J. Blais, and D. Houston, "Physical aging in the creep behavior of thermosetting and thermoplastic composites," *Composites Science and Technology*, vol. 47, no. 4, pp. 389–403, 1993.

[74] Technical Committee CEN/TC250, "CEN-TC250 Design of Fibre-Polymer Composite Structures Second Draft-20200430," 2020.

[75] L. Bank and A. Mosallam, "Creep and Failure of a Full-Size Plastic Pultruded Frame," *Composites Engineering*, vol. 2, no. 3, 1992.

[76] E. Kuiper and N. Ligterink, "Vehicle categories and weights of vehicle combinations on the Dutch highway based on axle combinations and loads.," p. 26, 2013.

[77] F. Ascione, V. P. Berardi, L. Feo, and A. Giordano, "An experimental study on the long-term behavior of CFRP pultruded laminates suitable to concrete structures rehabilitation," *Composites Part B: Engineering*, vol. 39, no. 7-8, pp. 1147–1150, 2008.

[78] A. Tobolsky and K. Murakami, "Existence of a Sharply Defined Maximum Relaxation Time for Monodisperse Polystyrene," *Journal of Polymer Science*, vol. XI, pp. 443–456, 2005.

[79] R. Schapery, "A simple collocation method for fitting viscoelastic models to experimental data," 1961.

[80] T. Cost and E. Becker, "A multidata method of approximate laplace transform inversion," vol. 2, no. May 1969, pp. 207–219, 1970.

[81] I. Emri and N. W. Tschoegl, "Generating line spectra from experimental responses. Part I: Relaxation modulus and creep compliance," *Rheologica Acta*, vol. 32, no. 3, pp. 311–322, 1993.

[82] A. Cottrell, *An introduction to metallurgy*. CRC Press, 2019.

[83] H. Altenbach, "Introduction to creep mechanics," in *Encyclopedia of Continuum Mechanics*, no. October, Springer, 2019.

[84] F. Nabarro, "Report of a conference on the strength of solids," *The Physical Society, London*, vol. 75, 1948.

[85] C. Herring, "Diffusional viscosity of a polycrystalline solid," *Journal of Applied Physics*, vol. 21, no. 5, pp. 437–445, 1950.

[86] W. Rachinger, "Relative grain translations in the plastic flow of aluminium," *J. Inst. Metals*, vol. 81, 1952.

[87] P. de Vries, S. Fennis, and S. Pasterkamp, *Veiligheid*. Bouwen met Staal, 2013.